DISCLAIMER

This report was prepared as an account of work sponsored by an agency of the United States Government. Neither the United States Government nor any agency thereof, nor any of their employees, makes any warranty, express or implied, or assumes any legal liability or responsibility for the accuracy, completeness, or usefulness of any information, apparatus, product, or process disclosed, or represents that its use would not infringe privately owned rights. Reference herein to any specific commercial product, process, or service by trade name, trademark, manufacturer, or otherwise does not necessarily constitute or imply its endorsement, recommendation, or favoring by the United States Government or any agency thereof. The views and opinions of authors expressed herein do not necessarily state or reflect those of the United States Government or any agency thereof. Reference herein to any social initiative (including but not limited to Diversity, Equity, and Inclusion (DEI); Community Benefits Plans (CBP); Justice 40; etc.) is made by the Author independent of any current requirement by the United States Government and does not constitute or imply endorsement, recommendation, or support by the United States Government or any agency thereof.

ORNL/SPR-2024/3615

Identify and Assess Technical Challenges in Safeguards Measurements of Spent Advanced Reactor Fuels

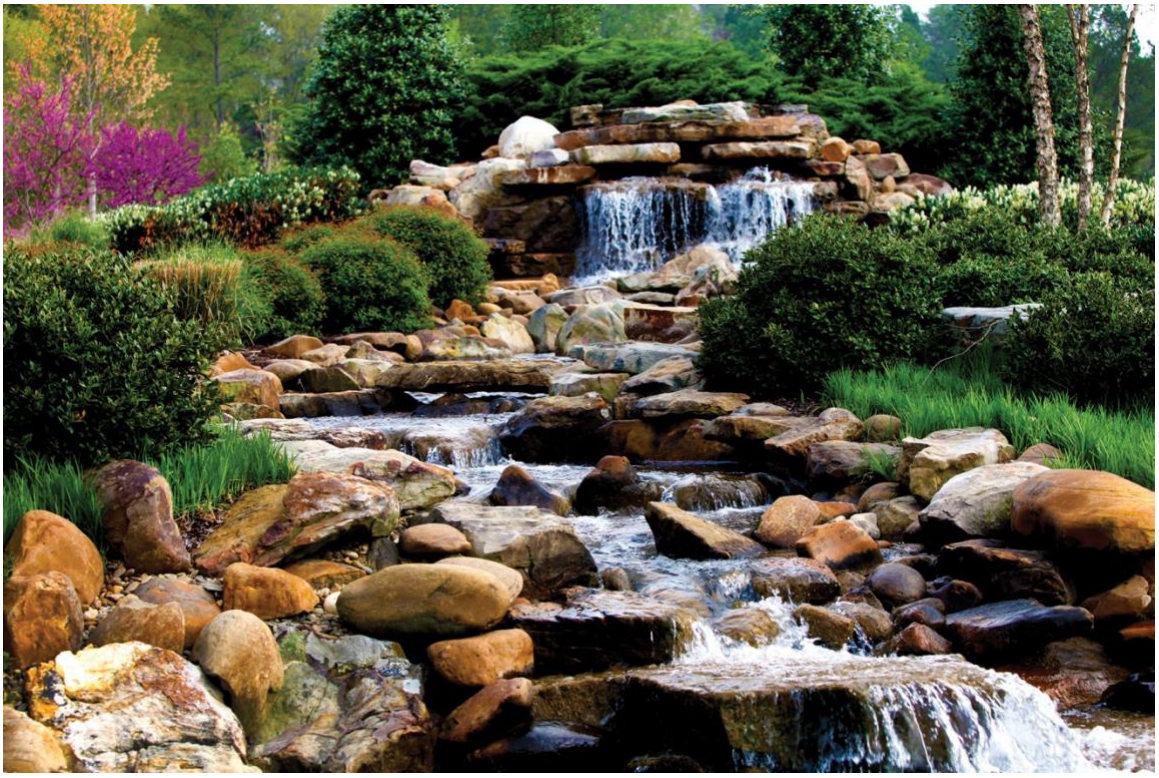

Donny Hartanto
Jianwei Hu

November 2024

OAK RIDGE National Laboratory

ORNL IS MANAGED BY UT-BATTELLE LLC FOR THE US DEPARTMENT OF ENERGY

ORNL/SPR-2024/3615

Nuclear Energy and Fuel Cycle Division

IDENTIFY AND ASSESS TECHNICAL CHALLENGES IN SAFEGUARDS MEASUREMENTS OF FRESH ADVANCED REACTOR FUELS

Donny Hartanto
Jianwei Hu

November 2024

Prepared by
OAK RIDGE NATIONAL LABORATORY
Oak Ridge, TN 37831
managed by
UT-BATTELLE LLC
for the
US DEPARTMENT OF ENERGY
under contract DE-AC05-00OR2272

CONTENTS

LIST OF FIGURES

LIST OF TABLES

ABBREVIATIONS

ANS	American Nuclear Society
ANSI	American National Standards Institute
AR	advanced reactor
ARDP	Advanced Reactor Demonstration Program
BANR	BWXT Advanced Nuclear Reactor
BEGe	broad energy germanium
CVD	Cerenkov viewing device
DCVD	digital Cerenkov viewing device
DOE	US Department of Energy
DU	depleted uranium
FDET	fork detector
GADRAS	Gamma Detector Response and Analysis Software
GWd/MTIHM	gigawatt-days/metric ton of initial heavy metal
GWd/MTU	gigawatt-days/metric ton of uranium
HALEU	high-assay low-enriched uranium
HDPE	high-density polyethylene
HM	heavy metal
HPGe	high-purity germanium
HTTR	high-temperature engineering test reactor
IAEA	International Atomic Energy Agency
ICRP	International Commission on Radiological Protection
ISOCS	In Situ Object Counting System
KP	Kairos Power
LWR	light-water reactor
MCNP	Monte Carlo N-Particle
ORIGEN	Oak Ridge Isotope Generation
PWR	pressurized water reactor
RCVD	robotized CVD
TRISO	tristructural-isotropic
USNC	Ultra Safe Nuclear Corporation
XE	X-energy

ACKNOWLEDGMENTS

We would like to acknowledge and thank the National Nuclear Security Administration of the US Department of Energy, Office of International Nuclear Safeguards, Advanced Reactor International Safeguards Engagement (ARISE) program for sponsoring this work. We would also like to thank Dr. Steve Skutnik for his detailed and insightful review on this report and Dr. Louise Evans for her guidance on this project.

EXECUTIVE SUMMARY

Advanced reactor (AR) designs use various nuclear fuel types that can be significantly different than conventional light-water reactor (LWR) fuels, including differences in sizes, compositions, and chemical forms (e.g., oxide, carbide, metal). Nearly all the proposed AR fuels use high-assay low-enriched uranium (HALEU), which will have higher enrichments (5–20 wt% ^{235}U) than LWR fuels (currently limited to <5 wt% ^{235}U). In advance of the wide use of these new fuel types around the world, international safeguards organizations such as the International Atomic Energy Agency (IAEA]) are working with some of the AR vendors to formulate safeguards approaches for these AR fuel cycles. As part of the overall safeguards approach, it is important to identify the potential technical challenges in performing safeguards verification measurements of these AR fuels (both fresh and spent fuels) in advance of the widespread adoption of these new fuel types, because new safeguards technologies can take several years to develop, test, and approve for use.

This report documents work performed in fiscal year 2024 based on modeling and simulation to assess the performance of the existing safeguards measurement technologies for ***irradiated or spent*** AR fuel elements or items. This work is a continuation of the work performed in fiscal year 2023 that focused on ***fresh*** AR fuels. Spent AR fuels have a distinct difference from their LWR counterparts: unlike the spent LWR fuels typically stored in a water-filled pool, some spent AR fuels—such as tristructural-isotropic (TRISO)-based fuels—will most likely be stored in air-filled hot cells. Because most safeguards measurements on spent fuel performed to date have been conducted under water, the air-filled hot cell environment could present unique challenges to safeguards measurements.

Fork detector (FDET) and Cerenkov viewing device (CVD) systems have been the two primary instruments used by the IAEA for several decades to measure spent LWR fuel assemblies stored in pools for safeguards verification purposes. Because the lower refractive index of air causes Cerenkov light to be of lower intensity in air than in water, existing CVDs are likely unable to perform safeguards verification measurements for spent fuel stored in an air-filled hot cell, as is the case for the TRISO-based spent fuel elements (e.g., pebbles, graphite fuel blocks). Unlike FDET measurements, CVD measurements do not require fuel be moved, so they are a simpler and faster to take than FDET measurements. **The inability to perform CVD measurements on the TRISO-based AR fuel types presents a major technical challenge in the effort to use existing technology to perform safeguards measurements on spent AR fuels.**

This study was mainly conducted through the modeling and simulation of an FDET or an FDET-like system on five spent AR fuel types, including one metallic fuel type and four TRISO-based fuel types in both pebble and graphite block forms in their respective storage configurations and environments. Because the various AR fuel types have significantly different dimensions, FDET systems must be adapted to accommodate them. Partial defect tests were also simulated in this study to assess the FDET's ability to detect potential fuel diversions. The FDET measures the fuel's total passive neutron and gamma emissions. The simulated FDET results from spent AR fuel items are compared against results from a typical spent pressurized water reactor (PWR) assembly. High-purity germanium (HPGe) gamma detector measurements were also simulated for the spent AR fuel types and the PWR assembly because the signature photopeaks have been used in LWR safeguards verifications, although HPGe is usually not used to detect diversions because of the fuel's self-attenuation effects on those photopeaks. The results indicate that these detectors have significant challenges in performing safeguards measurements of the spent AR fuel items, including incompatibilities between AR fuel items and existing FDETs, lower neutron count rates, lower sensitivities to fuel diversions in certain AR fuel items, and significantly higher interference from a neighboring fuel item when the measurement is performed in air. These results suggest that an

alternative technology or significant and timely technology development is needed to perform adequate safeguards measurements of some of these AR fuel items.

1. INTRODUCTION

1.1 BACKGROUND AND MOTIVATION

Dozens of advanced reactor (AR) designs are being pursued around the world [1]. These AR designs use various nuclear fuel types that are significantly different than conventional light-water reactor (LWR) fuels, including differences in sizes, compositions, and chemical forms (e.g., oxide, carbide, metal). Nearly all proposed AR fuels use high-assay low-enriched uranium (HALEU), which has higher enrichments (5 to 20 wt% ^{235}U) compared to LWR fuels (currently limited to <5 wt% ^{235}U). Because most existing safeguards measurement instruments were developed for LWR fuel elements, potential technical challenges are expected when these instruments are applied to the AR fuel elements. Identifying these challenges in advance of the widespread adoption of these new fuel types will provide international safeguards organizations such as the International Atomic Energy Agency (IAEA) with extra time to adapt existing technologies or develop alternative technologies to overcome the challenges. Identifying these challenges will also help domestic AR developers create plans to accommodate safeguards needs.

The current study focuses on identifying and assessing the potential technical challenges when using existing safeguards technologies to perform safeguards measurements on ***spent or irradiated*** AR fuel elements or items. ("Item" is used in this report as a broad term that can represent a fuel element or a collection of fuel elements such as a canister that holds a number of pebbles.) This is a continuation of the previous effort conducted using ***fresh*** AR fuel elements [2, 3]. Spent AR fuels have a distinct difference from their LWR counterparts: unlike the spent LWR fuels typically stored in water-filled pools, some spent AR fuel—such as tristructural-isotropic (TRISO)-based fuels—will most likely be stored in air-filled hot cells. Because most safeguards measurements on spent fuel performed to date have been conducted under water, the air-filled hot cell environment could present unique challenges to safeguards measurements.

This study was mainly conducted through the modeling and simulation of an existing fork detector (FDET) system [4, 5, 6] or adapted FDET systems for five AR fuel types, including one metallic fuel type and four TRISO-based fuel types in both pebble and graphite block forms in their respective storage configurations and environments. (These AR fuel types were selected based on results from a survey of domestic AR designs, as discussed in the next subsection.) Because the various AR fuel types have significantly different dimensions, FDET systems must be adapted to accommodate some of the AR fuel types. Partial defect tests were also simulated in this study to assess the FDET's ability to detect potential fuel diversions. The FDET measures the fuel's total passive neutron and gamma emissions. The simulated FDET results for spent AR fuel items are compared against those from a typical spent pressurized water reactor (PWR) assembly. FDETs are commonly employed to measure spent LWR fuel assemblies [3, 4, 5] to qualitatively and quantitatively verify the assembly's identity and integrity for safeguards verification purposes. High-purity germanium (HPGe) gamma detector measurements were also simulated for the spent AR fuel types and the PWR assembly because the signature photopeaks have been used in LWR safeguards verifications, although HPGe is usually not used to detect diversions because of the fuel's self-attenuation effects on those photopeaks.

Besides FDET systems, the various versions of Cerenkov viewing devices (CVDs) are the other primary instrument used by the IAEA to measure spent LWR fuels for safeguards verification purposes. However, unlike spent LWR fuels that are usually stored in a water-filled pool, the TRISO-based spent AR fuel types (e.g., pebbles, graphite blocks) are expected to be stored in an air-filled hot cell, which is a drastic departure from the environment in which IAEA conducts a typical spent fuel measurement. Because the lower refractive index of air causes Cerenkov light to be of lower intensity in air than in water, existing CVDs are likely unable to perform safeguards verification measurements for spent fuel stored in an air-filled hot cell, as is the case for the TRISO-based spent fuel elements or items. Unlike FDET

measurements, CVD measurements do not require fuel to be moved, so they are simpler and faster to take than the FDET measurements. **The reduced effectiveness or inability to perform CVD measurements on the TRISO-based AR fuel types presents a major technical challenge in the effort to use existing technology to perform safeguards measurements on spent AR fuels.** Brief descriptions of FDET and CVD systems are provided in the following subsection.

1.2 BRIEF DESCRIPTIONS OF FDET AND CVD SYSTEMS

The FDET and CVD systems have been the primary instruments used by the IAEA for several decades to measure spent LWR fuel assemblies stored in pools for safeguards verification purposes. The image on the left in Figure 1 shows an FDET measurement being conducted on a spent PWR assembly in a storage pool. As can be seen, the fuel assembly was lifted by a crane out of the storage racks, and the FDET measurement was taken at the usual measurement position, which is at mid-height of the fuel assembly. The middle image in Figure 1 shows an unmounted FDET head with arrows indicating the four fission chambers used for neutron detections [7]. Although it is not shown in this image, an FDET is also equipped with two ionization chambers for gamma-ray detection. The right image in Figure 1 shows a plot of the comparison of measured and calculated FDET neutron counts for a large set of LWR fuel assemblies [8]. By integrating the Oak Ridge Isotope Generation (ORIGEN) data analysis module into the IAEA's software that is used to analyze FDET neutron and gamma count rates, FDET's capability to quantitatively verify an LWR fuel assembly's identity and integrity has been substantially improved [5, 7, 8]. Because most of the FDET measurements performed to date were conducted in water-filled pools, comparing the historic data with data from the air-filled measurement environment presents additional challenges for FDET measurements of spent AR fuels.

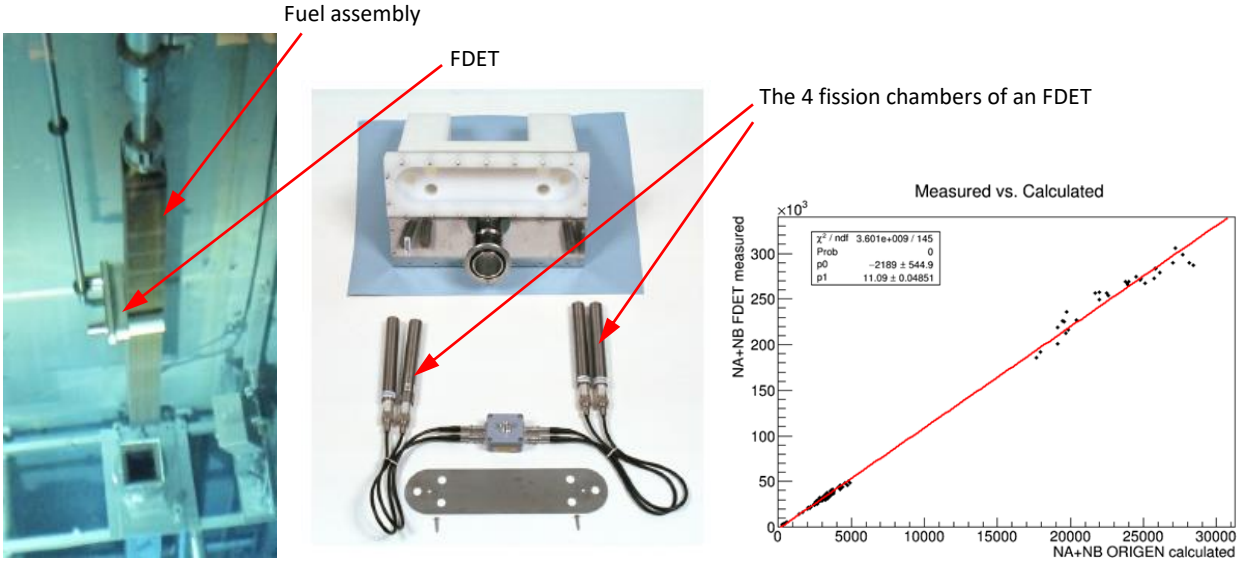

Figure 1. FDET measurement of a PWR spent fuel assembly in the storage pool (left), the unmounted FDET head [7] (middle), and plot comparing the measured and calculated FDET neutron counts [8] (right).

The IAEA has used various versions of CVDs for spent fuel safeguards verification measurements, particularly the digital Cerenkov viewing device (DCVD). The left image in Figure 2 shows a conventional CVD measurement being conducted at poolside [9]. As can be seen, the CVD is pointed downwards toward the spent fuel in the pool to collect the Cerenkov light from the fuel. The middle image in Figure 2 shows a Cerenkov image of a PWR assembly that was produced by a CVD [9]. The right image in Figure 2 shows testing of a robotized CVD (RCVD) in a spent fuel pool [10]. The RCVD

autonomously navigates a path across a used fuel storage pool while updating a real-time map with footage and data of the fuel assemblies being measured [11].

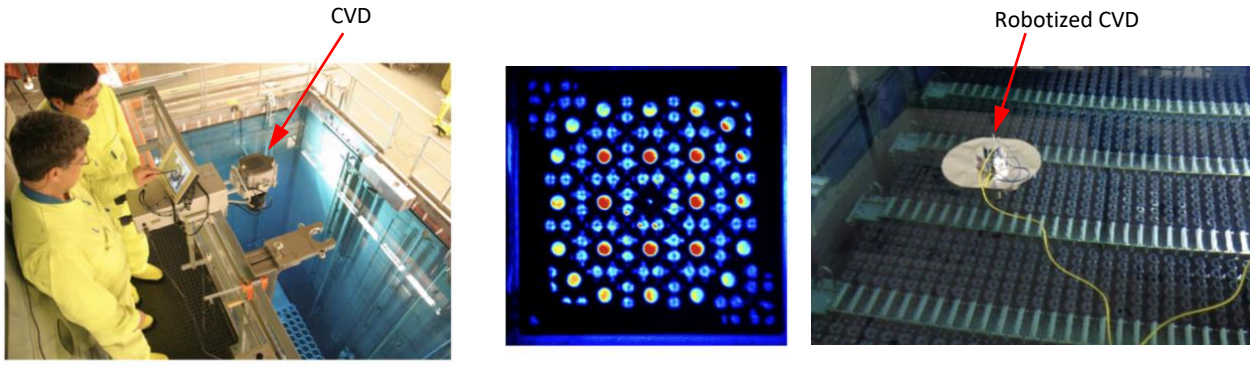

Figure 2. A conventional CVD measurement on at pool side [9] (left), a Cerenkov image of a PWR assembly [9] (middle), and robotized Cherenkov viewing device performing testing at a spent fuel pool [10] (right).

Various versions of CVDs have been used by the IAEA to qualitatively verify the presence of LWR spent fuel assemblies, although work is under way to use the CVDs to perform quantitative verifications. As aforementioned, existing CVDs are likely unable to perform safeguards verification measurements for spent fuel (e.g., the TRISO-based spent fuel) stored in an air-filled hot cell. Because metallic fuel bundles have much longer plenums (~8 times longer) above the active fuel region than an LWR assembly, and because CVDs collect signals from above the pool, it is expected that CVDs would be less effective in verifying metallic fuel bundles in a pool than in an LWR fuel assembly. With recent advancements in CVD technology for water-based measurements (e.g., RCVD), the ineffectiveness or inability to perform CVD measurements on several spent AR fuel types will become an increasingly important limitation for spent AR fuel safeguards inspections.

1.3 SURVEY OF THE ADVANCED REACTOR FUELS AND THE FORK DETECTOR

Because of the large number of AR designs being pursued by various organizations around the world, it is impractical to study all of them in this work. The US Department of Energy (DOE) Advanced Reactor Demonstration Program (ARDP) has down-selected the domestic AR designs and is currently supporting the ten designs [12] listed in Table 1, which also lists the associated fuel types. Of the ten ARs, five utilize TRISO-based fuel elements in pebble form or compacts in graphite blocks; two use metal fuel, two use UO_2 fuel, which is expected to be similar to existing LWR fuel; and one uses molten salt. This work focuses on the various types of TRISO-based fuel elements—pebbles, compacts, and graphite fuel blocks—and metallic fuel elements, together representing seven of the ten AR designs. The analysis also includes TRISO-based Ultra Safe Nuclear Corporation (USNC) fuel elements because their fuel design information is available in the public domain. Fuel types listed in boldface font in the table were included in this analysis.

Table 1. The 10 AR designs supported by DOE's ARDP program [12]

DOE program	Reactor name	Company name	Fuel type
Advanced Reactor Demonstration Program (ARDP)	Xe-100	X-energy (XE)	**Pebble (TRISO-based)**
	Natrium	TerraPower	**Metallic**
Risk Reduction for Future Demonstration Projects	Hermes Reduced-Scale Test Reactor	Kairos Power (KP)	**Pebble (TRISO-based)**
	eVinci Microreactor	Westinghouse	**Compact (TRISO-based)**
	BWXT Advanced Nuclear Reactor (BANR)	BWXT	**Compact (TRISO-based)**
	Holtec SMR-160 Reactor	Holtec	UO_2 (17 × 17)
	Molten Chloride Reactor Experiment	Southern Company	Molten salt
Advanced Reactor Concepts-20 Projects (ARC-20)	Inherently Safe Advanced SMR for American Nuclear Leadership	Advanced Reactor Concepts, LLC	**Metallic fuel**
	Fast Modular Reactor Conceptual Design	General Atomics	UO_2 in SiC cladding
	Horizontal Compact High Temperature Gas Reactor	MIT	**Compact (TRISO-based)**

Based on these AR designs and considering the publicly accessible data, the five spent AR fuels described below and presented in Figure 3 were simulated in this work:

1. **Metallic fuel bundle.** The design is based on the fuel assembly of ABTR-250 [13], which features 217 fuel pins per assembly. The design has been modified to use U-10Zr enriched fuel with 16.5 wt% of ^{235}U, achieving a final discharge burnup of 150 GWd/MTIHM [14].[1]
2. **Type 1 pebbles in a canister.** This configuration involves 2,000 irradiated pebbles randomly packed within a transportation canister. The pebble fuel design is derived from the PBMR-400 using UO_2 fuel with 9.6 wt% ^{235}U enrichment, achieving a final discharge burnup of 90 GWd/MTIHM [15].
3. **Type 2 pebbles in a canister.** Like the Type 1 canister configuration, this fuel type involves 2,000 irradiated pebbles randomly packed within a transportation canister. The pebble fuel design is derived from the Xe-100 reactor based on public information, utilizing UCO fuel with 15.5 wt% ^{235}U enrichment and achieving a final discharge burnup of 165 GWd/MTIHM [16].
4. **Type 1 prismatic graphite fuel block.** This graphite fuel block contains 54 fuel pins, each pin holding 60% TRISO particles by volume [17]. The TRISO particles are based on a UCO fuel kernel enriched to 19.75 wt% of ^{235}U, achieving a final discharge burnup of 100 GWd/MTIHM.
5. **Type 2 prismatic graphite fuel block.** In this design, the graphite fuel block contains 216 fuel pins, and each pin contains 40% of TRISO particles by volume [18]. Like the first prismatic fuel block, this fuel block also utilizes UCO fuel kernels enriched to 19.75 wt% of ^{235}U with a final discharge burnup of 100 GWd/MTIHM.

[1] The burnup unit gigawatt-days/metric ton of initial heavy metal (GWd/MTIHM) is used herein and is interchangeable with the unit GWd/MTU if fuel is initially loaded with only uranium with no uranium–plutonium mix. All LWR and AR fuel types modeled in this work are initially loaded with only uranium, although other AR fuel types may contain both uranium and plutonium in their initial loading.

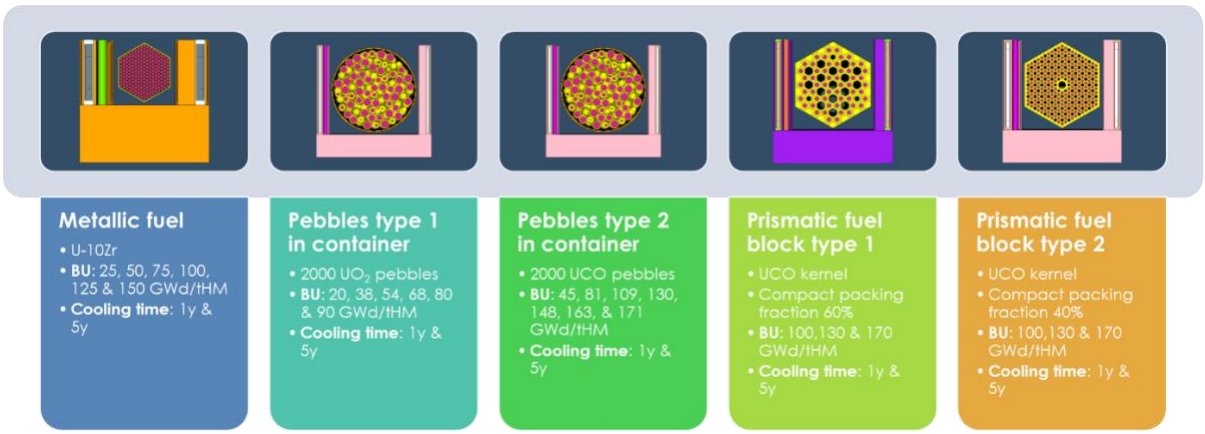

Figure 3. Simulated spent AR fuel items.

1.4 ATTRIBUTES OF SPENT ADVANCED REACTOR FUELS

Table 2 summarizes the characteristics of each of the five spent AR fuel items shown Figure 3 and a spent PWR assembly. These parameters are detailed for each fuel element, bundle, or block, but not for the pebbles, in which case the value reflects the assumption that 2,000 pebbles are contained within a single transportation canister.

Although AR fuels generally utilize HALEU and can achieve burnups significantly higher than those for typical PWR fuels, the neutron and gamma radiation source intensity per spent AR fuel item tends to be lower than that of a PWR fuel assembly. This lower intensity can be attributed to the fact that AR fuel designs often contain smaller quantities of fresh uranium and hence smaller quantities of neutron- and photon-emitting nuclides per individual item.

In a PWR, the large, densely packed fuel assemblies contain several hundred fuel rods that generate a high level of radioactivity because of their large quantities of fissile material content and the fission products they produce during irradiation. This high level of radioactivity results in intense neutron and gamma radiation emissions.

In contrast, AR designs, which often feature innovative fuel configurations like TRISO particles in pebbles or prismatic blocks, distribute the fuel in smaller, more dispersed elements. Metallic fuel elements are typically smaller and have shorter active regions than PWR fuel assemblies. As a result, the total quantity of radioactive material within each metallic fuel element is less than that of a typical PWR assembly. Consequently, the overall neutron and gamma radiation emitted by individual AR fuel elements is lower, as confirmed in the plots presented in Figures 4 and 5. This reduced radiation intensity in AR fuels will reduce the neutron and gamma count rates of an FDET measurement.

Table 2. Summary of key characteristics of the simulated spent PWR and AR fuels

Parameter	PWR fuel assembly	Metallic fuel bundle	Type 1 pebbles in canister	Type 2 pebbles in canister	Type 1 prismatic fuel block	Type 2 prismatic fuel block
Fuel width[1] (cm)	21.4	14.198	29.55	29.55	36	35.996
Fuel height[2] (cm)	360	80	167.58	167.58	80	79.299
Burnup (GWd/MTIHM)	50	150	90	163	100	100
Initial U (kg)	461.828	67.60	18.00	14.17	3.70	9.00
Initial ^{235}U (wt%)	4.2	15.5	9.6	15.5	19.75	19.75
Total Pu/HM at first cycle/pass (wt%)	0.58	1.47	0.49	0.95	N/A	N/A
Total Pu/HM at final discharge (wt%)	1.28	7.85	1.54	2.35	1.39	2.16
^{239}Pu/Pu at first cycle/pass (wt%)	78.08	98.51	84.11	68.91	N/A	N/A
^{239}Pu/Pu at final discharge (wt%)	51.50	88.71	42.86	34.44	50.81	56.65
Total fissile/HM at final discharge (wt%)	1.63	12.34	2.67	3.25	10.83	12.03
Neutron source intensity after 1 y cooling (1/s/cm)	1.6138E+06	1.4816E+04	8.5571E+04	3.1312E+05	2.0430E+04	7.7581E+04
Neutron source intensity after 5 y cooling (1/s/cm)	1.2349E+06	8.8245E+03	5.1263E+04	2.5050E+05	8.6020E+03	3.2801E+04
Gamma source intensity after 1 y cooling (1/s/cm)	1.0213E+14	1.0825E+14	1.6467E+13	1.8283E+13	6.6468E+12	1.0202E+13
Gamma source intensity after 5 y cooling (1/s/cm)	2.1151E+13	3.1578E+13	3.1438E+12	4.6639E+12	1.3184E+12	2.8633E+12

[1]pitch for hexagonal shape assembly; [2]only for active height

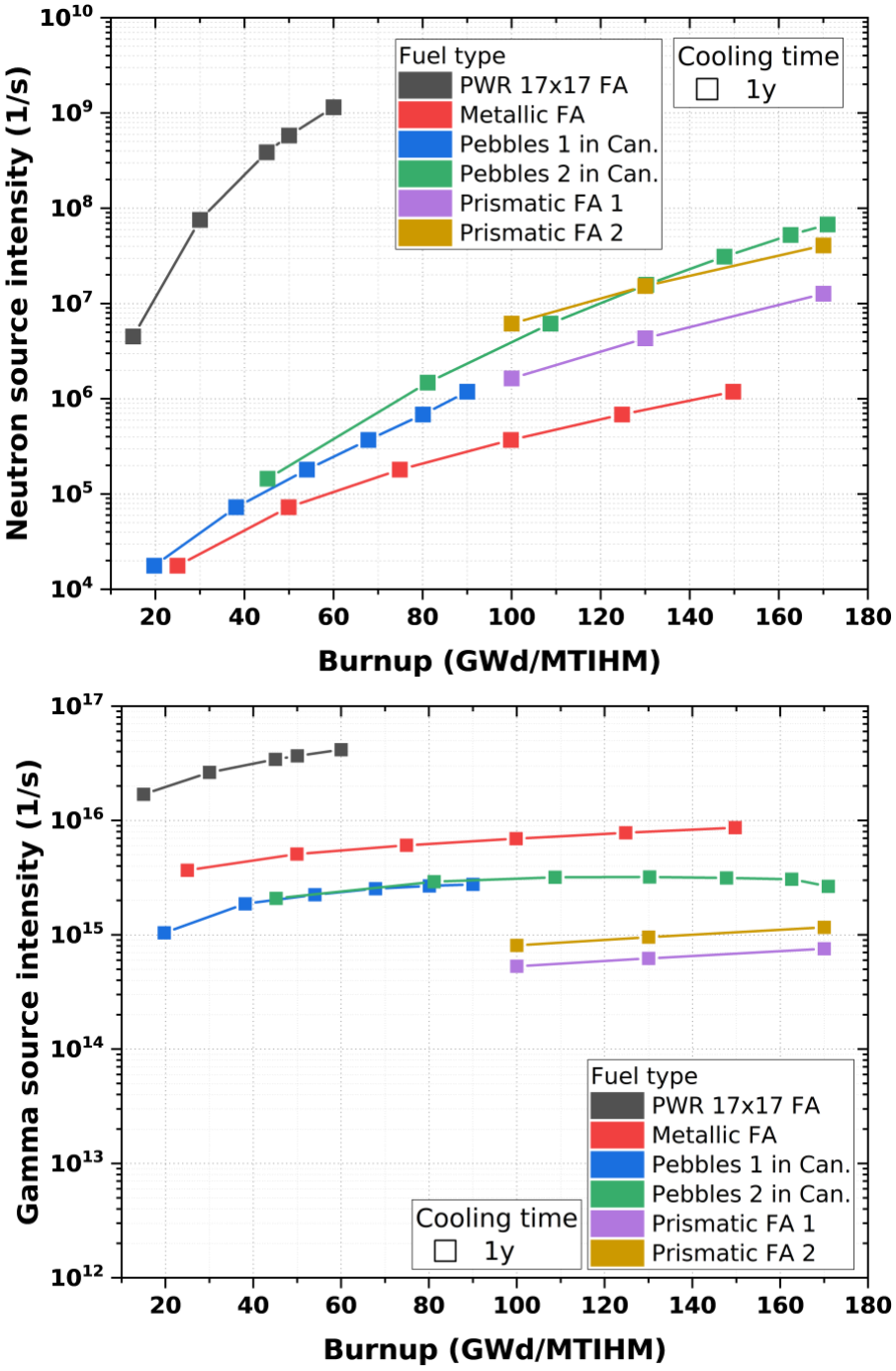

Figure 4. Neutron (top) and photon (bottom) intensity of spent PWR and AR fuels after one year of cooling time.

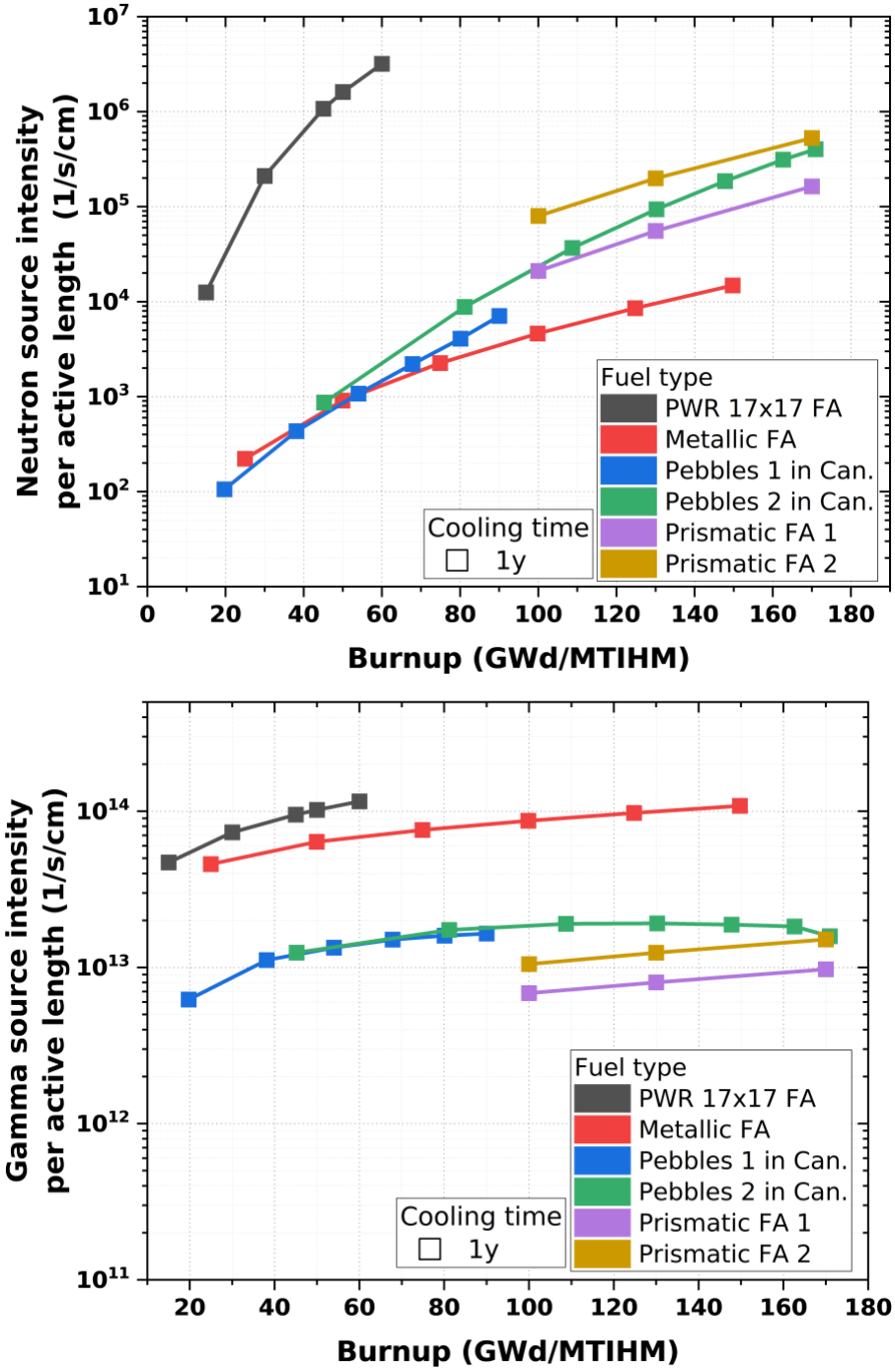

Figure 5. Neutron (top) and photon (bottom) intensity per unit of fuel active length of spent PWR and AR fuels after one year of cooling time.

Figure 6 compares the gamma dose at 1 meter away from the fuel item's outer surface as a function of cooling time between an irradiated PWR assembly and a transportation canister filled with irradiated pebbles with different burnups. As shown, at a given cooling time, the gamma dose rates for the irradiated pebbles are several orders of magnitude lower than those of an irradiated PWR assembly, which is expected because of the much higher initial uranium loading (see Table 2) and thus the higher irradiated fuel material in a PWR assembly. When such gamma dose rates are sufficiently high (e.g., 500 R/h), the

fuel can be considered as “self-protecting” against would-be fuel proliferators. Figure 6 shows that the irradiated pebbles are significantly less self-protecting than an irradiated PWR assembly. Similar conclusions can be made for the other four types of spent AR fuels, as indicated by the additional results included in APPENDIX A.

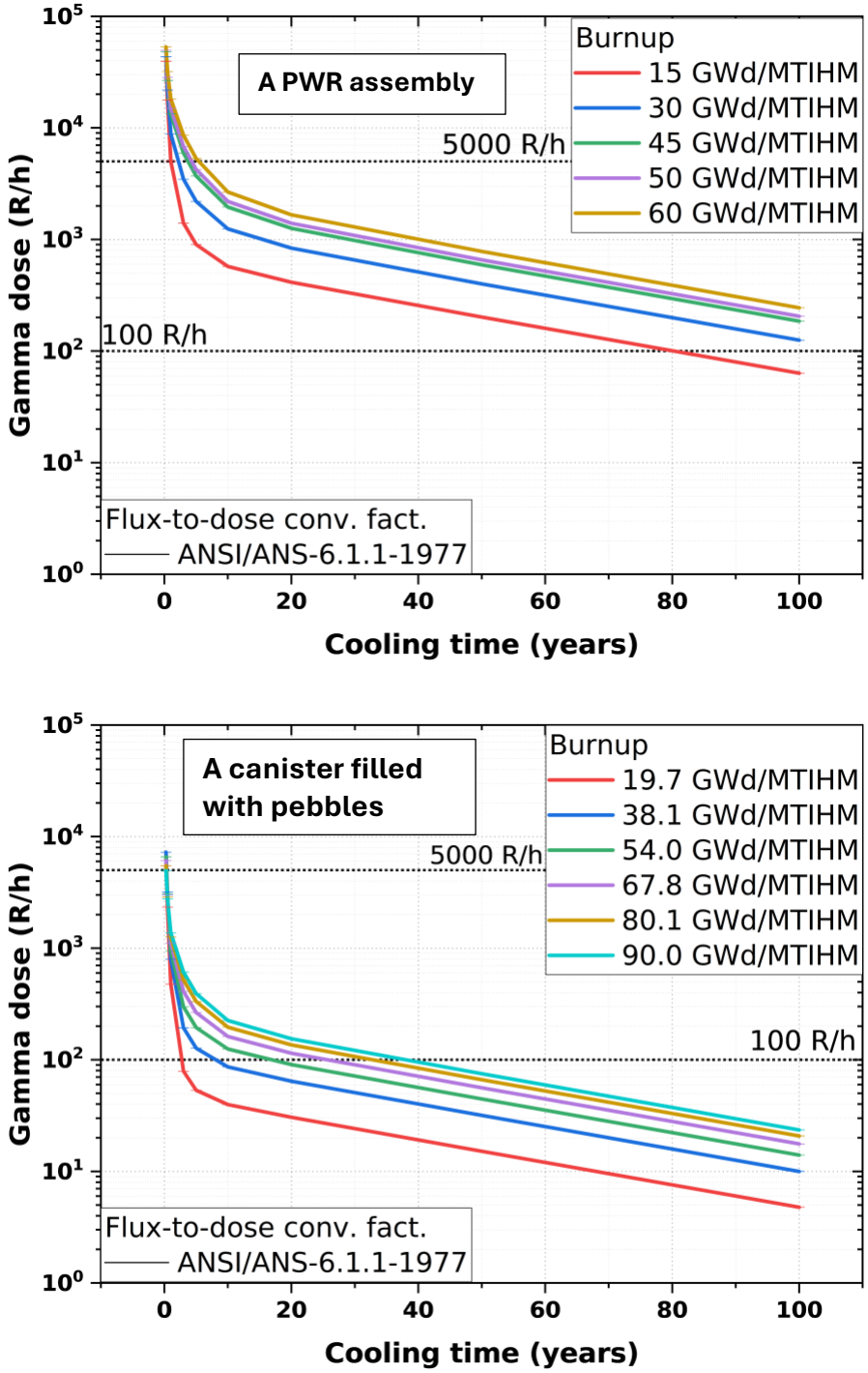

Figure 6. Self-protecting property of PWR fuel (top) and Type 1 pebbles in a transportation canister (bottom).

Figures 7 and 8 compare key characteristics of spent PWR and AR fuels: the ratio of total plutonium (Pu) to heavy metal (HM), and the ratio of ^{239}Pu to total Pu. Several spent AR fuel items (e.g., the metallic bundle, Type 2 pebbles) have higher concentrations of total Pu and/or ^{239}Pu than a PWR assembly. The metallic fuel bundle, which was irradiated in a fast reactor, exhibited a much higher Pu content and a greater ^{239}Pu fraction relative to the total Pu. This is because fast reactors operating with fast neutron energy spectra, which are more efficient at converting ^{238}U into ^{239}Pu, thus leading to increased plutonium production and a higher proportion of ^{239}Pu than in a PWR assembly.

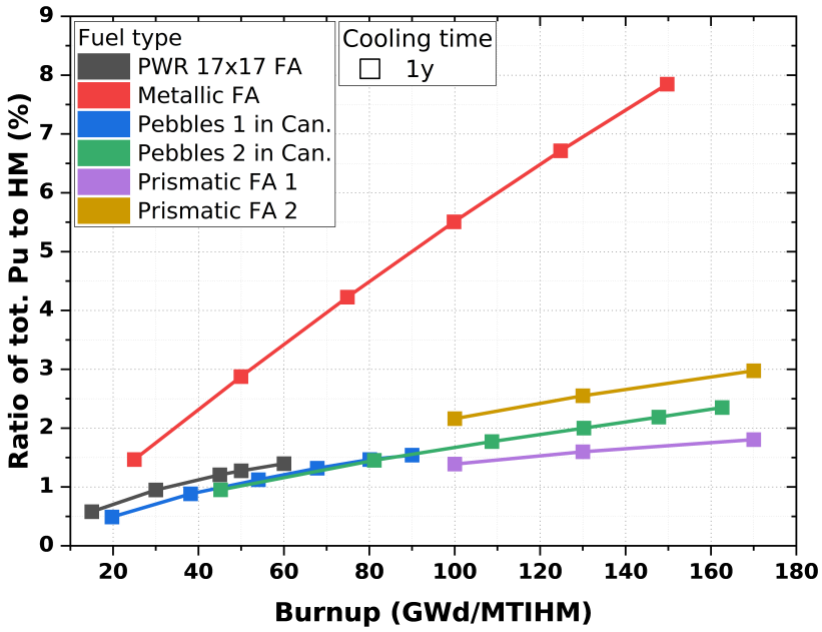

Figure 7. Ratio of total Pu to HM in spent PWR and AR fuels after one year of cooling time.

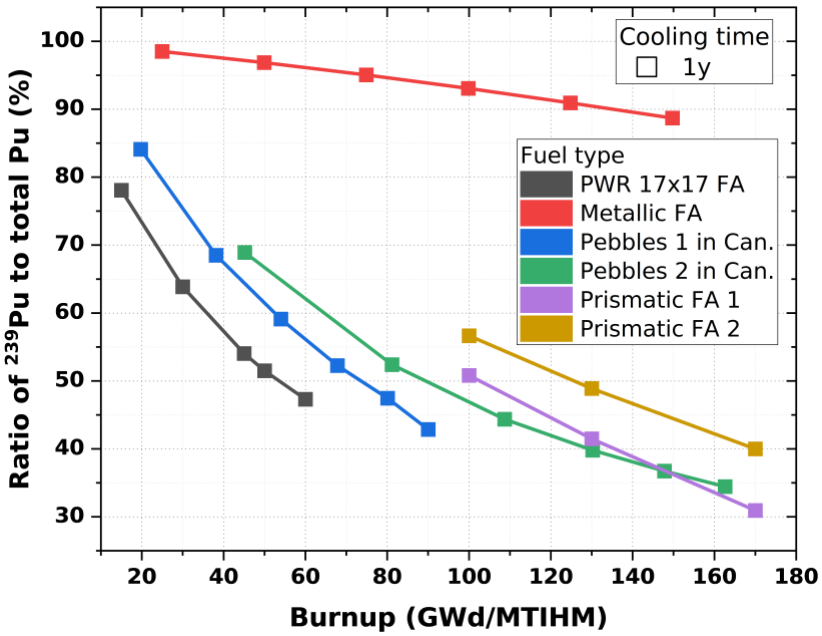

Figure 8. Ratio of ^{239}Pu to total Pu in spent PWR and AR fuels after one year of cooling time.

Figure 9 presents the neutron emission energy spectra comparing the spent PWR fuel assembly with the spent AR fuels after one year of cooling. Most of the neutron sources arises from spontaneous fission, primarily from isotopes such as ^{240}Pu, ^{242}Cm, and ^{244}Cm, with neutron energies ranging from 0.1 to 10 MeV following a Maxwellian distribution. The most probable energy, or the average energy, of these neutrons is usually approximately 1–2 MeV. All fuel types shown exhibit similar shapes of neutron energy spectra, although the intensities can be significantly different from one fuel type to another.

Figure 10 shows the photon emission energy spectra, comparing the spent PWR fuel assembly with the spent AR fuels after one year of cooling. The gamma energy spectra for both spent PWR and AR fuels are similar, with the magnitude being lower for spent AR fuels. The gamma source intensity in both spent PWR and AR fuels peaks within a few MeV, but it drops significantly beyond 3 MeV. Additional results regarding neutron and gamma emission energy spectra from the spent AR fuel types are included in APPENDIX B.

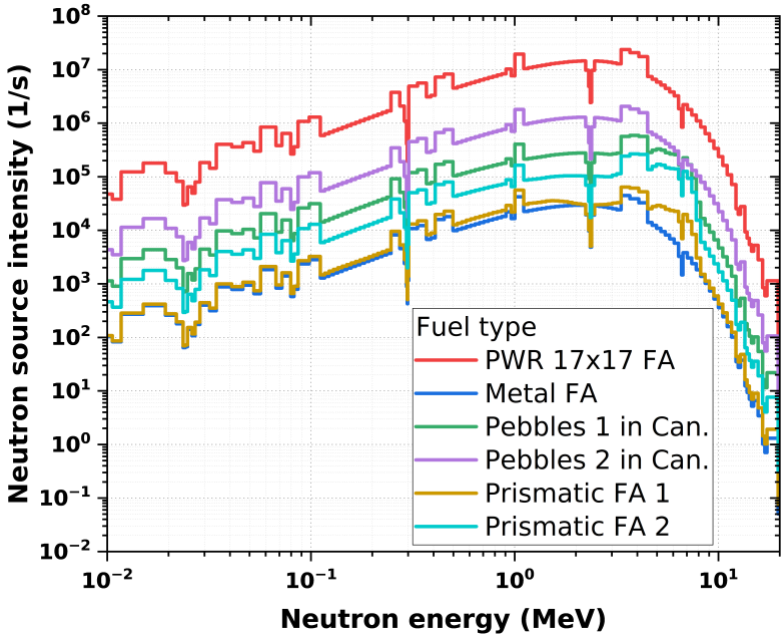

Figure 9. Neutron source intensity for the spent PWR and AR fuels after one year of cooling time.

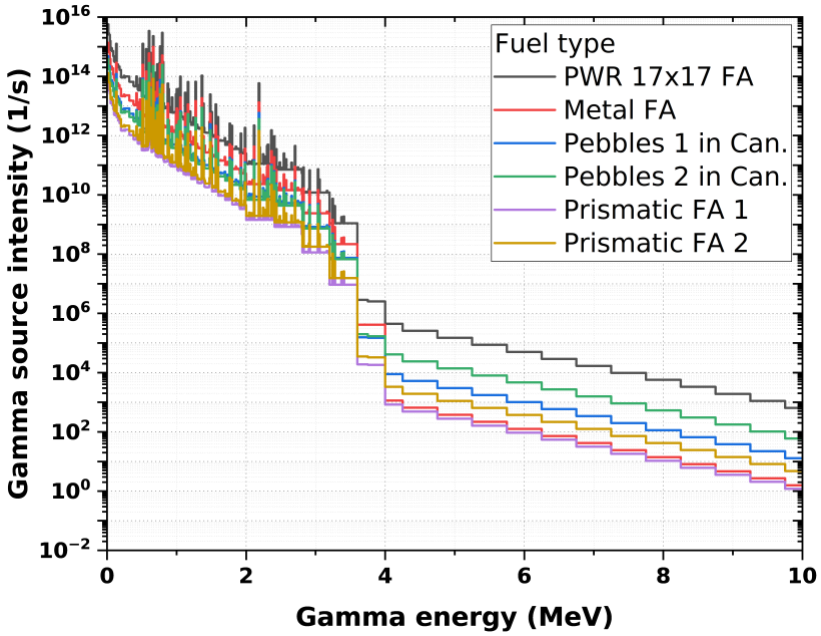

Figure 10. Gamma source intensity for the spent PWR and AR fuels after one year of cooling time.

In summary, the spent AR fuel items have several characteristics that are notably different from those of a spent LWR assembly: AR fuel items are much lighter (i.e., easier to be maneuvered), they contain less uranium per unit volume, and they emit lower self-protecting gamma dose rates when compared to a PWR assembly at a given cooling time. Some of the spent AR fuel items (e.g., metallic fuel) were found to have much higher total Pu and/or ^{239}Pu concentration than a spent PWR assembly; therefore, those spent AR fuel items likely require more stringent safeguards measures than spent PWR assemblies.

2. FORK DETECTOR MODELING OF SPENT ADVANCED REACTOR FUELS

This section documents the work performed to simulate the FDET measurements of the 17 × 17 PWR fuel assembly, the most popular PWR fuel design, and five spent AR fuel items, including a metallic fuel bundle, Types 1 and 2 prismatic graphite fuel blocks, and 2,000 Type 1 and 2 pebbles each in a transportation canister.

2.1 BRIEF INTRODUCTION OF THE FORK DETECTOR

The FDET models developed in previous studies [5, 6] were leveraged in this work. The detector consists of two arms, each equipped with an ionization (ion) chamber for gamma detection and two ^{235}U fission chambers for neutron measurement, as depicted in Figure 11 [4, 5, 6]. In the model, the ionization chamber and one of the two fission chambers are housed within a high-density polyethylene (HDPE) block which is further shielded by a cadmium lining. However, the other fission chamber is left unshielded. The fission chambers contain a thin layer of U_3O_8 coating with 93 wt% of ^{235}U enrichment.

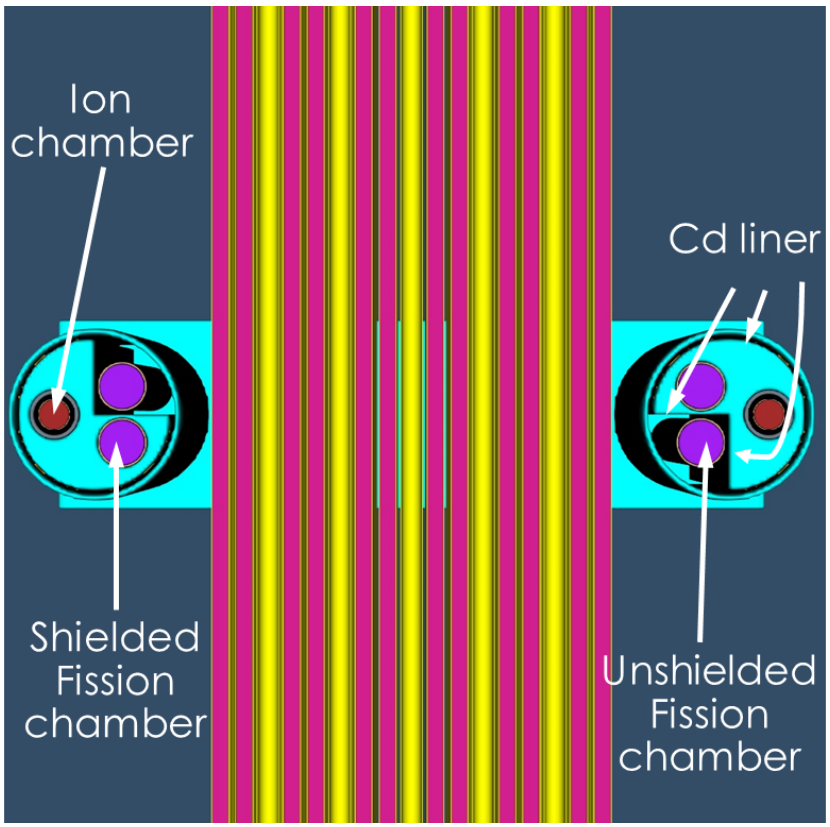

Figure 11. Vertical cross section through the FDET arms with a PWR fuel assembly.

The gamma signals from the two ionization chambers are combined to obtain the overall gamma signal. Simultaneously, the signals from the two unshielded fission chambers are combined to measure the detector response to mostly thermal neutrons. The cadmium shield effectively reduces the thermal neutron flux entering the shielded fission chambers, and the HDPE thermalizes the fast neutrons that manage to penetrate the cadmium lining. In contrast, the signals from the two cadmium-covered fission chambers are combined to detect the response for fast neutrons. To accommodate the varying sizes of the spent AR fuel items, the configuration and dimensions of the FDET were modified accordingly. The modified dimensions of the FDET to fit the spent AR fuel items are summarized in Table 3.

Table 3. Dimensions of the FDET models for simulated spent PWR and AR fuels

Parameter	PWR fuel assembly	Metallic fuel bundle	Type 1 pebbles in canister	Type 2 pebbles in canister	Type 1 prismatic fuel block	Type 2 prismatic fuel block
Fuel width[1] (cm)	21.4	14.198	29.55	29.55	36	35.996
Fuel height[2] (cm)	360	80	167.58	167.58	80	79.299
Detector dimension[3] (cm)	35.61 × 42.7 × 11.45	33.50 × 35.20 × 11.45	77.55 × 79.20 × 11.45	77.55 × 79.20 × 11.45	59.55 × 57.20 × 11.45	59.55 × 57.20 × 11.45
Detector arm length (cm)	23.56	17.80	61.8	61.8	43.8	43.8
Arm gap to assembly (cm)	1.45	1.30	0.85	0.85	1.40	1.40
Fission chamber dimension[4] (cm)	1.3 × 17.78	1.3 × 17.78	1.3 × 61.78	1.3 × 61.78	1.3 × 43.78	1.3 × 43.78
Ionization chamber dimension[4] (cm)	1.3 × 15.30	1.3 × 15.30	1.3 × 59.30	1.3 × 59.30	1.3 × 41.30	1.3 × 41.30

[1]pitch for hexagon shape fuel assembly; [2]only for active height; [3]length × width × height; [4]outer radius × length

The MCNP 6.2 code [19] was used to simulate the detector response with a fixed-source calculation mode with one billion particle histories in each run. Source particles were uniformly sampled within the fuel region. Neutron detection was assessed by analyzing the fission reaction rates within each fission chamber using the F4 tally. An eigenvalue calculation was also conducted using MCNP 6.2 to obtain the subcritical neutron multiplication (M) to correct the neutron count rate because M fission neutrons will be generated for each passive neutron emitted in the fuel [5].

The gamma response in the ionization chamber was calculated using the F2 tally. The gamma results were then converted to dose rates by employing flux-to-dose conversion factors from either the International Commission on Radiological Protection (ICRP) ICRP/23-1973 or the American National Standards Institute/American Nuclear Society (ANSI/ANS) ANSI/ANS-6.1.1-1977 standards. The radiation sources required for the MCNP simulation, including the spent fuel composition, photon and neutron source strength, and energy spectra, were generated using SCALE/ORIGEN code [20]. These radiation sources were generated at cooling times of 1 year and 5 years (both are commonly used measurement times for safeguards verification measurements) after final discharge using 200-group neutron and 999-group photon energy structures.

In addition to measuring neutron and gamma under normal conditions, the FDET was also employed to perform partial defect tests (also referred to as *diversion*) in which a fraction of the fuel was replaced by the depleted uranium (DU). Three sources of uncertainties were considered in these diversion cases, including counting statistic uncertainty, calculation uncertainty, and positioning uncertainty. Measurement uncertainty decreases with longer measurement times because higher total counts lead to improved precision. In this study, measurement times of 1 minute and 10 minutes were considered. Calculation uncertainty was derived from the results of MCNP simulations. Positioning uncertainty was also determined from MCNP calculations, where the fuel item was assumed to touch either one of the two arms of the FDET (instead of being perfectly centered between the two arms).

2.2 PWR FUEL ASSEMBLY

2.2.1 Simulated Count Rates

Performance of an FDET for conducting safeguards measurements for a spent LWR assembly was assessed to serve as a reference point for comparison with spent AR fuels. To accomplish this, a 17×17 PWR fuel assembly with an initial enrichment of 4.2 wt% and a burnup of 50 GWd/MTIHM was modeled for measurement using an FDET. The measurements were simulated in a pool filled with borated water containing 2,000 ppm (a typical concentration) of boron, as illustrated in Figure 12.

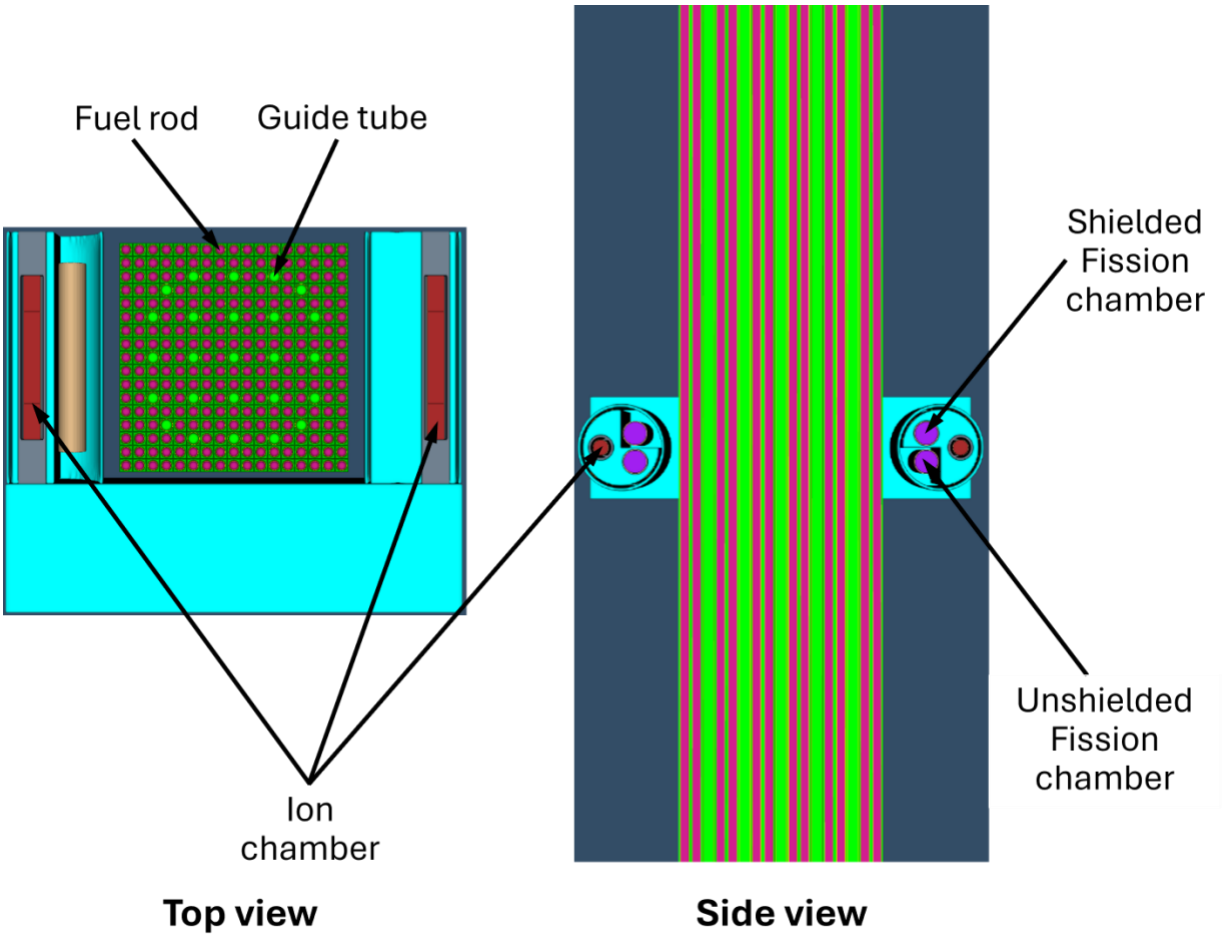

Figure 12. A cross-sectional view of the FDET measurement of a PWR fuel assembly.

The neutron count rates and gamma count rates for the two cooling times are depicted in Figure 13 and Figure 14, respectively. Note that the gamma count rates are referred to as *gamma units* in this report because the FDET electronic unit usually converts the electric current from the two ionization chambers into pulses, and the conversion factor can vary from one FDET unit to another, but the gamma units are proportional to the electric currents collected by the ionization chambers for a given FDET unit. Two neutron count rates were obtained from both unshielded and shielded fission chambers. The results indicated that unshielded (thermal) neutron count rates were lower than the shielded neutron count rates. This difference is attributed to the fact that most of neutrons emitted from the fuel are fast neutrons and they have an average energy of ~2 MeV (see Figure 9). Additionally, boron in the borated water absorbs thermal neutrons, reducing the number of neutrons that reach the unshielded fission chambers and

resulting in a lower response. In contrast, fast neutrons that penetrate the Cd liner on their way to the shielded fission chambers can be thermalized by the high-density polyethylene (HDPE) surrounding the fission chambers, leading to higher count rates in the shielded (fast) fission chambers. Furthermore, both neutron count rates decreased with longer cooling times, which is consistent with the expected reduction in the neutron emissions over time.

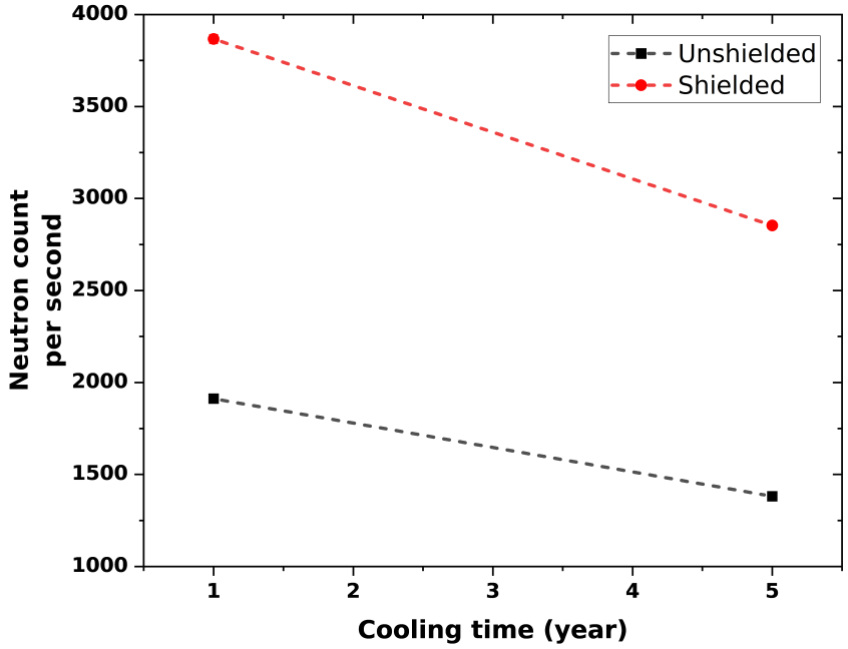

Figure 13. Simulated neutron count rates of the FDET measurement of a spent PWR fuel assembly.

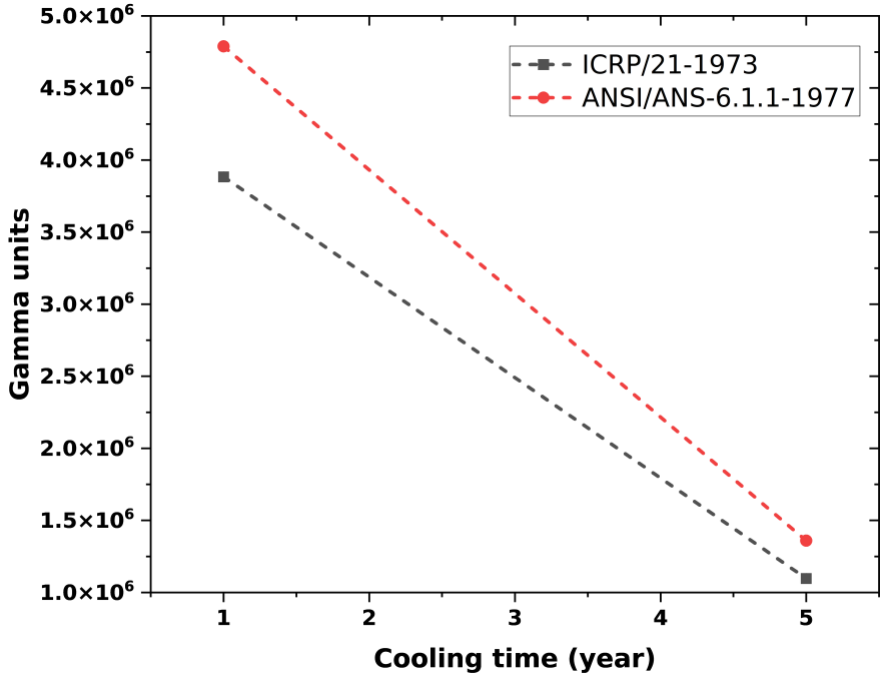

Figure 14. Simulated gamma units of the FDET measurement of a spent PWR fuel assembly.

Gamma results were obtained using two photon flux-to-dose standards: the ANSI/ANS and the ICRP standards. The results indicate that gamma units calculated using ANSI/ANS standards were higher than those obtained using ICRP standards. This difference arises because ANSI/ANS standards employ higher photon flux-to-dose conversion factors, as illustrated in Figure 15. Like the neutron count rates, the gamma responses also showed a decrease with longer cooling times, which can be attributed to the decay of photon-emitting nuclides in the fuel over time.

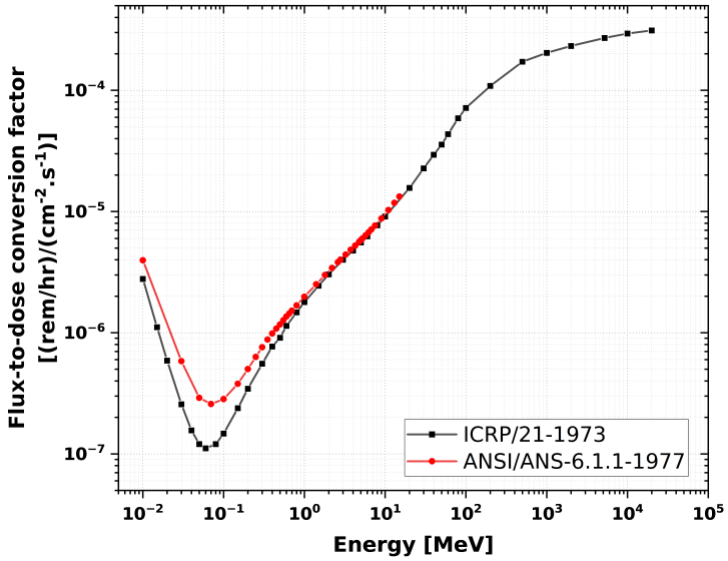

Figure 15. Photon flux-to-dose conversion factors of ICRP and ANSI/ANS standards.

2.2.2 Simulation of Partial Defect Tests

Three scenarios were simulated in the fuel diversion analysis as illustrated in Figure 16. In each scenario, a varying number of spent fuel rods that reached a burnup of 50 GWd/MTIHM were replaced with fresh DU rods that were evenly distributed across the fuel assembly.

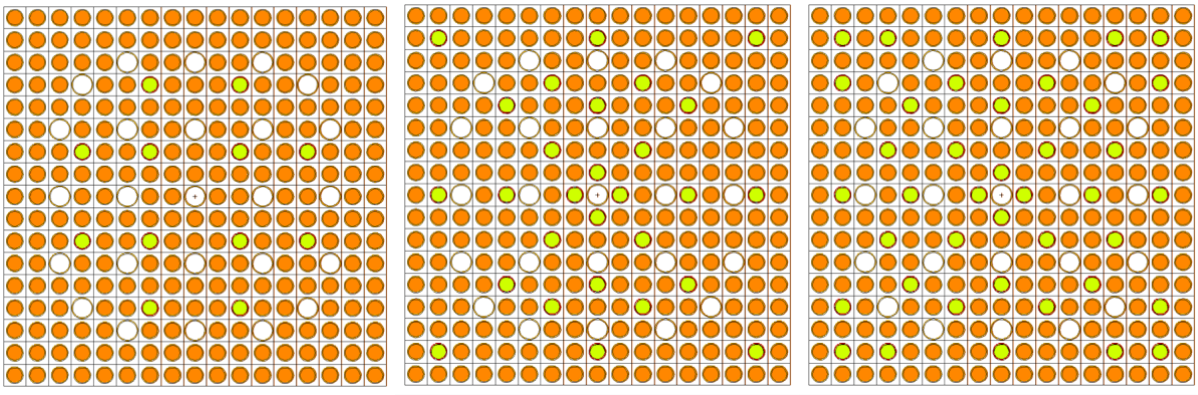

5% diversion *11% diversion* *15% diversion*

Figure 16. Simulated diversion cases for a PWR fuel assembly.
Green rods are filled with DU instead of spent fuel.

Tables 4, 5, and 6 summarize the performance of gamma and neutron detector responses in FDET for detecting these diversions with measurement durations of 1 minute and 10 minutes.

For each diversion scenario, when the relative reduction in responses resulting from fuel diversion exceeds two times the uncertainty (2σ) of the response, a YES is recorded in the box under 2σ, representing 95% confidence; otherwise, a NO is entered. The boxes under 3σ, representing 99.7% confidence, are similarly filled, except that the relative reduction of responses were compared to three times the uncertainty (3σ) of the response. Positioning uncertainty was the largest contributor to the overall uncertainty for each response, with values of 5.35% for gamma, 1.02% for unshielded neutrons, and 6.59% for shielded neutrons. Notably, the positioning uncertainty had a minimal impact on the unshielded neutron response because thermal neutrons are significantly absorbed by borated water in the storage pool, thus reducing the influence of positioning variations.

As indicated in Table 5, the unshielded (thermal) fission chambers were found to be more sensitive to diversions in the PWR assembly than the shielded (fast) chambers and the ionization chambers. The gamma response was found to be insensitive to fuel diversions in a PWR assembly, which is expected because of the self-attenuation effect of the high-density PWR fuel on gamma-rays. The shielded (fast) fission chambers can detect diversions only when larger fractions of pins were replaced.

Table 4. Assessment of the use of gamma units from FDET to detect diversions in PWR fuel assembly

Number of diverted pins	Diverted pins [%]	Gamma count rate reduction [%]	Total sigma [%]	Ability to detect diversion within 1 min measurement time		Ability to detect diversion within 10 min measurement time	
				2σ	3σ	2σ	3σ
12	5	-1.3	5.4	NO	NO	NO	NO
28	11	-5.7	5.4	NO	NO	NO	NO
40	15	-10.0	5.4	NO	NO	NO	NO

Table 5. Assessment of the use of unshielded neutron count rates from FDET to detect diversions in PWR fuel assembly

Number of diverted pins	Diverted pins [%]	Unshielded neutron count rate reduction [%]	Total sigma [%]	Ability to detect diversion within 1 min measurement time		Ability to detect diversion within 10 min measurement time	
				2σ	3σ	2σ	3σ
12	5	-5.2	1.2	YES	YES	YES	YES
28	11	-12.8	1.2	YES	YES	YES	YES
40	15	-18.7	1.2	YES	YES	YES	YES

Table 6. Assessment of the use of shielded neutron count rates from FDET to detect diversions in PWR fuel assembly

Number of diverted pins	Diverted pins [%]	Shielded neutron count rate reduction [%]	Total sigma [%]	Ability to detect diversion within 1 min measurement time		Ability to detect diversion within 10 min measurement time	
				2σ	3σ	2σ	3σ
12	5	-5.5	6.6	NO	NO	NO	NO
28	11	-12.8	6.6	NO	NO	NO	NO
40	15	-18.6	6.6	YES	YES	YES	YES

2.3 METALLIC FUEL BUNDLE

2.3.1 Simulated Count Rates

The first AR spent fuel item simulated using an FDET was a metallic fuel bundle derived from the ABTR-250 design [13]. This bundle was loaded with HALEU fuel enriched to 16.50% and achieved a

final burnup of 150 GWd/MTIHM [14]. As in the spent PWR fuel assembly case, the measurements were simulated in a storage pool environment filled with borated water containing 2,000 ppm of boron, as shown in Figure 17. Other axial regions of the assembly, including the lower reflector, upper plenum, and upper reflector, were also included in the model. The FDET was positioned at the mid-height of the active fuel region, which is the usual FDET measurement location.

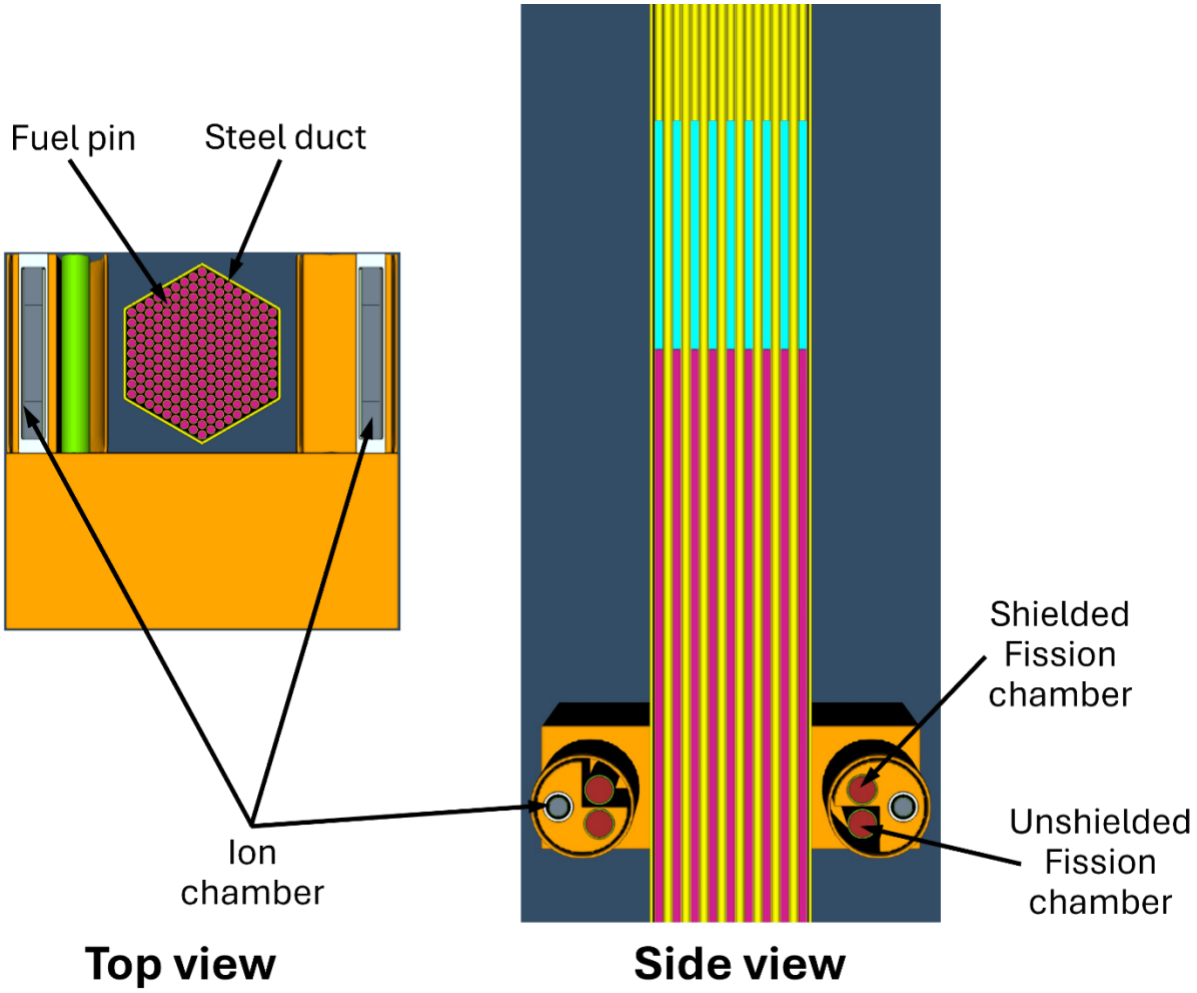

Figure 17. A cross-sectional view of the FDET measurement of a metallic fuel bundle.

Neutron count rates and gamma units for various burnups and two cooling times follow a trend similar to those of the spent PWR fuel assembly, as depicted in Figures 18 and 19, respectively. Specifically, the unshielded (thermal) neutron count rates were lower than those recorded by the shielded fission chambers. This is because a significant portion of the neutrons emitted from the fuel have higher energies. The absorption of thermal neutrons by the boron in the pool water further reduces the count rates of the unshielded fission chambers. Conversely, fast neutrons penetrating the Cd liner surrounding the shielded fission chambers are thermalized by the HDPE surrounding the chambers, resulting in higher shielded neutron counts.

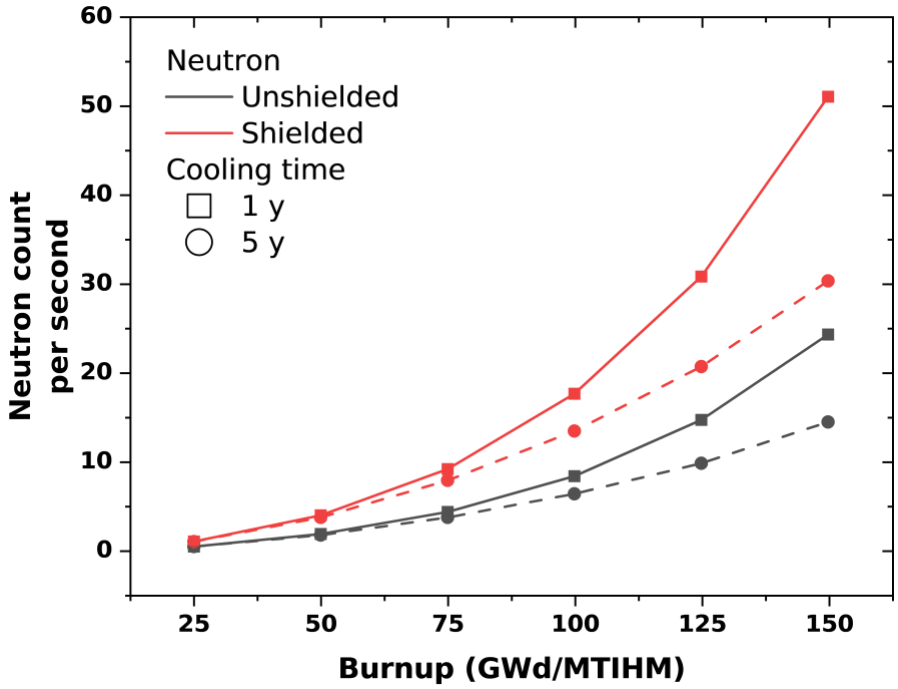

Figure 18. Simulated neutron count rates of the FDET measurement for spent metallic fuel bundle.

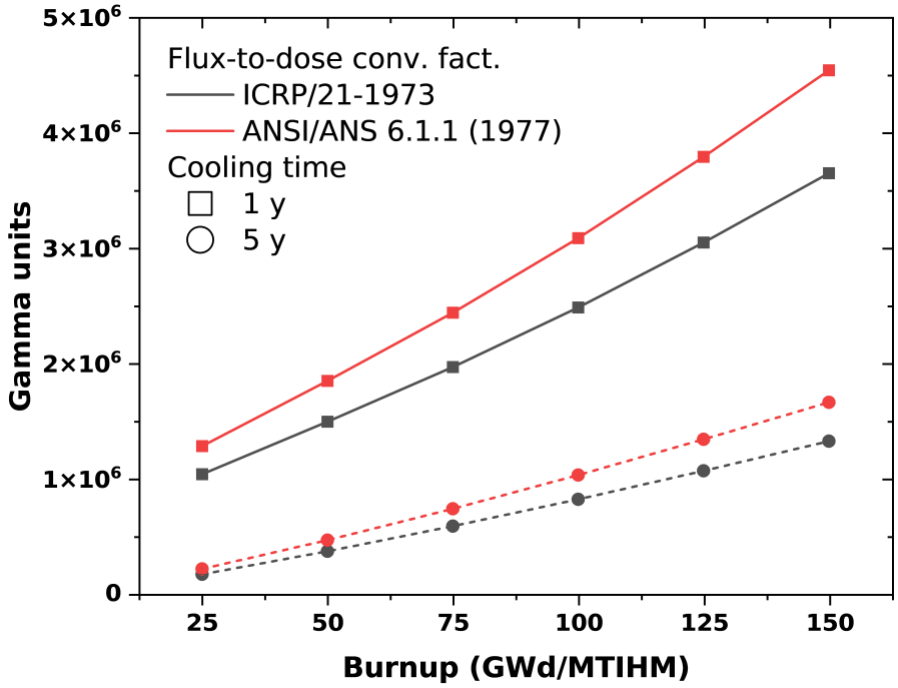

Figure 19. Simulated gamma units of the FDET measurement for a spent metallic fuel bundle.

Gamma measurements in the metallic fuel bundle were analyzed using the ANSI/ANS and ICRP photon flux-to-dose conversion standards. As in the PWR case, gamma units calculated using ANSI/ANS standards were higher than those obtained with ICRP standards because of the higher photon flux-to-dose conversion factors employed by the ANSI/ANS standards.

Both neutron and gamma count rates in the metallic fuel bundle increased with burnup and decreased with cooling times. The increase in count rates with burnup was caused by the greater accumulation of fission products and actinides, which are the primary sources of radiation. In contrast, the decrease in count rates with cooling times was a result of the decay of the neutron and photon-emitting nuclides in the fuel after being discharged from the reactor core.

2.3.2 Simulation of Partial Defect Tests

Three diversion scenarios in the metallic fuel bundle were simulated as illustrated in Figure 20. In each scenario, a varying number of spent fuel pins that reached a burnup of 150 GWd/MTIHM were replaced with fresh DU pins evenly distributed across the fuel assembly.

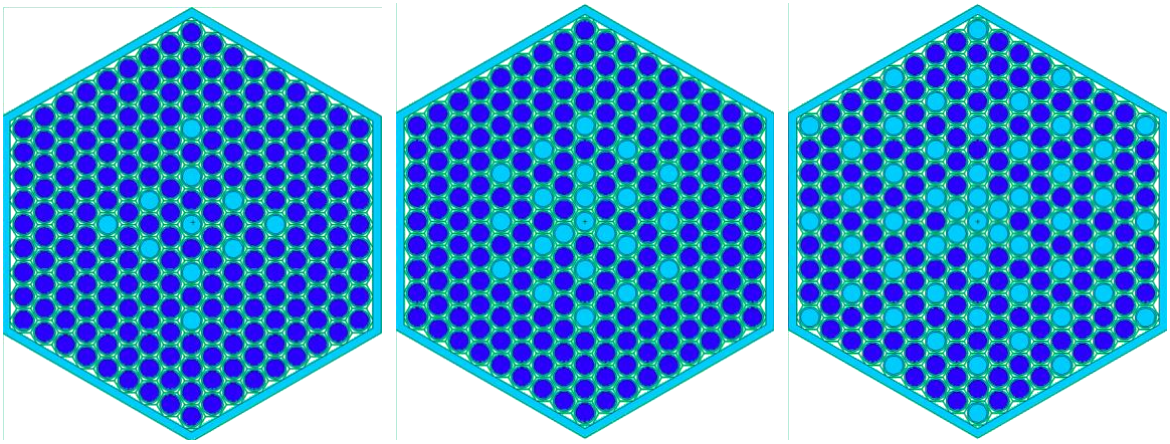

Figure 20. Simulated diversion cases for metallic fuel bundle.
Light blue pins are filled with DU instead of spent fuel.

Tables 7, 8, and 9 summarize the performance of gamma and neutron responses in FDET for detecting these diversions, with measurement taken at durations of 1 minute and 10 minutes.

Table 7. Assessment of the use of gamma units from FDET to detect diversions in metallic fuel bundle

Number of diverted pins	Diverted pins [%]	Gamma count rate reduction [%]	Total sigma [%]	Ability to detect diversion within 1 min measurement time		Ability to detect diversion within 10 min measurement time	
				2σ	3σ	2σ	3σ
11	5	−0.8	2.0	NO	NO	NO	NO
22	10	−1.9	2.0	NO	NO	NO	NO
55	25	−23.4	2.0	YES	YES	YES	YES

Table 8. Assessment of the use of unshielded neutron count rates from FDET to detect diversions in metallic fuel bundle

Number of diverted pins	Diverted pins [%]	Unshielded neutron count rate reduction [%]	*Total sigma [%]	Ability to detect diversion within 1 min measurement time		Ability to detect diversion within 10 min measurement time	
				2σ	3σ	2σ	3σ
11	5	−5.6	7.5 / 6.8	NO	NO	NO	NO
22	10	−11.2	7.5 / 6.8	NO	NO	NO	NO
55	25	−27.0	7.7 / 6.8	YES	YES	YES	YES

*Measurement time 1 min / 10 mins

Table 9. Assessment of the use of shielded neutron count rates from FDET to detect diversions in metallic fuel bundle

Number of diverted pins	Diverted pins [%]	Shielded neutron count rate reduction [%]	*Total sigma [%]	Ability to detect diversion within 1 min measurement time		Ability to detect diversion within 10 min measurement time	
				2σ	3σ	2σ	3σ
11	5	−5.7	2.3 / 0.8	YES	NO	YES	YES
22	10	−11.2	2.4 / 0.9	YES	YES	YES	YES
55	25	−27.6	2.6 / 0.9	YES	YES	YES	YES

*Measurement time 1 min / 10 mins

Unlike the case of the spent PWR fuel assembly, the shielded (fast) neutron was found to be more sensitive in detecting diversion in the metallic fuel bundle compared to the unshielded (thermal) neutron and gamma responses, as summarized in Table 9. This can be attributed to the more compact fuel bundle design and thus tighter coupling between the fuel and the detector in the metallic fuel than the PWR fuel. With longer measurement durations of up to 10 minutes, shielded neutrons can detect diversions in which as little as 5% of the pins were diverted. In contrast, unshielded neutrons and gamma units can detect diversion only when larger fractions of pins were replaced. Positioning uncertainty was again the largest contributor to the overall uncertainty, with values of 2.03% for gamma, 6.71% for unshielded neutrons, and 0.42% for shielded neutrons. The difference in positioning uncertainty between the PWR fuel assembly and the metallic fuel bundle is likely caused by the differences in the fuel designs. For example, the fuel pins in the metallic fuel bundle are smaller and more tightly packed than those in the PWR assembly. Such fuel design differences between a metallic bundle and a PWR assembly cause the neutrons emitted from the fuel to experience different amounts of thermalization (especially between the fuel pins) before being detected, which are likely the main contributor to the different sensitivities to the FDET positioning variations in both the shielded and unshielded neutron detectors.

2.4 TYPE 1 PEBBLES IN A CANISTER

2.4.1 Simulated Count Rates

The next AR spent fuel simulated using the FDET involved Type 1 pebbles contained in a transportation canister. These Type 1 pebbles are modeled to simulate the pebbles discharged from a PBMR-400 [15] reactor. Each pebble contains approximately 15,000 TRISO particles with UO_2 kernel enriched to 9.6 wt% ^{235}U. During reactor operation, these pebbles typically circulate the core an average of six times (or passes) to achieve an average discharged burnup of 90 GWd/MTIHM. The isotopic compositions of the pebbles after each pass through the core were calculated in a previous study [21] and were used as input data in this work.

In this study, approximately 2,000 Type 1 pebbles were randomly packed inside a cylindrical transportation canister using the random sampling feature in Serpent [24]. The canister dimensions were 170.78 cm in height and 29.55 cm in radius, which yielded a packing fraction of 0.55 for the 2,000 pebbles. The canister had a stainless-steel wall with a thickness of 1.6 cm.

To simplify the complex geometry of the TRISO particles and their surrounding graphite matrix, the region containing the TRISO particles and the surrounding graphite matrix within each pebble, with a combined radius of 2.5 cm, was treated as a homogenized mixture. This homogenized region was encapsulated by an outer graphite layer 0.5 cm thick. The simulation model is illustrated in Figure 21, with the FDET positioned at the mid-height of the canister. Unlike previous cases in which the detector and the canister were immersed in borated water, in this case, the detector and canister were surrounded by air because the canister would most likely be stored in an air-filled hot cell.

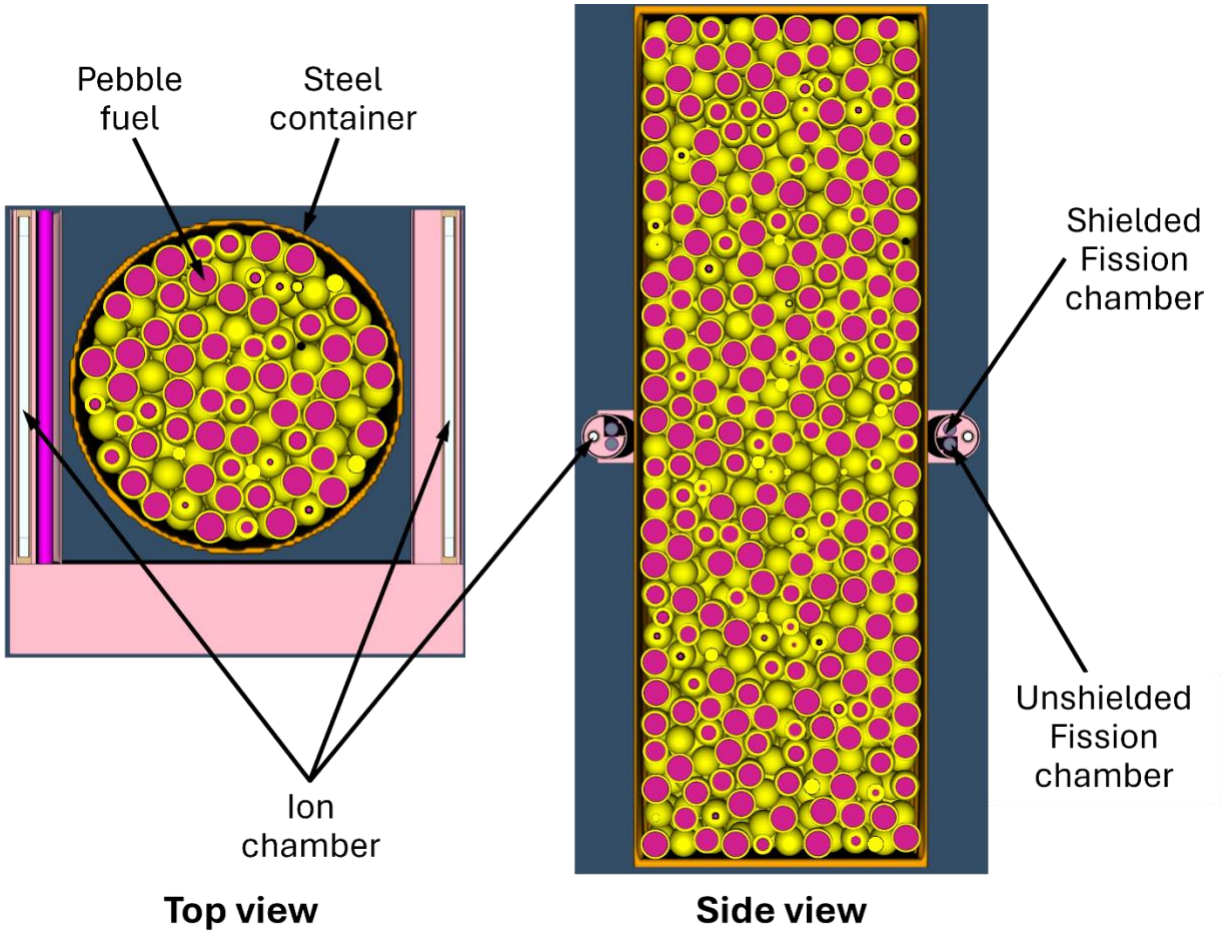

Figure 21. A cross-sectional view of the FDET measurement of Type 1 pebbles in canister.

The neutron count rates and gamma units for various burnups representing each pass and two cooling times are depicted in Figures 22 and 23, respectively.

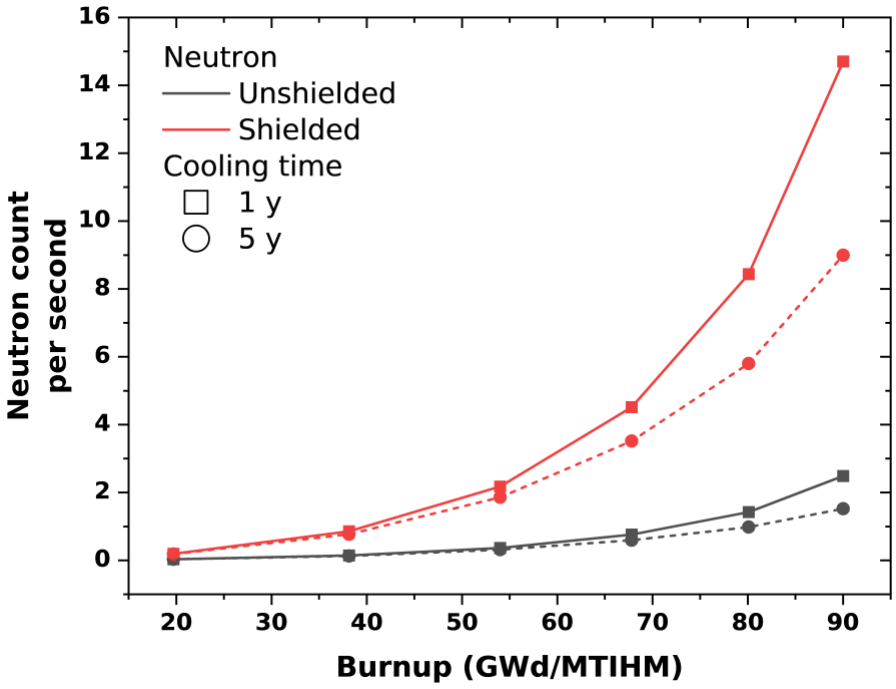

Figure 22. Simulated neutron count rates of the FDET measurement for Type 1 pebbles in canister.

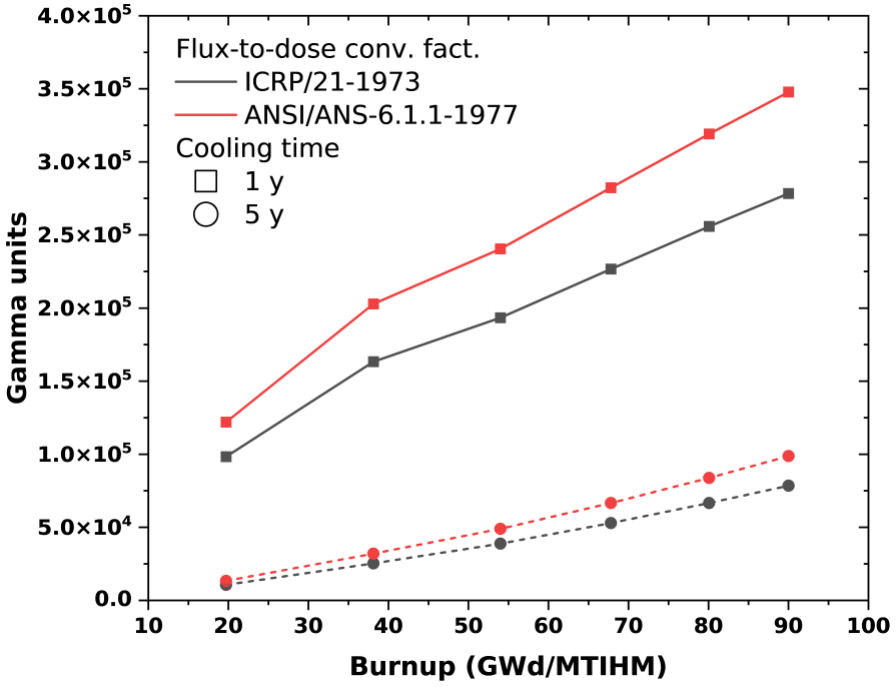

Figure 23. Simulated gamma units of the FDET measurement for Type 1 pebbles in canister.

Although the detector and canister were not immersed in borated water, the neutron response followed a trend similar to that observed in previous cases. Specifically, the shielded neutron count rates were higher than the unshielded neutron count rates. Both neutron count rates increased with burnup; however, the overall count rates remained relatively low, even at the maximum burnup of a Type 1 pebble (90

GWd/MTIHM). This was caused by the much smaller amount of initial uranium loading (and hence irradiated fuel) in the pebbles than in a PWR assembly. Additionally, as expected, longer cooling times led to a decrease in neutron count rates.

Gamma measurements for Type 1 pebbles in canister were also analyzed using the ANSI/ANS and ICRP photon flux-to-dose conversion standards. Consistent with other cases, the gamma units calculated using the ANSI/ANS standards were higher than those obtained with the ICRP standards because of the higher photon flux-to-dose conversion factors employed by the ANSI/ANS standards. Similar to the neutron response, higher burnup resulted in higher gamma units, whereas longer cooling times led to a decrease in the gamma response.

2.4.2 Simulation of Partial Defect Tests

Three diversion scenarios in the canister containing Type 1 pebbles were simulated. In each scenario, a varying number of irradiated fuel pebbles that reached a burnup of 90 GWd/MTIHM were replaced with pebbles containing fresh DU that were randomly distributed within the canister. Tables 10, 11, and 12 summarize the performance of gamma and neutron responses detected by FDET under these scenarios, with measurement taken at 1- and 10-minute durations.

Table 10. Assessment of the use of gamma units from FDET to detect diversions in a canister with Type 1 pebbles

Number of diverted pebbles	Diverted pebbles [%]	Gamma count rate reduction [%]	Total sigma [%]	Ability to detect diversion within 1 min measurement time		Ability to detect diversion within 10 min measurement time	
				2σ	3σ	2σ	3σ
100	5	−4.7	0.2	YES	YES	YES	YES
200	10	−9.1	0.2	YES	YES	YES	YES
500	25	−25.4	0.2	YES	YES	YES	YES

Table 11. Assessment of the use of unshielded neutron count rates from FDET to detect diversions in a canister with Type 1 pebbles

Number of diverted pebbles	Diverted pebbles [%]	Unshielded neutron count rate reduction [%]	*Total sigma [%]	Ability to detect diversion within 1 min measurement time		Ability to detect diversion within 10 min measurement time	
				2σ	3σ	2σ	3σ
100	5	−4.6	8.6 / 2.9	NO	NO	NO	NO
200	10	−8.3	8.8 / 2.9	NO	NO	YES	NO
500	25	−25.4	9.7 / 3.2	YES	NO	YES	YES

*Measurement time 1 min / 10 mins

Table 12. Assessment of the use of shielded neutron count rates from FDET to detect diversions in a canister with Type 1 pebbles

Number of diverted pebbles	Diverted pebbles [%]	Shielded neutron count rate reduction [%]	*Total sigma [%]	Ability to detect diversion within 1 min measurement time		Ability to detect diversion within 10 min measurement time	
				2σ	3σ	2σ	3σ
100	5	−5.0	3.6 / 1.5	NO	NO	YES	YES
200	10	−9.3	3.7 / 1.5	YES	NO	YES	YES
500	25	−26.2	4.1 / 1.6	YES	YES	YES	YES

*Measurement time 1 min / 10 mins

The simulation results indicate that the gamma response from the FDET was more sensitive to fuel diversions in the canister with Type 1 pebbles compared to the neutron responses, as detailed in Table 10, because the pebbles had a lower average fuel density and hence smaller self-attenuation than that of a PWR assembly. However, with longer measurement durations of up to 10 minutes, both unshielded and shielded neutron detectors were able to detect diversions in which 10% of the irradiated pebbles were diverted. The positioning uncertainty emerged as the largest contributor to the overall uncertainty in each response. Specifically, the uncertainty values were 0.12% for gamma and 0.90% for unshielded and shielded neutrons. The positioning uncertainty in this case was lower than that observed in the in-water measurement cases, which can be attributed to the smaller impacts on the neutron and photon particles by air than by water.

2.5 TYPE 2 PEBBLES IN A CANISTER

2.5.1 Simulated Count Rates

The setup for simulating the FDET measurement of Type 2 pebbles, as illustrated in Figure 24, was similar to that used for Type 1 pebbles. Approximately 2,000 Type 2 pebbles were randomly distributed within the transportation canister. Type 2 pebbles are used in the Xe-100 [16], and each pebble contains approximately 19,000 TRISO particles with a UCO kernel enriched to 15.5 wt% in ^{235}U. Like the PBMR-400, these pebbles also circulate through the core an average of six times (i.e., six passes) to achieve an average discharged burnup of ~165 GWd/MTIHM. The isotopic compositions of the pebbles after each pass through the core were calculated in a previous study [22] and were used as input data in this work.

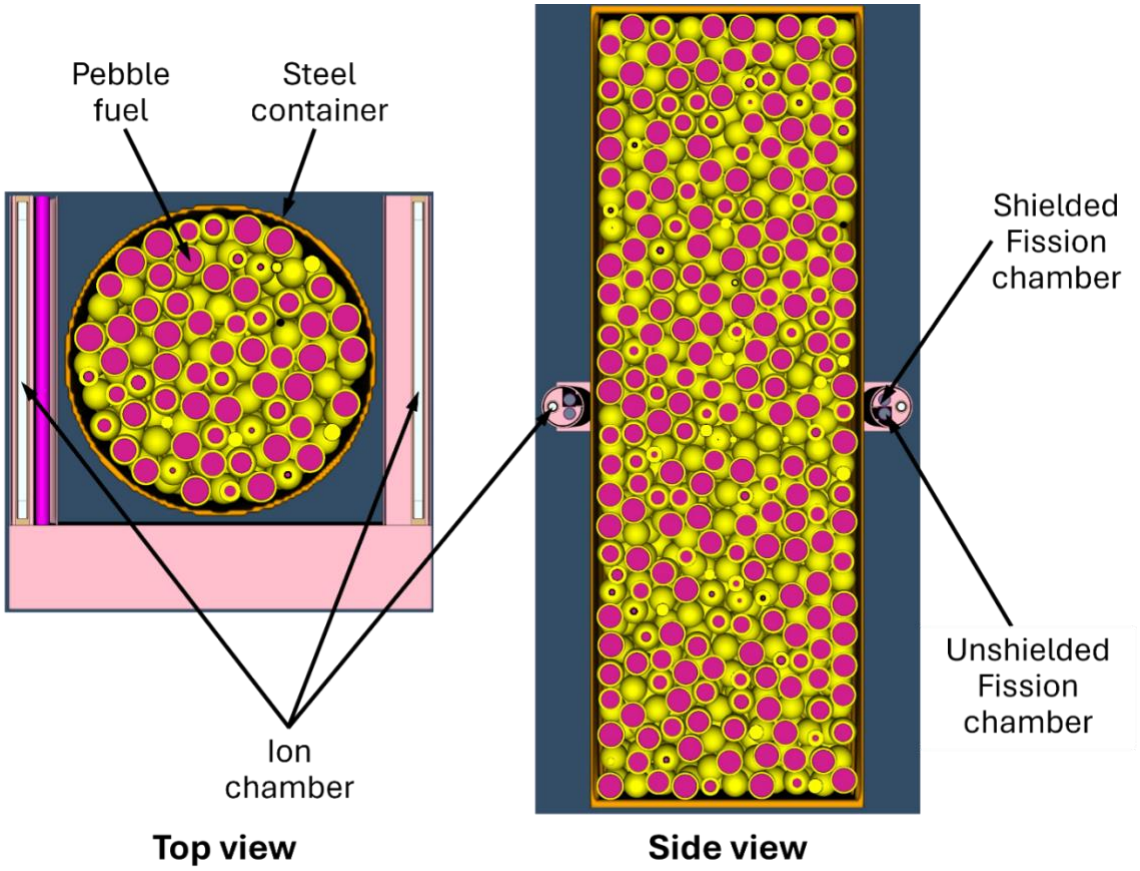

Figure 24. A cross-sectional view of the FDET measurement of Type 2 pebbles in canister.

The neutron count rates and gamma units for various burnups (representing each pass) and two cooling times are depicted in Figures 25 and 26, respectively. The results show a trend similar to those observed in Type 1 pebbles. After the sixth pass, the neutron count rates for Type 2 pebbles were higher than those of Type 1 pebbles because of the greater burnup. The increase of neutron count rates with burnup can be attributed to the accumulation of neutron-emitting nuclides such as ^{242}Cm and ^{244}Cm, which build up with each pass through the core.

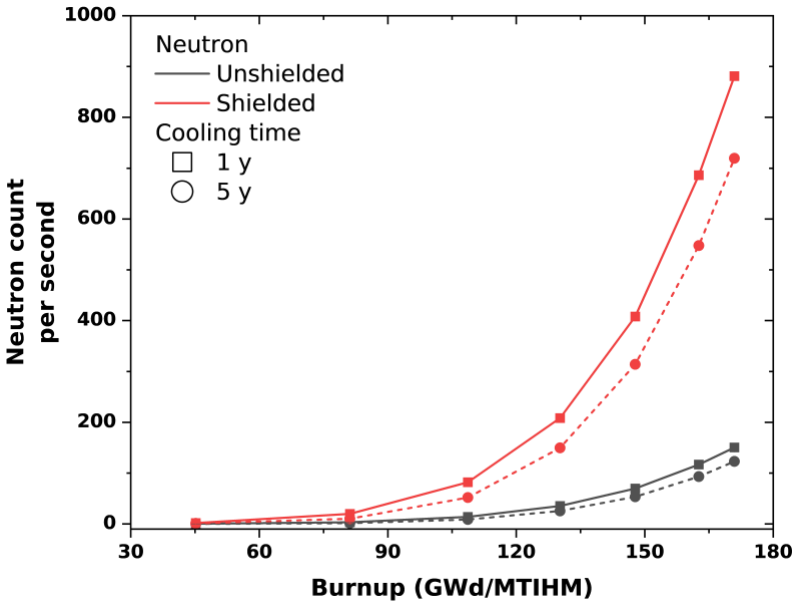

Figure 25. Simulated neutron count rates of the FDET measurement for Type 2 pebbles in canister.

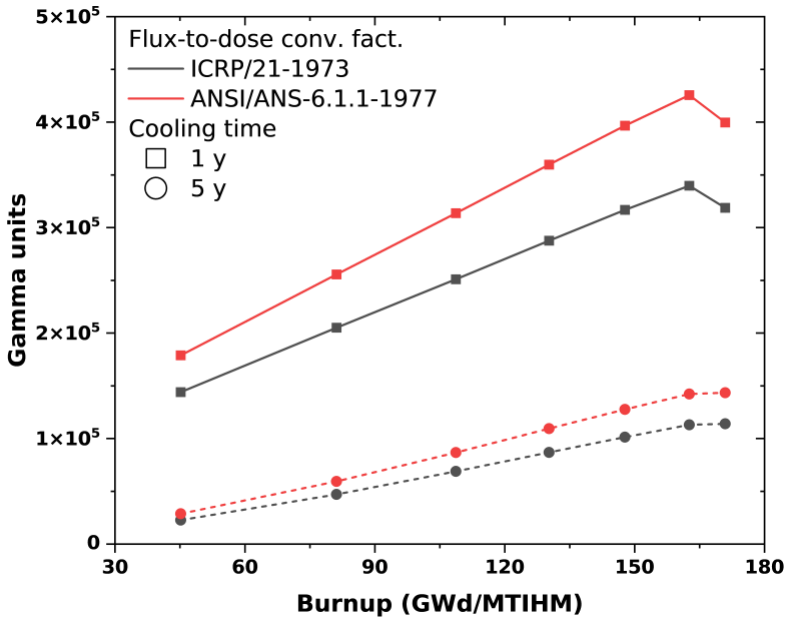

Figure 26. Simulated gamma units of the FDET measurement for Type 2 pebbles in canister.

Additionally, the composition after the seventh pass, corresponding to a burnup of ~171 GWd/MTIHM, was also analyzed. The neutron results increased from the sixth to seventh pass, whereas the gamma units decreased after the sixth pass. The decrease can be attributed to the lower specific power the pebble experienced in the seventh pass than in previous passes due to the diminish of the pebble's remaining fissile material and that the photon emissions at short cooling time are largely dependent on the specific power.

2.5.2 Simulation of Partial Defect Tests

Three diversion scenarios in the canister containing Type 2 pebbles were also simulated. In these scenarios, a varying number of irradiated fuel pebbles, each having achieved a burnup of ~165 GWd/MTIHM, were replaced with fresh DU pebbles that were randomly distributed within the canister. The performance of the gamma and neutron responses in FDET under these conditions is summarized in Tables 13, 14, and 15, with measurements taken at durations of 1 minute and 10 minutes.

In line with the findings from Type 1 pebbles, the gamma response from the FDET proved to be more sensitive in detecting diversions within the canister of Type 2 pebbles compared to neutron responses, as summarized in Table 13. However, unlike analyses using Type 1 pebbles, both unshielded and shielded neutron detectors were capable of detecting diversions in which 5% of the irradiated Type 2 pebbles were removed. This increased detection capability was the result of the neutron source strength of Type 2 pebbles which, at a burnup of ~165 GWd/MTIHM, was approximately 44 times higher than that of Type 1 pebbles at a burnup of 90 GWd/MTIHM. Positioning uncertainty again presented as the largest contributor to overall response uncertainty, with values of 0.15% for gamma, 1.00% for unshielded neutrons, and 0.56% for shielded neutrons. These positioning uncertainty values are consistent with those observed for Type 1 pebbles.

Table 13. Assessment of the use of gamma units from FDET to detect diversions in a canister with Type 2 pebbles

Number of diverted pebbles	Diverted pebbles [%]	Gamma count rate reduction [%]	Total sigma [%]	Ability to detect diversion within 1 min measurement time		Ability to detect diversion within 10 min measurement time	
				2σ	3σ	2σ	3σ
100	5	-4.9	0.2	YES	YES	YES	YES
200	10	-13.8	0.2	YES	YES	YES	YES
500	25	-36.7	0.2	YES	YES	YES	YES

Table 14. Assessment of the use of unshielded neutron count rates from FDET to detect diversions in a canister with Type 2 pebbles

Number of diverted pebbles	Diverted pebbles [%]	Unshielded neutron count rate reduction [%]	*Total sigma [%]	Ability to detect diversion within 1 min measurement time		Ability to detect diversion within 10 min measurement time	
				2σ	3σ	2σ	3σ
100	5	−4.7	1.6 / 1.1	YES	NO	YES	YES
200	10	−13.8	1.7 / 1.2	YES	YES	YES	YES
500	25	−36.5	1.9 / 1.2	YES	YES	YES	YES

*Measurement time 1 min / 10 mins

Table 15. Assessment of the use of shielded neutron count rates from FDET to detect diversions in a canister with Type 2 pebbles

Number of diverted pebbles	Diverted pebbles [%]	Shielded neutron count rate reduction [%]	*Total sigma [%]	Ability to detect diversion within 1 min measurement time		Ability to detect diversion within 10 min measurement time	
				2σ	3σ	2σ	3σ
100	5	−5.2	0.8 / 0.7	YES	YES	YES	YES
200	10	−14.1	0.8 / 0.7	YES	YES	YES	YES
500	25	−37.2	0.9 / 0.7	YES	YES	YES	YES

*Measurement time 1 min / 10 mins

2.6 TYPE 1 PRISMATIC FUEL BLOCK

2.6.1 Simulated Count Rates

The first prismatic fuel block configuration simulated using the FDET was based on a USNC design [17]. Each prismatic block contains 54 fuel pins (i.e., a stack of cylindrical SiC compacts), with each compact containing TRISO particles at a 60% packing fraction. The TRISO particles feature UCO fuel kernels enriched to 19.75 wt% in ^{235}U. The fuel is designed to achieve a burnup of 100 GWd/MTIHM.

To simplify the complex geometry of the fuel compacts, the region containing the TRISO particles and the surrounding SiC matrix, with a combined radius of 0.92 cm, was treated as a homogenized mixture. This homogenized region was surrounded by a 0.23 cm thick outer SiC layer. The simulation model illustrated in Figure 27 shows the FDET positioned at the mid-height of the fuel block. In this scenario, the detector and the fuel block were surrounded by air instead of water because this type of fuel block would most be likely stored in a hot cell.

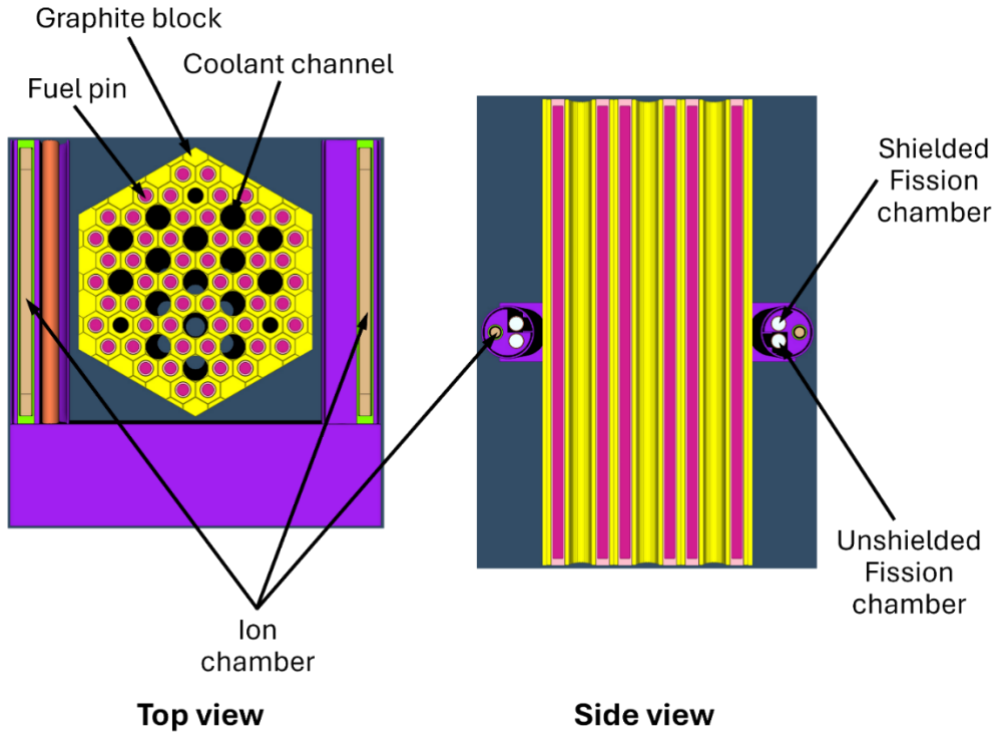

Figure 27. A cross-sectional view of the FDET measurement of a Type 1 prismatic fuel block.

Because of the lack of detailed design information for a USNC core configuration, a depletion calculation was performed using the high-temperature engineering test reactor (HTTR) core design [23] to obtain the isotopic compositions for the irradiated Type 1 fuel block. In the depletion calculation, the Type 1 fuel blocks were inserted into the HTTR core, which was simulated at a power level of 45 MWth/MTIHM using the Serpent Monte Carlo code [24] to utilize the existing Serpent model for HTTR [23].

The complete HTTR core configuration consists of 30 columns dedicated to fuel blocks, 16 columns for control rods, 3 columns for irradiation testing, and 12 columns serving as replaceable graphite reflectors. The HTTR core is surrounded by a permanent graphite reflector which enhances neutron economy and contributes to the overall stability of the core. Each prismatic fuel column within the core houses five fuel blocks.

The neutron count rates and gamma units for various burnups (100, 130, and 170 GWd/MTIHM) and two cooling times are depicted in Figures 28 and 29, respectively. The results for neutron and gamma measurements follow trends consistent with those observed in previous simulated cases. Specifically, shielded neutron count rates were higher than unshielded rates. As the burnup increased, both neutron and gamma count rates rose, reflecting the greater accumulation of fission products and neutron-emitting actinides at higher burnup levels. Conversely, longer cooling times led to a decrease in both neutron and gamma responses, consistent with the decay of radioactive sources over time.

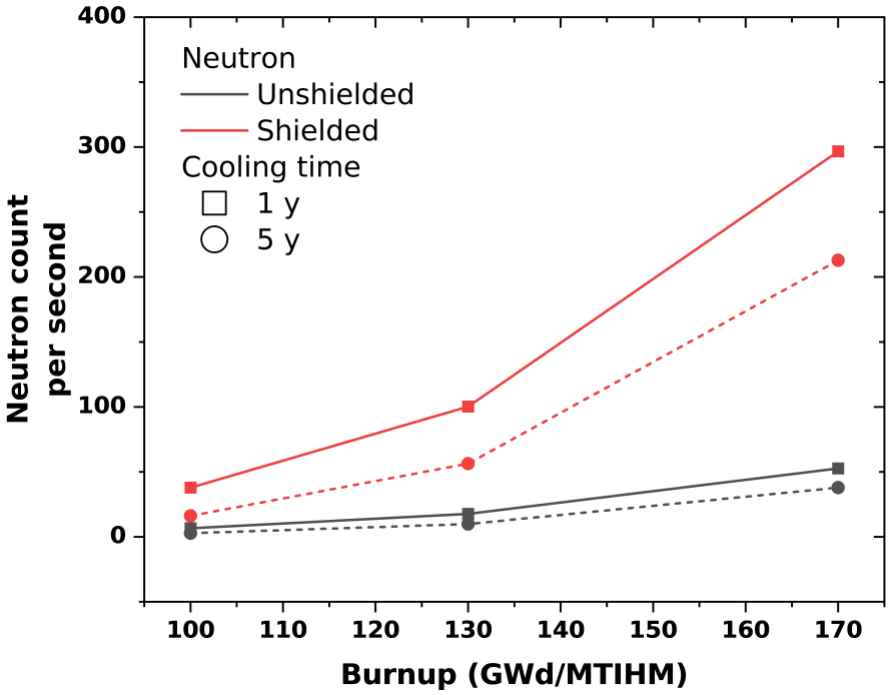

Figure 28. Simulated neutron count rates of the FDET measurement for a Type 1 prismatic fuel block.

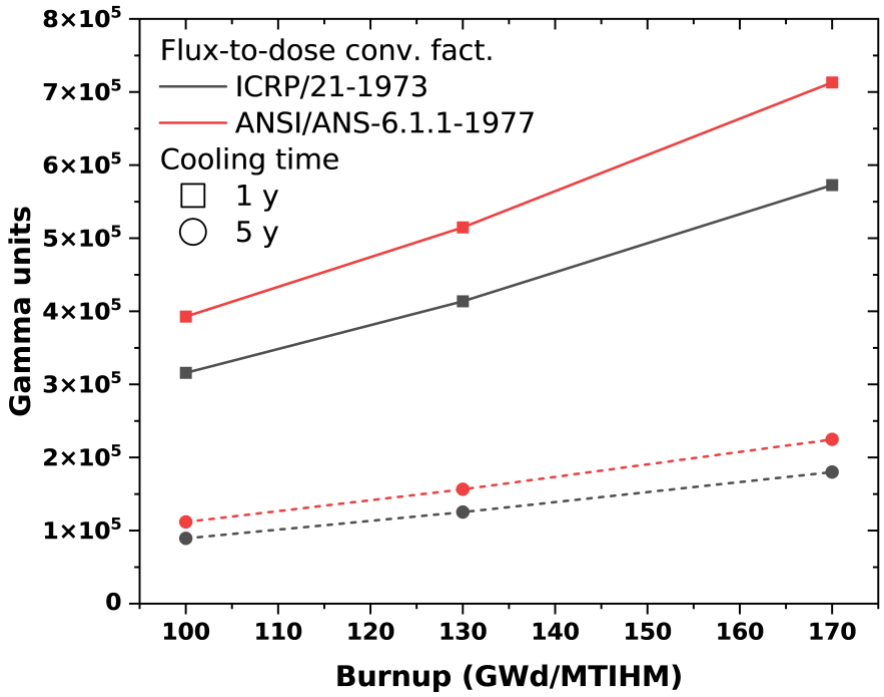

Figure 29. Simulated gamma units of the FDET measurement for a Type 1 prismatic fuel block.

2.6.2 Simulation of Partial Defect Tests

To evaluate the FDET's capability in detecting partial defects in Type 1 prismatic fuel block, three diversion scenarios were simulated, as shown in Figure 30. In each scenario, a varying number of irradiated fuel pins, each with a burnup of approximately 100 GWd/MTIHM, were replaced with fresh depleted uranium (DU) pins. The performance of the gamma and neutron responses in FDET under these scenarios is summarized in Tables 16, 17, and 18, with measurements taken at durations of 1 minute and 10 minutes.

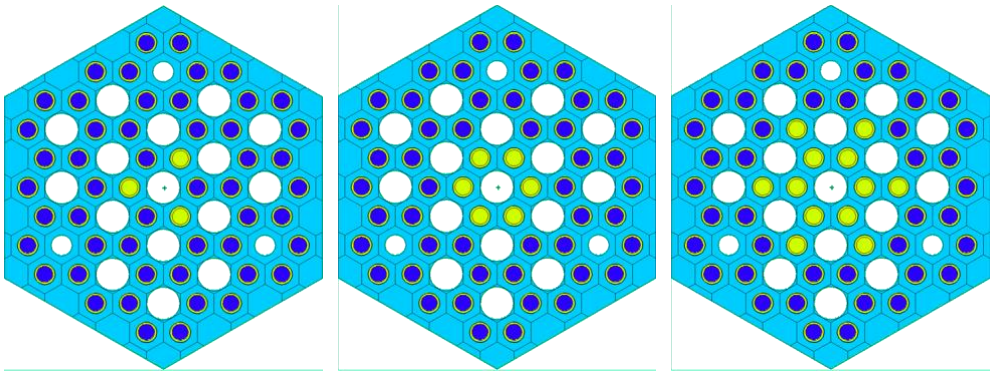

Figure 30. Simulated diversion cases for Type 1 prismatic fuel block.
Green pins are filled with DU instead of spent fuel.

In line with the findings from pebbles, the gamma response from the FDET proved to be more sensitive in detecting diversions within the Type 1 prismatic fuel block compared to neutron responses, as summarized in Table 16. Both unshielded and shielded neutron detectors were capable of detecting diversions in which at least 10% of the irradiated pebbles were diverted. However, the gamma response

provided a clearer indication of these diversions. As in previous tests, positioning uncertainty again presented as the largest contributor to overall response uncertainty, with values of 0.27% for gamma, 1.66% for unshielded neutrons, and 1.23% for shielded neutrons. It is noteworthy that the positioning uncertainty for both unshielded and shielded neutrons is within a similar range, unlike previous cases involving pebble fuels. This similarity is attributed to the higher graphite content in the fuel block than other fuel types, which leads to an over-moderation of the neutrons.

Table 16. Assessment of the use of gamma units from FDET to detect diversions in a canister with Type 1 prismatic fuel block

Number of diverted pins	Diverted pins [%]	Gamma count rate reduction [%]	Total sigma [%]	Ability to detect diversion within 1 min measurement time		Ability to detect diversion within 10 min measurement time	
				2σ	3σ	2σ	3σ
3	6	−2.9	0.3	YES	YES	YES	YES
6	11	−6.0	0.3	YES	YES	YES	YES
12	22	−13.2	0.3	YES	YES	YES	YES

Table 17. Assessment of the use of unshielded neutron count rates from FDET to detect diversions in a canister with Type 1 prismatic fuel block

Number of diverted pins	Diverted pins [%]	Unshielded neutron count rate reduction [%]	*Total sigma [%]	Ability to detect diversion within 1 min measurement time		Ability to detect diversion within 10 min measurement time	
				2σ	3σ	2σ	3σ
3	6	−6.2	5.5 / 2.4	NO	NO	YES	NO
6	11	−12.5	5.7 / 2.4	YES	NO	YES	YES
12	22	−24.4	6.1 / 2.5	YES	YES	YES	YES

*Measurement time 1 min / 10 mins

Table 18. Assessment of the use of shielded neutron count rates from FDET to detect diversions in a canister with Type 1 prismatic fuel blocks

Number of diverted pins	Diverted pins [%]	Shielded neutron count rate reduction [%]	*Total sigma [%]	Ability to detect diversion within 1 min measurement time		Ability to detect diversion within 10 min measurement time	
				2σ	3σ	2σ	3σ
3	6	−6.4	2.5 / 1.4	YES	NO	YES	YES
6	11	−12.4	2.5 / 1.4	YES	YES	YES	YES
12	22	−24.8	2.6 / 1.4	YES	YES	YES	YES

*Measurement time 1 min / 10 mins

2.7 TYPE 2 PRISMATIC FUEL BLOCK

2.7.1 Simulated Count Rates

The second prismatic fuel block configuration simulated using the FDET was intended to represent the BWXT BANR design [25]. However, because publicly available information is limited, it was assumed that the fuel block design resembled the General Atomics prismatic fuel block configuration [18]. Each block consists of 216 fuel pins (i.e., a stack of cylindrical graphite compacts) containing TRISO particles with a packing fraction of 40%. These TRISO particles utilize UCO fuel kernels enriched to 19.75 wt%. Unlike the Type 1 prismatic fuel block, these TRISO particles are embedded in graphite matrix instead of SiC matrix. The fuel block is assumed to achieve a burnup of 170 GWd/MTIHM.

To manage the complexity of the fuel compacts' geometry, the region containing the TRISO particles and the surrounding graphite matrix—together with a combined radius of 0.615 cm—was treated as a homogenized mixture in the simulation. This homogenized region was encased in a 0.085 cm thick outer graphite layer. Figure 31 illustrates the simulation model, with the FDET located at the mid-height of the fuel block. As with the Type 1 prismatic fuel block, the detector and the fuel block were surrounded by air.

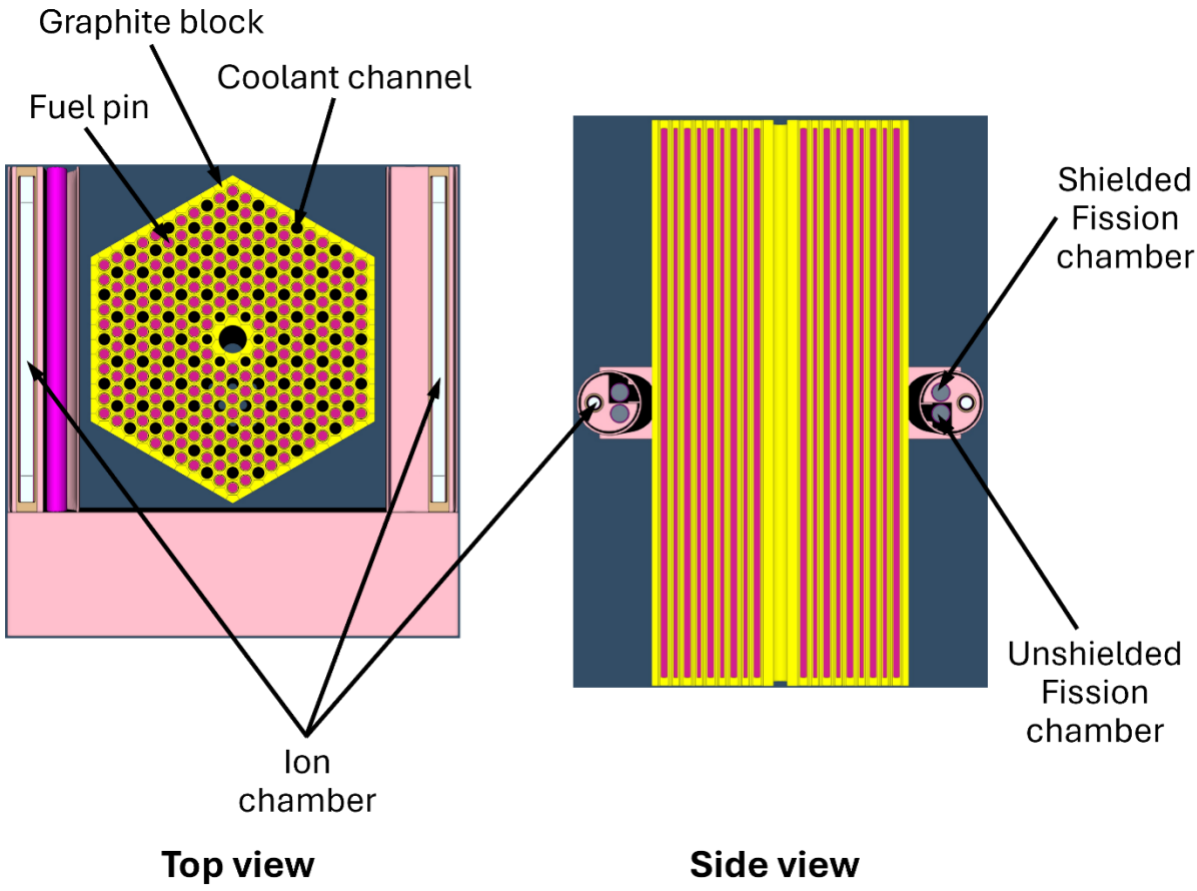

Figure 31. A cross-sectional view of the FDET measurement of Type 2 prismatic fuel block.

As with the previous fuel block case, a depletion calculation was conducted using the Serpent Monte Carlo code [24] to determine the radiation source terms. The design of the Type 2 fuel block was also incorporated into the HTTR core design and depleted at a power level of 50 MWth/MTIHM. This approach was adopted as a substitute because detailed information on the specific core configuration for the BANR design was unavailable.

Figures 32 and 33 illustrate the neutron count rates and gamma units for different burnup levels (100, 130, and 170 GWd/MTIHM) and two cooling periods. The observed trends in neutron and gamma measurements align with those seen in previous simulations involving pebbles and the Type 1 fuel block. Shielded neutron count rates were higher than the unshielded ones. As burnup levels increased, both neutron and gamma count rates also rose, indicating a greater accumulation of fission products and neutron-emitting nuclides at higher burnups. In contrast, longer cooling times resulted in a decline in both neutron and gamma responses, reflecting the natural decay of radioactive materials over time.

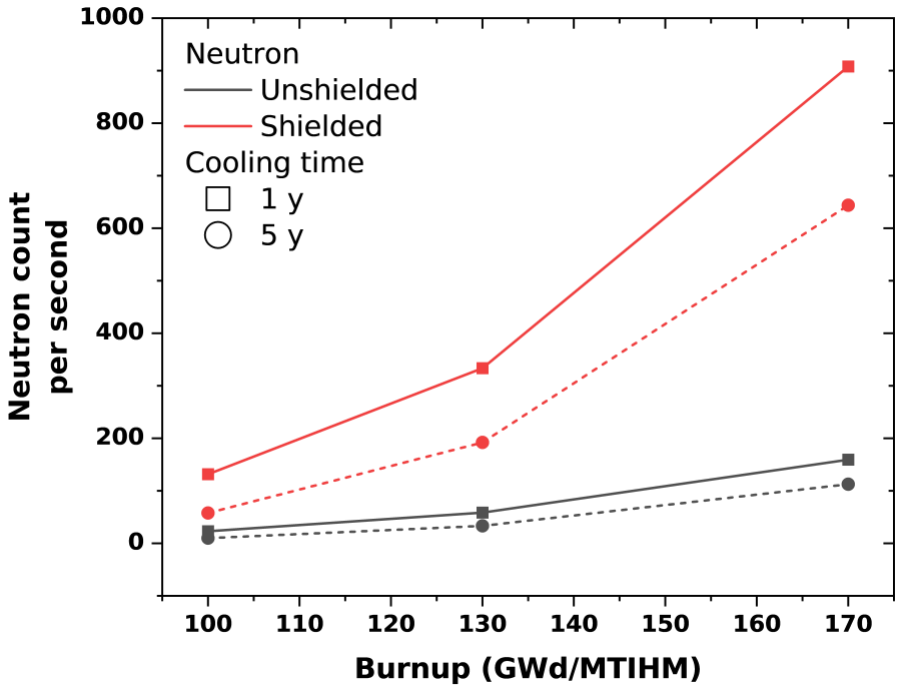

Figure 32. Simulated neutron count rates of the FDET measurement for a Type 2 prismatic fuel block.

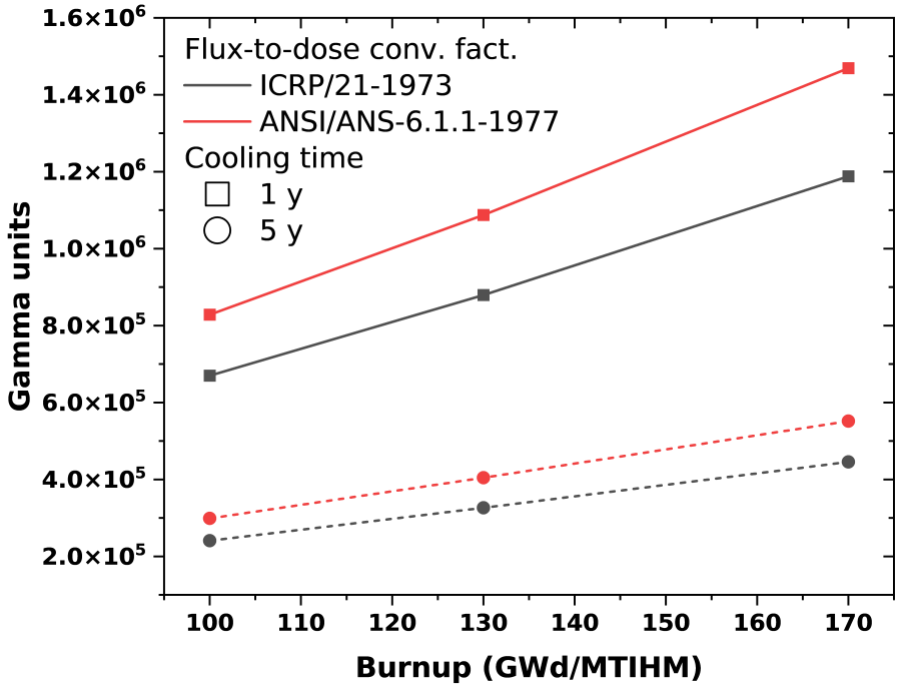

Figure 33. Simulated gamma units of the FDET measurement for a Type 2 prismatic fuel block.

2.7.2 Simulation of Partial Defect Tests

To assess the FDET's effectiveness in detecting partial defects within the Type 2 prismatic fuel block, three diversion scenarios were simulated as shown in Figure 34. In each scenario, a specific number of irradiated fuel pins—each with a burnup of approximately 100 GWd/MTIHM—were substituted with fresh DU pins. The performance of the gamma and neutron responses in the FDET under these conditions is detailed in Tables 19, 20, and 21, with measurements recorded after 1 minute and 10 minutes.

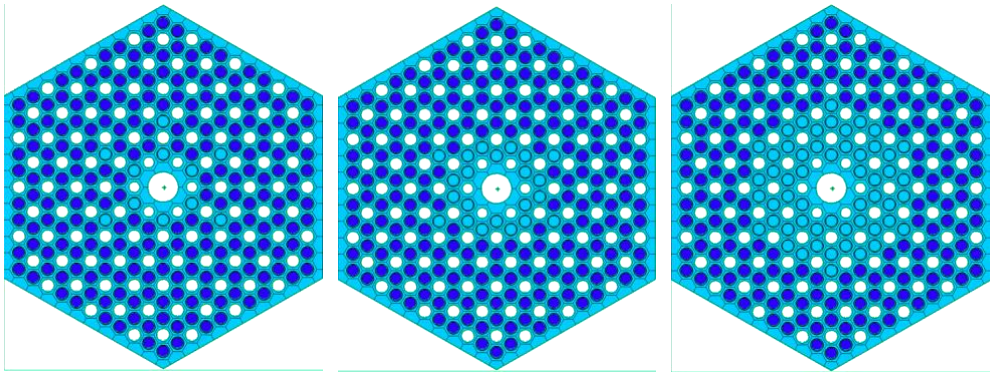

Figure 34. Simulated diversion cases for Type 2 prismatic fuel block.
Light blue pins are filled with DU instead of spent fuel.

Consistent with findings from the Type 1 fuel block, the gamma response of the FDET demonstrated greater sensitivity to diversions within the Type 2 prismatic fuel block compared to the neutron responses, as shown Table 19. Both shielded and unshielded neutron detectors were able to detect diversions in which 10% or more of the irradiated fuel pins were diverted. However, the gamma response provided a more distinct indication of these diversions. As observed in previous cases, the uncertainty in detector positioning emerged as the most significant source of overall response uncertainty, with values of 0.31% for gamma measurements, 1.37% for unshielded neutrons, and 1.54% for shielded neutrons.

Table 19. Assessment of the use of gamma units from FDET to detect diversions in a canister with Type 2 prismatic fuel block

Number of diverted pins	Diverted pins [%]	Gamma count rate reduction [%]	Total sigma [%]	Ability to detect diversion within 1 min measurement time		Ability to detect diversion within 10 min measurement time	
				2σ	3σ	2σ	3σ
11	5	−2.7	0.3	YES	YES	YES	YES
22	10	−5.3	0.3	YES	YES	YES	YES
55	25	−14.7	0.3	YES	YES	YES	YES

Table 20. Assessment of the use of unshielded neutron count rates from FDET to detect diversions in a canister with Type 2 prismatic fuel block

Number of diverted pins	Diverted pins [%]	Unshielded neutron count rate reduction [%]	*Total sigma [%]	Ability to detect diversion within 1 min measurement time		Ability to detect diversion within 10 min measurement time	
				2σ	3σ	2σ	3σ
11	5	−5.6	3.1 / 1.7	NO	NO	YES	YES
22	10	−11.5	3.2 / 1.7	YES	YES	YES	YES
55	25	−27.8	3.5 / 1.7	YES	YES	YES	YES

*Measurement time 1 min / 10 mins

Table 21. Assessment of the use of shielded neutron count rates from FDET to detect diversions in a canister with Type 2 prismatic fuel blocks

Number of diverted pins	Diverted pins [%]	Shielded neutron count rate reduction [%]	*Total sigma [%]	Ability to detect diversion within 1 min measurement time		Ability to detect diversion within 10 min measurement time	
				2σ	3σ	2σ	3σ
11	5	−5.8	1.9 / 1.6	YES	NO	YES	YES
22	10	−11.8	2.0 / 1.6	YES	YES	YES	YES
55	25	−28.4	2.0 / 1.6	YES	YES	YES	YES

*Measurement time 1 min / 10 mins

2.8 IMPACT OF HAVING A NEIGHBORING FUEL ITEM

Because the TRISO-based spent AR fuel items (used in five of the 10 ARDP designs, as shown in Table 1) are most likely stored in an air-filled hot cell instead of a water-filled pool, the impacts of a neighboring fuel item on a spent fuel measurement are expected to be different for the TRISO-based spent AR fuel items than a PWR assembly due to the significantly different radiation shielding characteristics of the air than those of the water. Some simple simulations of the FDET measurements with and without a neighboring spent fuel item were performed in this study. The models used in these analyses considered the measured fuel item placed at the center of the concrete room with a wall thickness of 1 m. The neighboring fuel item was located at the distance of 3 feet or 9 feet in each case from the outer surface of the measured fuel item. The simulation model is illustrated in Figure 35, and the results are summarized in Table 22.

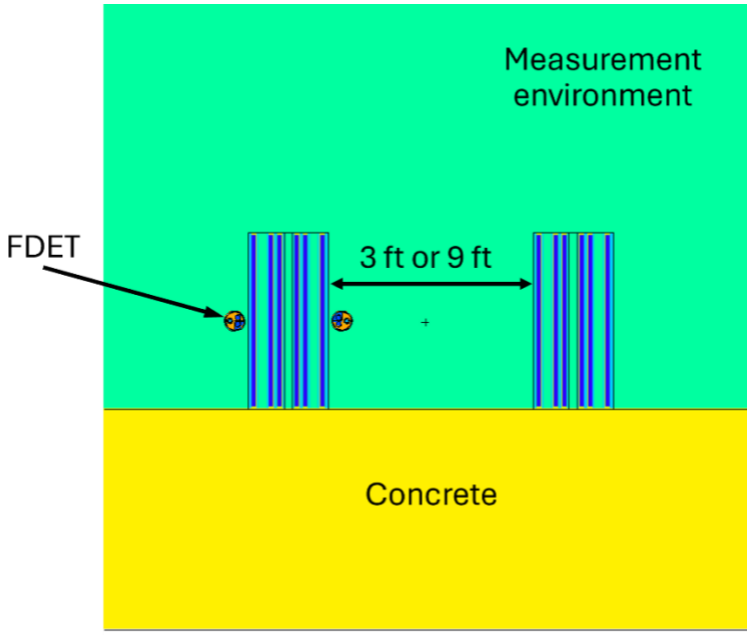

Figure 35. MCNP model considering neighboring fuel item on FDET measurement.

The results show that for in-air FDET measurement the gamma count rate for the pebble canister increased by about 15% when there is a neighbor canister 3 feet away. Similarly, the count rate increased for unshielded and shielded neutrons increased by about 17% and 20%, respectively. The rate changes were more prominent for the pebbles in the container than for the prismatic fuel blocks. However, the impact of neighboring fuel item decreased when the distance between the two fuel items increased. Conversely, the impacts of neighboring fuel item were negligible when the FDET measurements were performed in borated water. Unlike in air, gamma radiation is attenuated, and neutrons are absorbed by borated water, reducing the effect of neighboring fuel items on the measurements. These results show that adequate separation (and hence space) is needed to suppress the interference of the neighboring fuel items on the FDET measurements in air, which might be challenging when there are hundreds to thousands of spent fuel items are stored in a given space.

Table 22. Relative change of the FDET gamma units and neutron count rates due to neighboring fuel element.

Spent fuel element	Measurement environment	Gamma count rate change [%]		Unshielded neutron count rate change [%]		Shielded neutron count rate change [%]	
		3 ft	9 ft	3 ft	9 ft	3 ft	9 ft
PWR 17x17	Borated water	0.12	0.05	0.36	0.20	0.36	0.20
Metallic fuel	Borated water	0.10	0.03	0.05	0.05	0.34	0.34
Type 1 pebbles in container	Air	15.18	2.69	16.79	4.79	19.76	4.47
Type 2 pebbles in container	Air	15.29	2.79	16.36	4.66	18.97	4.08
Type 1 prismatic fuel block	Air	7.21	1.05	8.02	1.34	9.73	1.50
Type 2 prismatic fuel block	Air	6.82	0.94	8.37	1.58	9.74	1.44

2.9 SUMMARY OF FORK DETECTOR RESULTS

Figures 36 and 37 present a comparative analysis of the unshielded and shielded neutron count rates of FDET as a function of burnup between the spent PWR fuel assembly and spent AR fuel items considering cooling periods of 1 year and 5 years. The data reveal that the neutron count rates from the spent PWR fuel assembly at the discharge burnup of 50 GWd/MTIHM are significantly higher than those observed for any spent AR fuel items at their respective discharge burnups, even though these AR fuel items typically had significantly higher burnups.

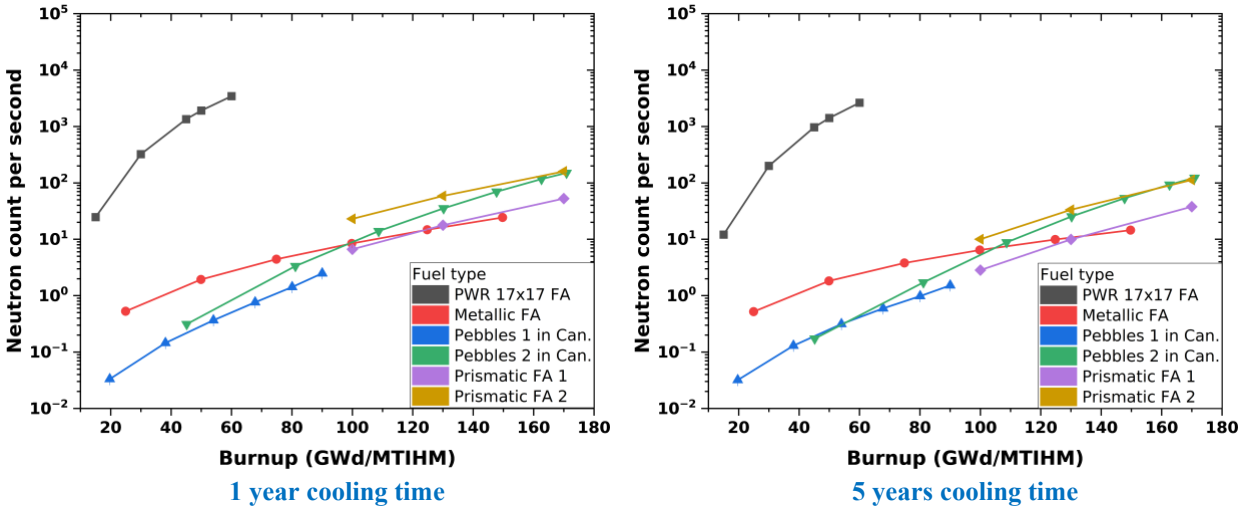

Figure 36. Summary of the unshielded neutron count rates of an FDET.

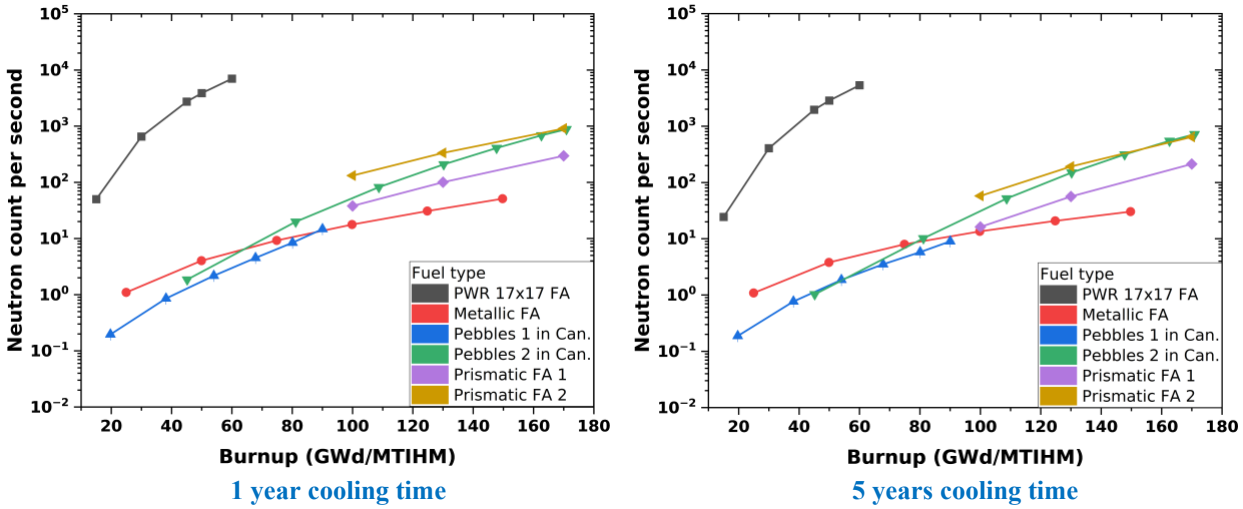

Figure 37. Summary of the shielded neutron count rates of an FDET.

As discussed in Section 1.4, this observed difference, can be attributed to the inherently lower neutron radiation source intensities in the AR fuel items. The reduced intensity is primarily a consequence of the design characteristics of AR fuel types, which generally contain less initial uranium and hence less irradiated fuel materials in them compared to a typical PWR fuel assembly. As a result, even though AR fuel achieve higher burnup, the total neutron emission in these items remains lower. The primary contributors to the neutron source in cooled discharged fuel assemblies are spontaneous neutron emissions, which predominantly arise from specific actinides, including ^{242}Cm, ^{244}Cm, and ^{240}Pu.

Because of the inherently lower neutron count rates of spent AR fuel items, particularly at lower burnup levels, achieving a desired counting precision in measurement requires significantly longer measurement times. For instance, in the specific case of Type 1 pebbles stored in a canister with a burnup of 19.71 GWd/MTIHM, it is estimated that a measurement time of approximately 36.39 hours is necessary to achieve a counting uncertainty of 1%. This longer measurement duration may pose a challenge to accurately performing safeguards measurement for AR fuel items using neutron detection in FDET, particularly for scenarios in which an inspector must measure a large number of AR fuel items during an inspection.

Similar observations can be made for the FDET gamma signals for these spent AR fuel items. As shown in Figure 38, when comparing the gamma units of the spent PWR fuel assembly and the spent AR fuel items (results based on the ANSI/ANS standards), the gamma units from the spent PWR fuel assembly at a discharge burnup of 50 GWd/MTIHM are consistently higher than those observed for any spent AR fuel items at their respective discharge burnups. Similarly, the lower gamma signals can be attributed to the lower mass and volume of irradiated fuel in the AR fuel items compared to that seen in the PWR fuel assembly. However, because the magnitudes of the gamma units are large in all cases, a short measurement time is sufficient to obtain satisfactory counting statistics for the spent AR fuel items.

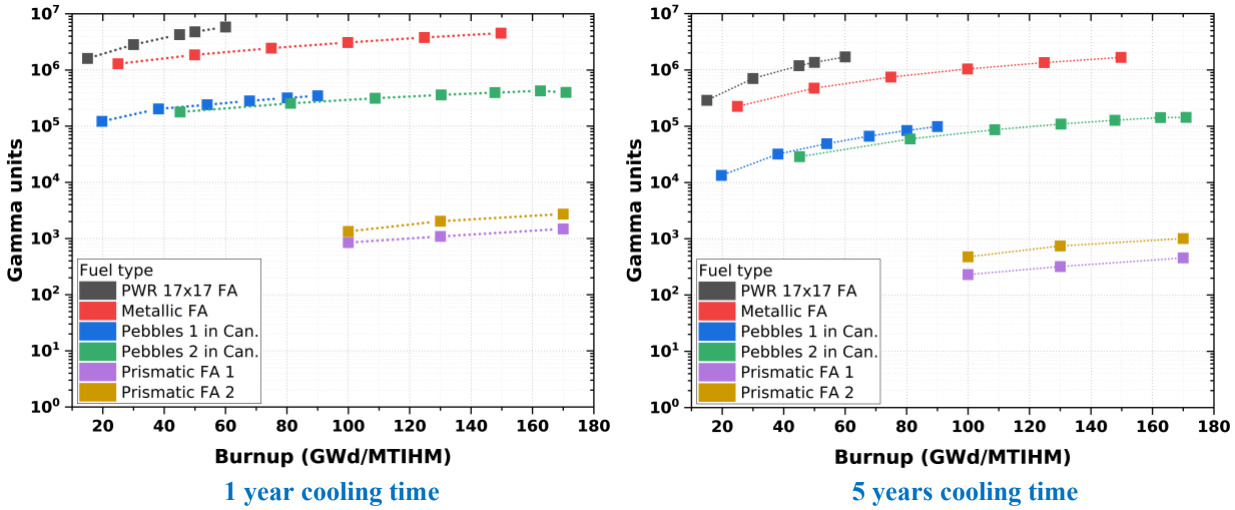

Figure 38. Summary of the gamma units of an FDET.

3. GAMMA SPECTROMETRY MODELING OF SPENT ADVANCED REACTOR FUELS

3.1 GADRAS MODELING OF GAMMA SPECTROMETRY MEASUREMENTS

This section documents the work performed to simulate the HPGe gamma spectrometry measurements of the spent AR fuel items described in previous sections. For LWR fuels, HPGe measurements are not routinely performed for spent fuel safeguards verifications, although such measurements are performed on special occasions (e.g., recovery from a loss of continuity-of-knowledge event). Because of the high radiation dose rates associated with spent fuel, fuel pins are usually not extracted from LWR fuel assemblies for safeguards measurements, although such measurements are sometimes performed by the reactor operator to examine fuel performance or to collect data to benchmark calculations. Therefore, the spent AR fuel items were modeled on a fuel "assembly" level in this work. Compared with the gamma signals from the ionization chambers (e.g., those used in an FDET), the gamma spectra collected by an HPGe detector can reveal the concentrations of certain key isotopes in the fuel, such as ^{134}Cs and ^{137}Cs, which have often been used as burnup indicators for LWR fuel. One caveat is that such gamma spectra can be heavily affected by the self-attenuation of a fuel item, especially if the average density of the fuel is high. As a result, the gamma spectra are usually dominated by the outer row of the fuel pins in an LWR assembly given that the fuel pins are tightly packed and the densities of the fuel and cladding materials are relatively high. Therefore, gamma spectra are not usually used to detect diversions within a fuel assembly, so diversion analysis was not performed in this part of work. However, gamma spectra analysis is useful for determining the burnup value of the irradiated fuel, including the spent AR fuel items simulated in this work.

A series of models for the Gamma Detector Response and Analysis Software (GADRAS) [26] were developed to simulate the expected gamma spectra from the HPGe measurements of four of the five AR fuel items shown in Figure 3. (Note that a Type 1 pebble has physical characteristics similar to those of a Type 2 pebble, but a Type 2 pebble has a wider range of burnup values; therefore, only a Type 2 pebble was modeled for this task.) HPGe measurements of a spent PWR assembly were also modeled for comparison. GADRAS version 19.3.5 was used in this work, and the built-in response function for a coaxial HPGe detector with 60% efficiency was used. Given that GADRAS performs radiation transport only in simple geometries, the four AR fuel items and the PWR assembly were simplified in the GADRAS models as cylinders that preserve the volumes of the respective fuel items. The materials inside the fuel item were blended to form a homogeneous material, with the mass of each isotope preserved as in the original fuel item. For example, in the case of a graphite fuel block, the TRISO particles, the graphite matrix, the carbon or SiC shell of the fuel compact, and the graphite block are all blended to form one homogenous material. If there is a structure (or a shell) outside the fuel blend—for example, the graphite shell at the outer surface of a graphite fuel block, the canister wall, or the duct wall of a metallic fuel bundle—then it was modeled explicitly with GADRAS. Table 23 lists the main physical characteristics of the simplified GADRAS models used for these spent fuel items.

Table 23. Main physical characteristics of the simplified GADRAS models used for the spent fuel items

Spent fuel items	Fuel blend density (g/cc)	Equivalent fuel blend radius (cm)	*Shell* density (g/cc)	*Shell* thickness (cm)
PWR assembly	4.47	12.07	None	None
Metallic fuel bundle	7.45	7.14	7.65	0.32
Type 2 pebbles in a canister	0.54	7.95	8.03	1.6
Type 1 prismatic fuel block	1.46	18.13	1.74	0.77
Type 2 prismatic fuel block	1.47	18.23	1.74	0.66

For the isotopic concentrations of the fuel itself, burnup calculations were performed using SCALE or Serpent, as described in the previous section, to calculate such concentrations for various relevant burnup levels (e.g., low, medium, and high burnups). Once the isotopic concentrations in each material are fed into GADRAS, it will generate the photon emission source terms using its built-in data libraries that cover all relevant physical processes. GADRAS treats most types of gamma source terms in materials comprehensively, including neutron-induced (e.g., [n, γ] reaction) photons, electron-induced (e.g., bremsstrahlung radiation) photons, and decay photons [26]. GADRAS then performs the radiation transport and simulates the detector response according to the detector response function specified by the user. To facilitate comparison of gamma spectra from different fuel items, the standoff (distance between the fuel and the detector) was set as 500 cm, and the live time was set as 300 s for all simulation cases in this work.

Given that spent fuel can emit high gamma dose rates, attenuation and collimation are generally required for an HPGe measurement to reduce the dose rates on the detector. The requirement for attenuation and collimation was assessed based on the fuel item with the highest gamma dose rates (i.e., the hottest), which is the PWR assembly with a burnup of 60 GWd/MTIHM and a cooling time of one year. After a few runs with GADRAS, it was found that by using a layer of 2.5 cm thick lead and a reduction of the photon source intensity by four orders of magnitude for all energies (such reduction can be achieved by using a pin-hole collimator [e.g., 3 mm wide]) allowed GADRAS to produce a reasonable gamma spectrum for the hottest fuel item considered in this work. (If the gamma dose rates on the detector are too high, then the GADRAS run would either suspend or return an empty spectrum.) Because the goal of this work is to compare the different gamma spectra characteristics of different fuel items, the same combination of attenuation and collimation effect was used for all fuel items simulated in this work, even though such a combination is not necessarily optimal for a particular fuel item.

The left image in Figure 39 shows a top view of the GADRAS model for a spent metallic fuel bundle simulated in this work. The right image in Figure 39 shows a side view of this model.

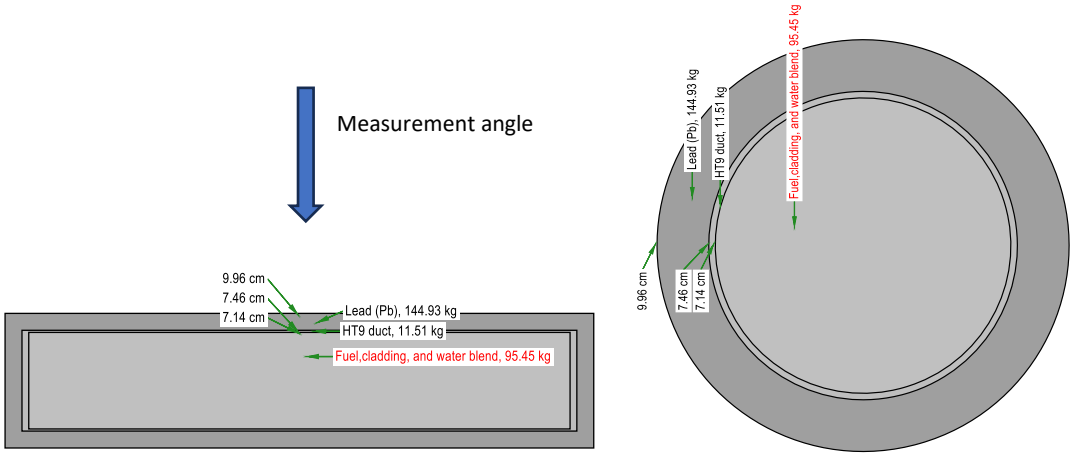

Figure 39. Top view of the GADRAS model for a metallic fuel bundle encased in 2.5 cm thick lead (left), and a side view of the model (right).

As shown in Figure 39, three regions of materials were included in this model: the homogenous region blended with fuel, cladding, and water; the HT9 duct wall; and the 2.5 cm thick lead. As previously mentioned, the interior of the fuel bundle was modeled as a cylinder filled with a homogenous material that preserves the mass of each isotope contained in the original item. As indicated by the blue arrow, the

HPGe detector was simulated to point to the mid-height of the cylinder from the side. This measurement angle was used for all fuel items in this work. Similarly, Figure 40 shows the GADRAS model for a canister filled with Type 2 pebbles. The interior of the canister is modeled with blended material with irradiated TRISO particles and graphite matrix materials.

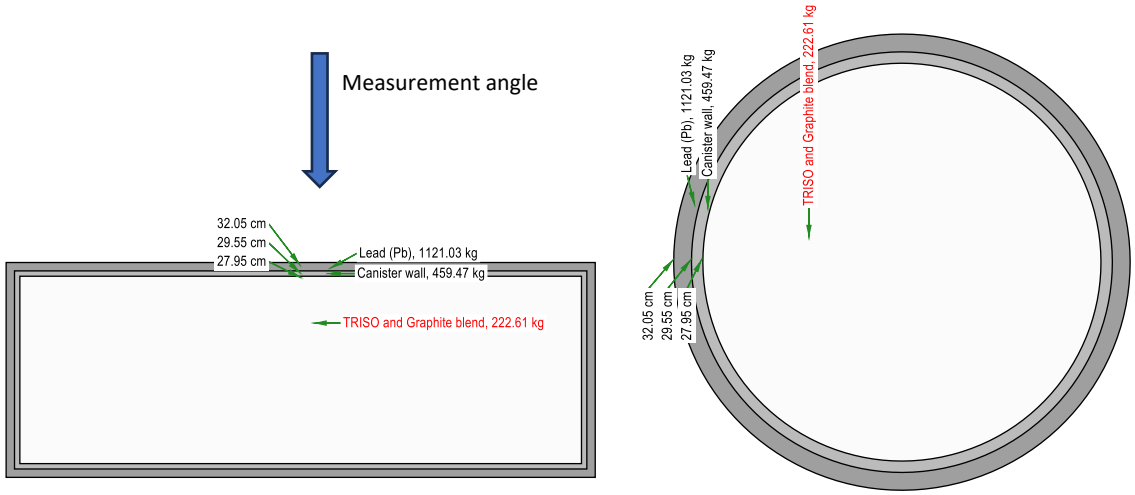

Figure 40. Top view of the GADRAS model for a spent pebble-containing canister encased in 2.5 cm thick lead (left), and a side view of model (right).

3.2 SIMULATED GAMMA SPECTRA

Figure 41 and Figure 42 show the simulated HPGe gamma spectra from an irradiated metallic fuel bundle with three burnups and cooling times of one year and five years, respectively. (Note that *G* in the figures in this section indicates GWd/MTIHM.) The major photopeaks from the three most important burnup-indicator nuclides (^{134}Cs, ^{137}Cs, and ^{154}Eu) are labeled in this figure, along with their respective half-lives and branching ratios shown in the parentheses. Because lower energy photopeaks have higher detection efficiency and the 796 keV photopeak is somewhat interfered with by the neighboring 802 keV peak (also from ^{134}Cs), the 605 keV and 662 keV peaks were the two primary peaks used to determine the fuel's burnup values. As shown, higher photopeaks and continuums are seen at higher burnups, which is unsurprising because of the higher accumulations of photon-emitting fission products in fuels with higher burnups.

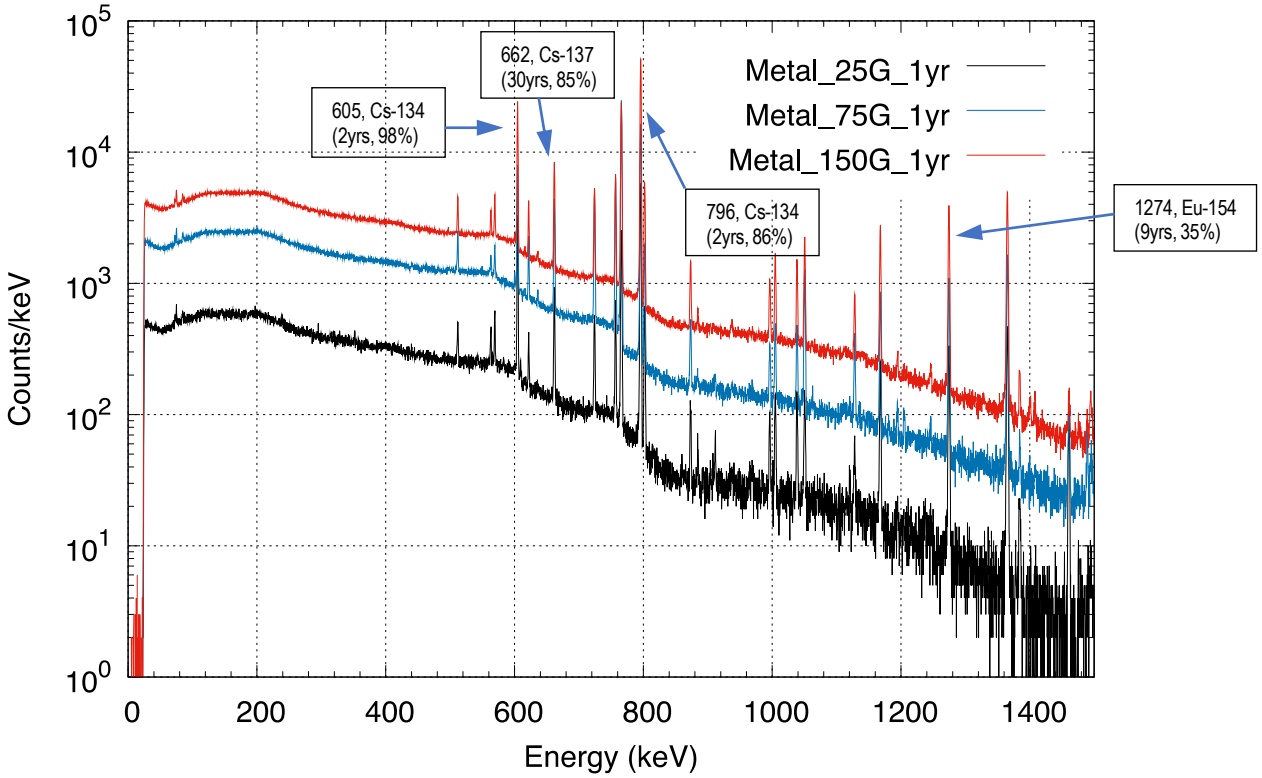

Figure 41. Simulated HPGe gamma spectra from an irradiated metallic fuel bundle with three burnups and a cooling time of one year.

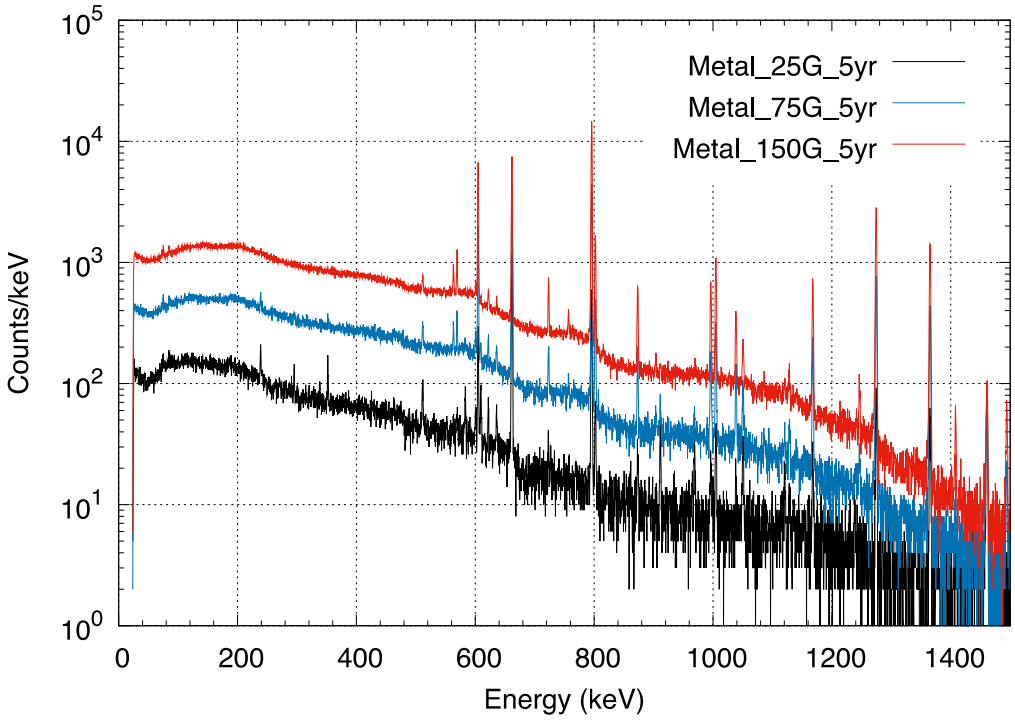

Figure 42. Simulated HPGe gamma spectra from an irradiated metallic fuel bundle with three burnups and a cooling time of five years.

Figure 43 compares the gamma spectra of the metallic fuel at cooling times of one year and five years at the same burnup of 150 GWd/MTIHM (i.e., the nominal discharge burnup). The spectrum continuum for the one-year cooled time is approximately four times higher than that of the five-year cooling time. Compared with the one-year cooled case, the 662 keV photopeak of ^{137}Cs for the five-year cooled case is much stronger than the two ^{134}Cs peaks, which is expected because the half-life of ^{137}Cs is much longer than that of ^{134}Cs. Another noticeable difference between the two cases is that several peaks either disappeared or became significantly weaker in the five-year cooled case because of the decay of the corresponding source nuclides. For example, the 757 keV peak (primarily from ^{95}Zr) became much weaker, and the 766 keV peak (primarily from ^{95}Nb) disappeared in the five-year cooled case.

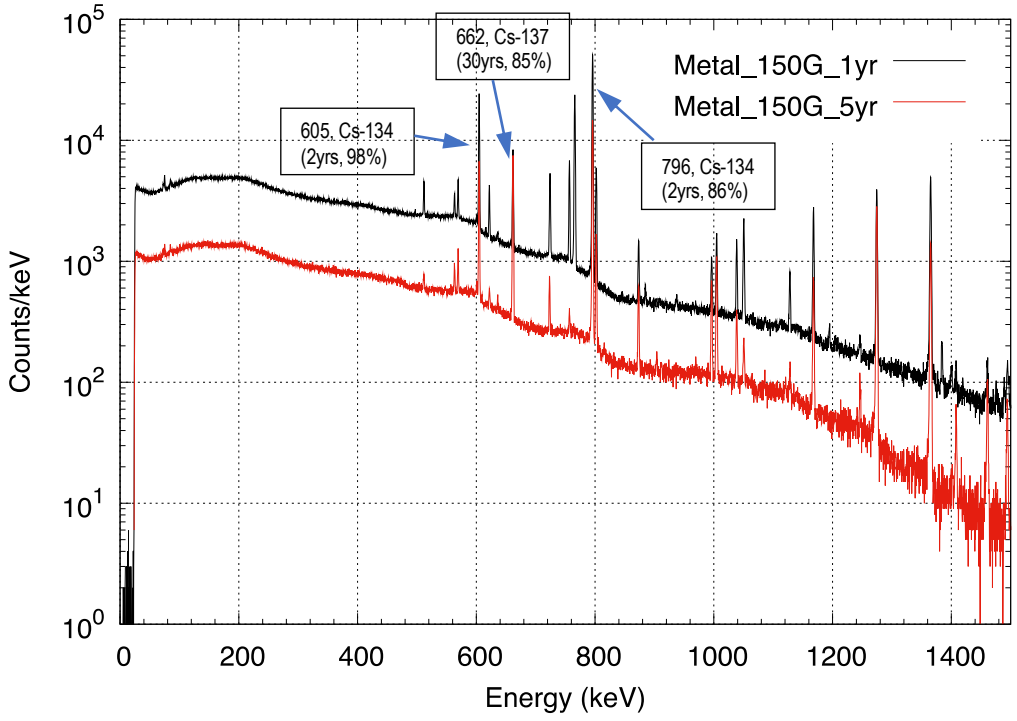

Figure 43. Simulated HPGe gamma spectra from an irradiated metallic fuel bundle with a burnup of 150 GWd/ MTIHM and a cooling time of one year vs. five years.

Similarly, Figure 44 and Figure 45 show the simulated HPGe gamma spectra from a canister filled with irradiated Type 2 pebbles with three burnups and cooling times of one and five years, respectively. (Note that *Pebble2* in the figure indicates Type 2 pebbles.)

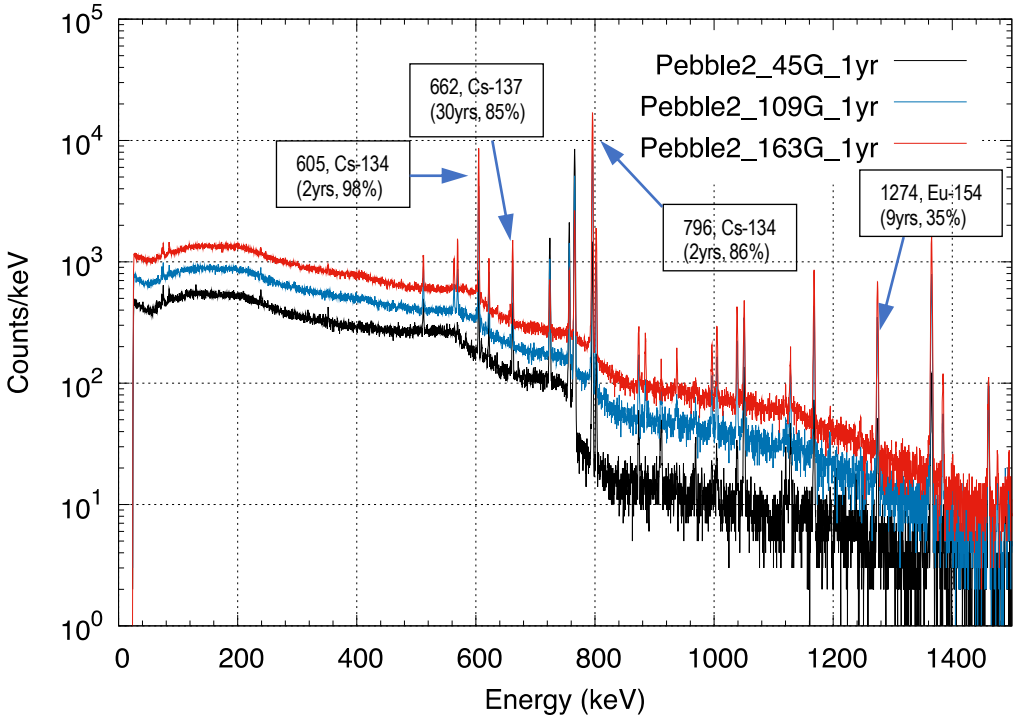

Figure 44. Simulated HPGe gamma spectra from a canister filled with irradiated Type 2 pebbles with three burnups and a cooling time of one year.

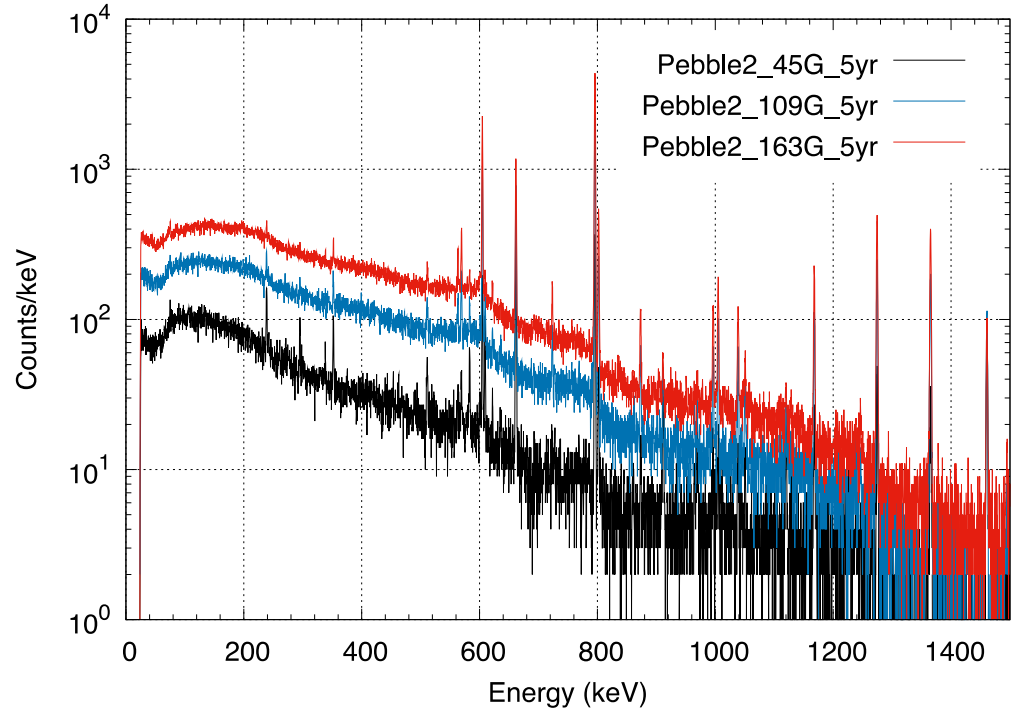

Figure 45. Simulated HPGe gamma spectra from a canister filled with irradiated Type 2 pebbles with three burnups and a cooling time of five years.

Figure 46 compares the gamma spectra of the pebble canister fuel at cooling times of one year and five years at the nominal discharge burnup. Compared with the respective spectra from the metallic fuel, these pebble spectra have similar characteristics, except the magnitude of these spectra are much smaller, which can be attributed to the smaller amounts of source fission product nuclides in the pebble case. Furthermore, the 1.6 cm stainless steel canister wall in the pebble case further reduced the magnitudes of the spectra.

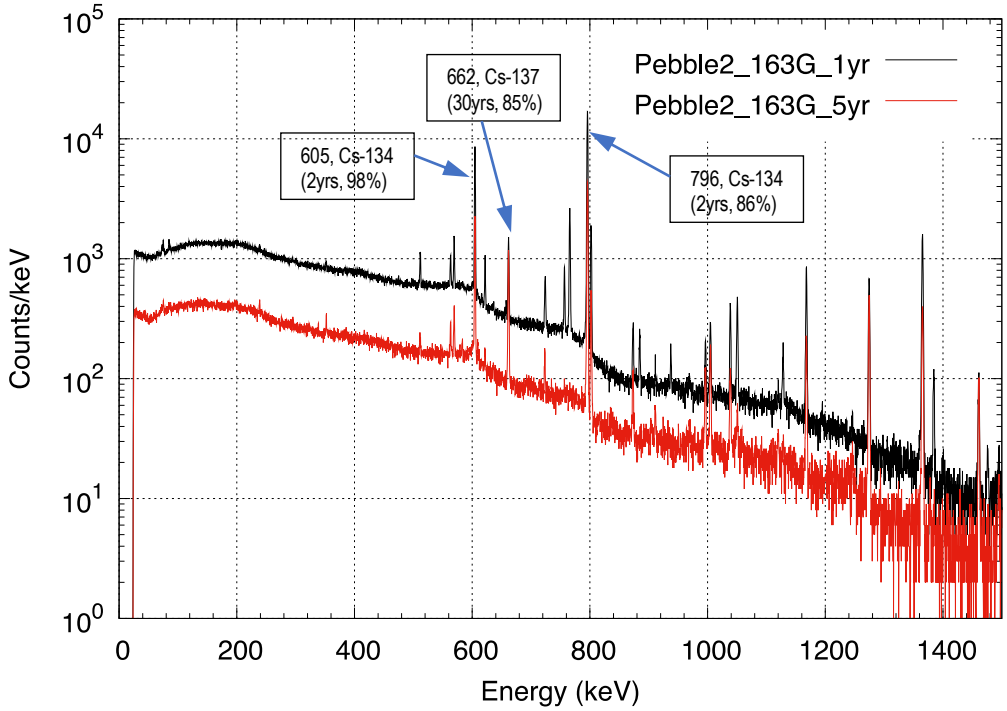

Figure 46. Simulated HPGe gamma spectra from a canister filled with irradiated Type 2 pebbles with a burnup of 163 GWd/ MTIHM and cooling times of one and five years.

Figure 47 and Figure 48 show the simulated HPGe gamma spectra of the four spent AR fuel items and a PWR assembly—all at their respective nominal discharge burnups—with cooling times of one and five years, respectively. The details of each fuel item can be found in Table 2. Similar shapes and photopeaks are seen among different fuel items, except the magnitudes can be significantly different because of the different amounts of photon-emitting fission products and self-attenuation effects in each item. Because the photon emission intensity of the PWR assembly is significantly higher than those of the spent AR fuel items, it is expected that gamma spectrometry measurements will be easier to perform on AR fuel items than on a PWR assembly, although ample attenuation, collimation, and standoff distance are required for all of these AR items, as described in Section 3.1.

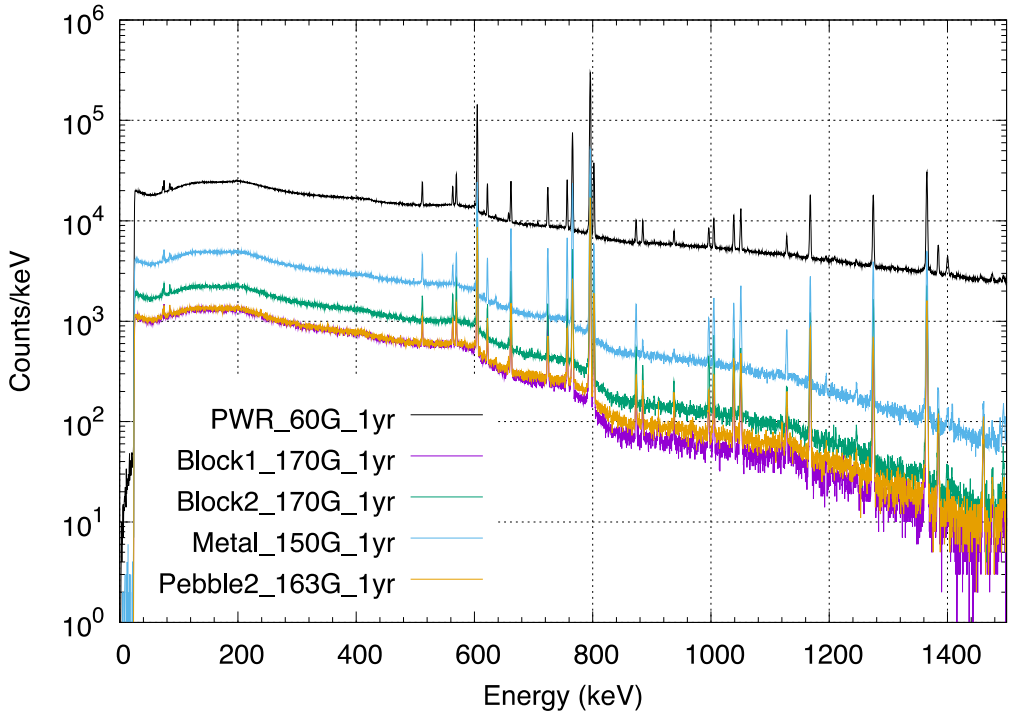

Figure 47. Simulated HPGe gamma spectra from the four different spent AR fuel items and the PWR assembly, each with their respective nominal discharge burnups (all with one-year cooling times).

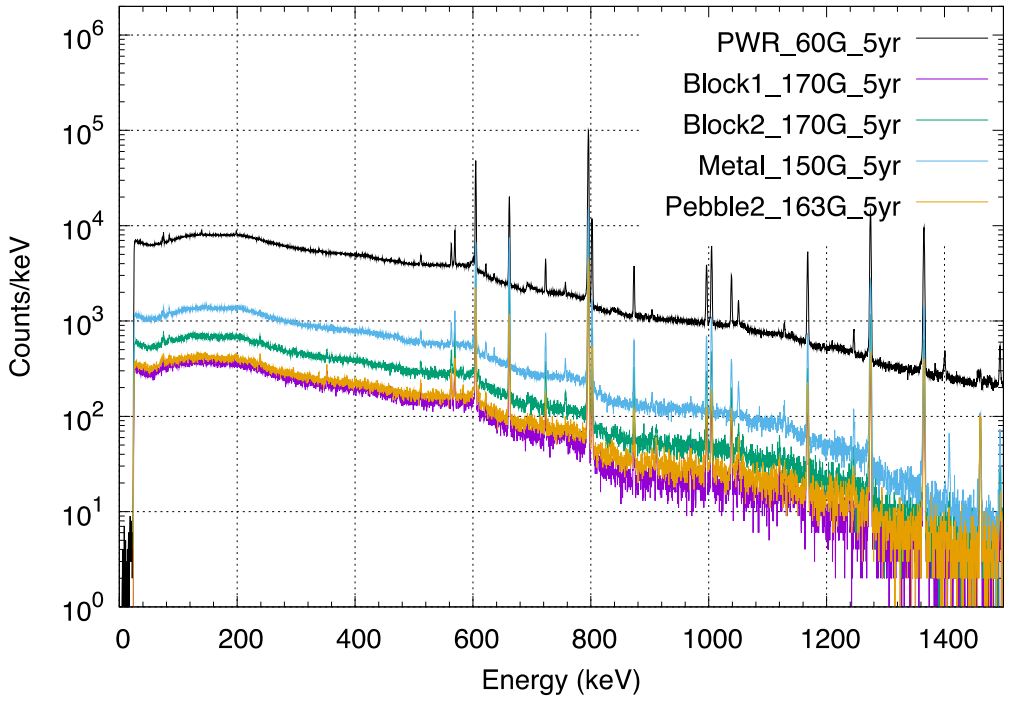

Figure 48. Simulated HPGe gamma spectra from the four different spent AR fuel items and the PWR assembly, each with their respective nominal discharge burnups (all with five-year cooling times).

Figure 49 shows the 662 keV peak area rate (in a log scale) as a function of burnup for two types of AR fuel items and the PWR assembly at a cooling time of one year. Somewhat linear trends with burnup can be seen for all three fuel types, which can be attributed to the fact that both ^{235}U and ^{239}Pu have similar fission yield of ^{137}Cs in both thermal and fast neutron irradiation spectra. ^{137}Cs has been considered as a reliable burnup indicator for LWR fuels. The differences in magnitude and the slopes of the trend for each fuel type were caused by the different amount of ^{137}Cs and attenuation in each fuel type. The other three TRISO-based AR fuel items are expected to have trends similar to those of Pebble2 because they all have similar fuel and reactor physics characteristics.

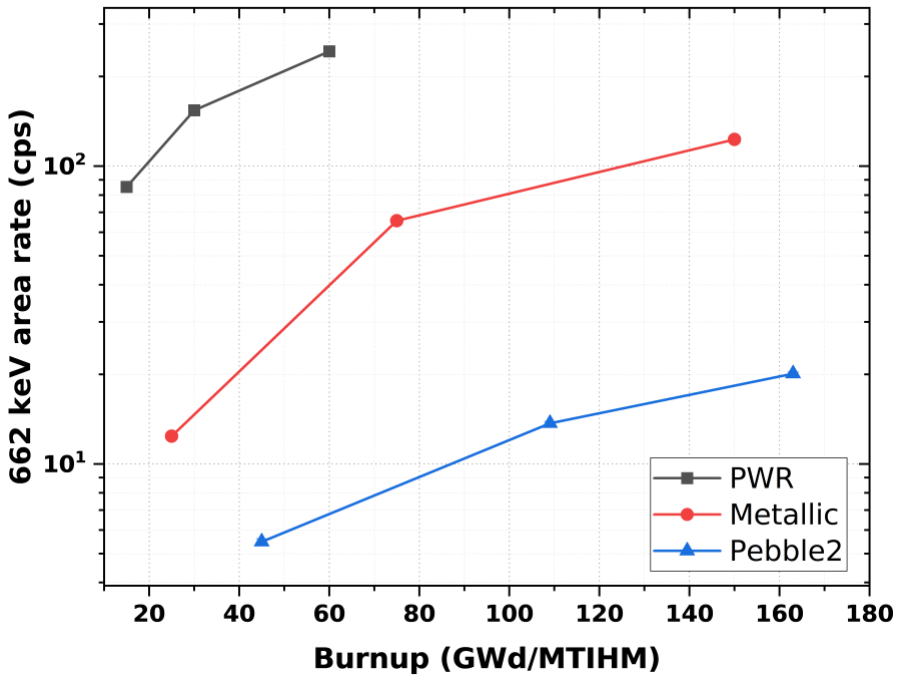

Figure 49. The 662 keV peak area rate as a function of burnup at a cooling time of one year.

Figure 50 shows the 605/662 peak area ratio as a function of burnup for two types of AR fuel items and the PWR assembly at a cooling time of one year. Linear trends with burnup can be seen for Pebble2 and PWR. However, the metallic fuel item exhibited a very nonlinear trend with burnup. Although $^{134}Cs/^{137}Cs$ ratio has been considered as another reliable burnup indicator for LWR fuels, the yield of ^{134}Cs is known to vary with the neutron spectra in a reactor because a large fraction of ^{134}Cs comes from the neutron absorption reaction of ^{133}Cs, which has a cross section that varies with the neutron energy spectra in the reactor. Because of the significantly harder neutron energy spectra that the metallic fuel has been exposed while the reactor than all other fuel types considered herein, it is unsurprising to see a very different trend in the 605/662 ratio for the metallic fuel than for the other fuel types.

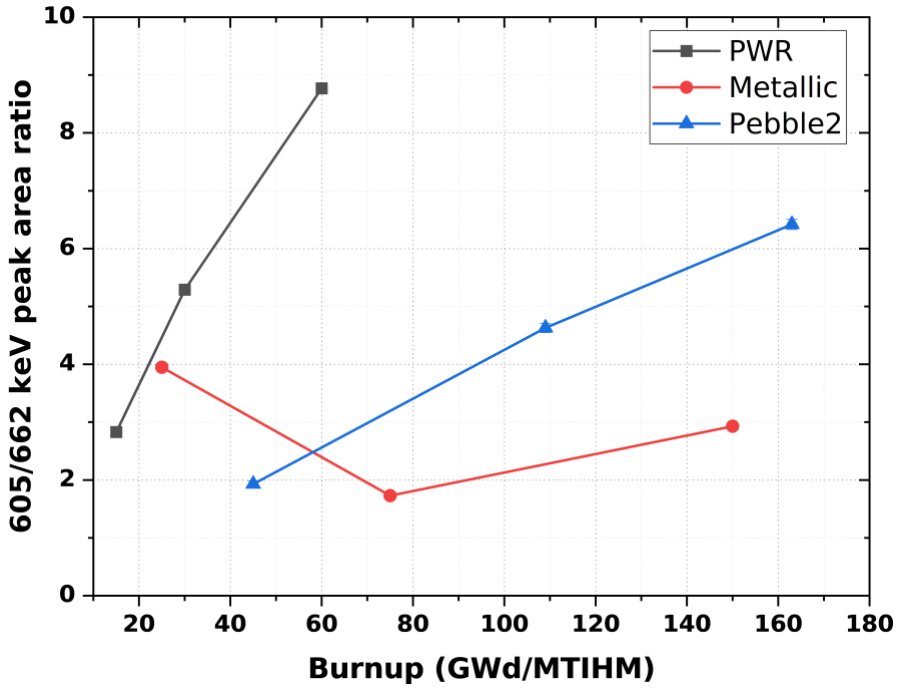

Figure 50. The 605/662 keV peak area ratio as a function of burnup at a cooling time of one year.

4. SUMMARY AND CONCLUSIONS

This work focused on assessing performance of existing safeguards measurement technologies for ***irradiated or spent*** AR fuels through modeling and simulation as a continuation of the FY23 effort that focused on ***fresh*** AR fuels. In addition to the differences in the fuel designs and enrichments used for AR and LWR fuel types (much higher enrichments are typically used in the AR fuel designs), several other characteristics of spent AR fuel items may warrant more stringent safeguards measures than spent LWR assemblies: (1) all spent AR fuel items are found to have significantly lower self-protecting gamma dose rates than a PWR assembly mainly due to the lower initial U loading in the AR fuel items, and (2) some of the spent AR fuel items (e.g., metallic fuel) were found to have significantly higher Pu content (per unit mass of heavy metal) or higher ^{239}Pu concentration than a spent PWR assembly.

Because the TRISO-based spent AR fuel items (used in five of the 10 ARDP designs, as shown in Table 1) are most likely stored in an air-filled hot cell instead of a water-filled pool, it is expected that the CVD measurement (one of the two primary safeguards measurements of spent LWR fuel) is unlikely to function on those fuel items in a hot cell. This is because the intensity of Cerenkov light produced in air is lower than in water because of the lower refractive index of air. The inability or reduced effectiveness of CVD measurements on spent AR fuel items presents a major technical challenge in the effort to use existing technology to perform safeguards measurements on spent AR fuels, especially when RCVDs are being developed to automatically perform safeguards measurements on spent LWR fuel assemblies stored in a pool. In addition, significantly higher interference from a neighboring fuel item was found on the FDET measurements when the measurement is performed in air than in water.

This study was mainly conducted using modeling and simulation of FDET measurements of five AR fuel types, including one metallic fuel type and four TRISO-based fuel types in both pebble and graphite block forms in their respective storage configurations and environment. HPGe gamma spectrometry measurements were also simulated on the spent AR fuel types and the PWR assembly because the signature photopeaks measured by an HPGe detector have been used in LWR safeguards verifications.

The following significant challenges were identified in performing FDET detector safeguards measurements of spent AR fuels:

- Incompatibilities were found between the AR fuel configurations and the existing FDET because the dimensions of the AR fuels were significantly different from the LWR assembly dimensions. For example, the prismatic fuel blocks are much wider than the existing FDETs.
- All spent AR fuel items were found to have much lower neutron count rates than a PWR assembly, especially when the burnup of the AR fuel was relatively low. This means that a longer measurement time would be required for the spent AR fuel to reach the same counting precision as that for a PWR assembly.
- FDET was found to be less effective in detecting fuel diversions in some of the spent AR fuel items (e.g., a transportation canister filled with Type 1 pebbles) than in a spent PWR assembly.

One significant challenge was identified when performing **gamma** spectrometry detector safeguards measurements of spent AR fuel elements:

- The 605/662 keV photopeak ratio (indicating the ratio of ^{134}Cs/^{137}Cs) was found to be nonlinear with the burnup for the irradiated metallic fuel bundle, which means that one of the frequently used burnup indicators cannot be applied to the metallic fuel.

These results suggest that either an alternative technology or other significant and timely technology development is needed to perform adequate safeguards measurements of some of these spent AR fuel elements/items, such as neutron detectors with higher sensitivity that can withstand the spent fuel's high gamma dose rates.

5. REFERENCES

[1] World Nuclear Association, "Advanced Nuclear Power Reactors," [Online]. Available: https://world-nuclear.org/information-library/nuclear-fuel-cycle/nuclear-power-reactors/advanced-nuclear-power-reactors.aspx. [Accessed 1st December 2023].

[2] J. Hu, D. Hartanto, R. Venkataraman and R. McElroy, "Identify and Assess Technical Challenges in Safeguards Measurements of Fresh Advanced Reactor Fuels," in *Advances in Nuclear Nonproliferation Technology and Policy Conference (ANTPC 2023)*, Washington, DC, 2023.

[3] D. Hartanto, J. Hu, R. McElroy, R. Venkataraman, J. W. Bae and B. Hiscox, "Identity and Assess Technical Challenges in Safeguards Measurements of Fresh Advanced Reactor Fuels," ORNL/SPR-2023/3237, Oak Ridge National Laboratory, Oak Ridge, TN, 2024.

[4] B. Murphy and P. De Baere, "Monte Carlo Modeling of a Fork Detector System," in *27th Annual Meeting Symposium on Safeguards and Nuclear Material Management*, London, UK, 2005.

[5] S. Vaccaro, I. Gauld, J. Hu, P. De Baere, J. Peterson, P. Schwalbach, A. Smejkal, A. Tomanin, A. Sjoland, S. Tobin and D. Wiarda, "Advancing the Fork Detector for Quantitative Spent Nuclear Fuel Verification," *Nuclear Instruments and Methods in Physics Research Section A: Accelerators, Spectrometers, Detectors and Associated Equipment,* vol. 888, pp. 202-217, 2018.

[6] J. Hu, I. C. Gauld, S. Vaccaro, T. Honkamaa and G. Ilas, "Validation of ORIGEN for VVER-440 Spent Fuel with Application to Fork Detector Safeguards Measurements," *ESARDA Bulletin - The International Journal of Nuclear Safeguards and Non-proliferation,* vol. 60, pp. 28-42, 2020.

[7] S. Vaccaro et al., "A New Approach to Fork Measurements Data Analysis by RADAR-CRISP and ORIGEN Integration," *IEEE TRANSACTIONS ON NUCLEAR SCIENCE,* vol. 61, pp. 2161-2168, 2014.

[8] E. Rapisarda, "Advanced Analysis of the IAEA Fork Detector Data for Partial Defect Verification," in *Institute of Nuclear Materials Management*, Vienna, Austria, 2023.

[9] Channel Systems, "Cerenkov Light Imaging for Nuclear Safeguards," [Online]. Available: https://channelsystems.ca/applications/cerenkov-light-imaging-nuclear-safeguards. [Accessed 25 September 2024].

[10] J. Wagman and T. Nicula-Golovei, "The Evolution of Safeguards Technology," [Online]. Available: https://www.iaea.org/bulletin/the-evolution-of-safeguards-technology. [Accessed 1 September 2024].

[11] World Nuclear News, "Robot developed to assist verification of used fuel," [Online]. Available: https://world-nuclear-news.org/Articles/Robot-developed-to-assist-verification-of-used-fue. [Accessed 26 September 2024].

[12] US DOE, "Advanced Reactor Demonstration Program," [Online]. Available: https://www.energy.gov/ne/advanced-reactor-demonstration-program. [Accessed 1st December 2023].

[13] T. K. Kim, "Benchmark Specification of Advanced Burner Test Reactor," ANL/NSE-20/65, Argonne National Laboratory, Argonne, IL, 2020.

[14] D. Hartanto, G. Radulescu, F. Bostelmann, R. Elzohery and W. Wieselquist, "SCALE Demonstration for Sodium-Cooled Fast Reactor Fuel Cycle Analysis," ORNL/TM-2023/3214, Oak Ridge National Laboratory, Oak Ridge, TN, 2024.

[15] NEA, "PBMR Coupled Neutronics/Thermal-Hydraulics Transient Benchmark: The PBMR-400 Core Design - Volume 1: The Benchmark Definition," NEA/NSC/DOC(2013)10, OECD Publishing, Paris, 2013.

[16] E. J. Mulder and W. A. Boyes, "Neutronics Characteristics of a 165 MWth Xe-100 Reactor," *Nuclear Engineering and Design,* vol. 357, p. 110415, 2020.

[17] Ultra Safe Nuclear Corporation, "Micro Modular Reactor," [Online]. Available: https://www.usnc.com/mmr. [Accessed December 2023].

[18] International Atomic Energy Agency, "Prismatic High-Temperature Reactor Design," 2013. [Online]. Available: https://aris.iaea.org/PDF/PrismaticHTR.pdf.

[19] C. J. Werner (ed.), "MCNP User's Manual Code Version 6.2," LA-UR-17-29981, Los Alamos National Laboratory, NM, USA, 2017.

[20] W. A. Wieselquiest and R. Lefebvre, "SCALE 6.3.1 User Manual," ORNL/TM-SCALE-6.3.1, Oak Ridge National Laboratory, Oak Ridge, TN, 2023.

[21] D. Kovacic, P. Gibbs, J. Hu, D. Hartanto, C. Ball, R. McElroy Jr., N. Luciano, R. Hunneke and T. Pham, "Nuclear Material Control & Accounting for Pebble Bed Reactors," ORNL/SPR-2023/2988, Oak Ridge National Laboratory, Oak Ridge, TN, 2023.

[22] Z. Richter, E. Davidson, S. Skutnik and M. Munk, "Modeling and Simulation of an Xe-100 type Pebble Bed Gas-Cooled Reactor with SCALE," ORNL/TM-2023/2959, Oak Ridge National Laboratory, Oak Ridge, TN, 2023.

[23] J. D. Bess and N. Fujimoto, "Benchmark Evaluation of Start-Up and Zero-Power Measurements at the High-Temperature Engineering Test Reactor," *Nuclear Science and Engineering ,* vol. 178, no. 3, pp. 414-427, 2014.

[24] J. Leppänen, M. Pusa, T. Viitanen, V. Valtavirta and T. Kaltiaisenaho, "The Serpent Monte Carlo code: Status, development and applications in 2013," *Annals of Nuclear Energy,* vol. 82, pp. 142-150, 2015.

[25] BWXT, "Terrestrial Micro RX," BWXT, [Online]. Available: https://www.bwxt.com/what-we-do/advanced-technologies/terrestrial-micro-rx. [Accessed December 2023].

[26] S. M. Horne, G. G. Thoreson, L. A. Theisen, D. J. Mitchell, L. T. Harding and S. E. O'Brien, "GADRAS Version 18 User's Manual," SAND2019-14305, Sandia National Laboratory, Albuquerque, NM, 2019.

APPENDIX A. SELF-PROTECTING RESULTS

APPENDIX A. SELF-PROTECTING RESULTS

An important aspect to consider in the context of safeguards for spent nuclear fuel is the fuel's self-protecting nature, which is driven by the high levels of radiation dose rates emitted, particularly when only a short amount of cooling time has transpired. This intense radiation acts as a natural deterrent against unauthorized handling or diversion because it poses a significant hazard to human health. The figures below present the gamma dose of the spent PWR fuel assembly and the spent AR fuel items analyzed in this report using the ANSI/ANS standards. The gamma dose was calculated at the distance of 1 meter from the outermost surface of the fuel assembly or item and at the mid elevation in an air environment. Using a threshold of 100 R/h as the self-protecting dose limit, a discharged PWR fuel assembly maintains its self-protecting characteristics for more than a century. This type of self-protecting time threshold can be significantly shorter for some spent AR fuel items. For example, it is less than 35 years for a Type 1 prismatic fuel block (see Figure A-5). However, the contrast is starker when comparing a spent PWR assembly and the spent AR fuel items if a higher threshold dose limit is deemed necessary for a spent fuel item to be considered self-protecting.

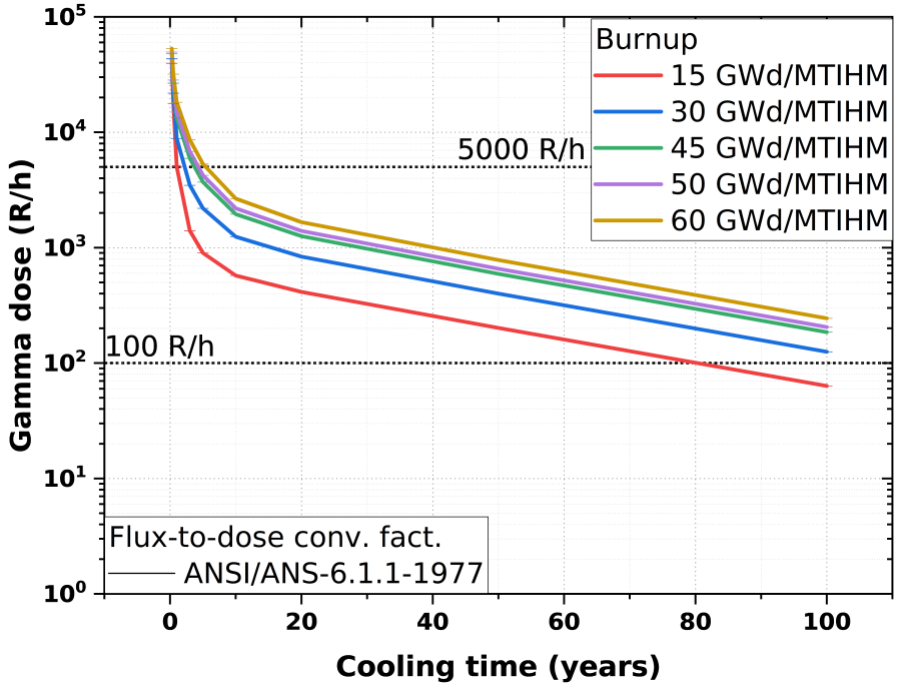

Figure A-1. Gamma dose from a PWR fuel assembly as a function of cooling time.

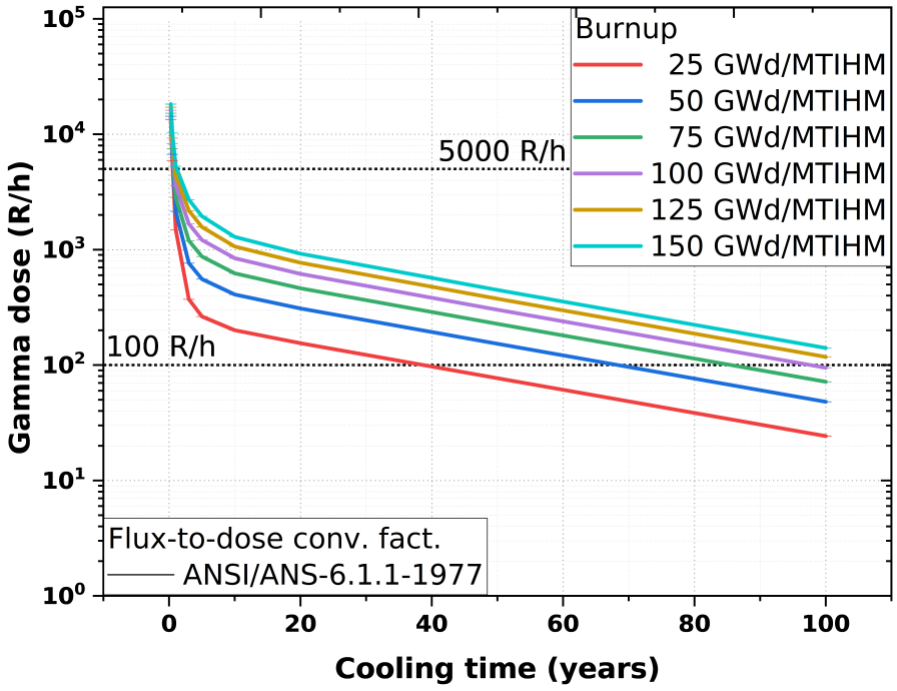

Figure A-2. Gamma dose from a metallic fuel bundle as a function of cooling time.

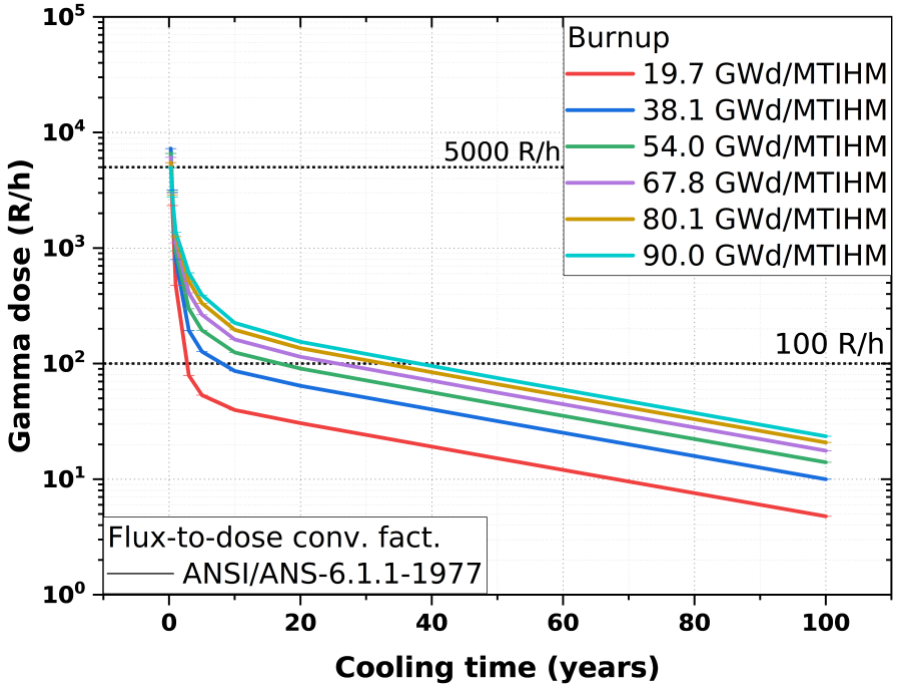

Figure A-3. Gamma dose from Type 1 pebbles in canister as a function of cooling time.

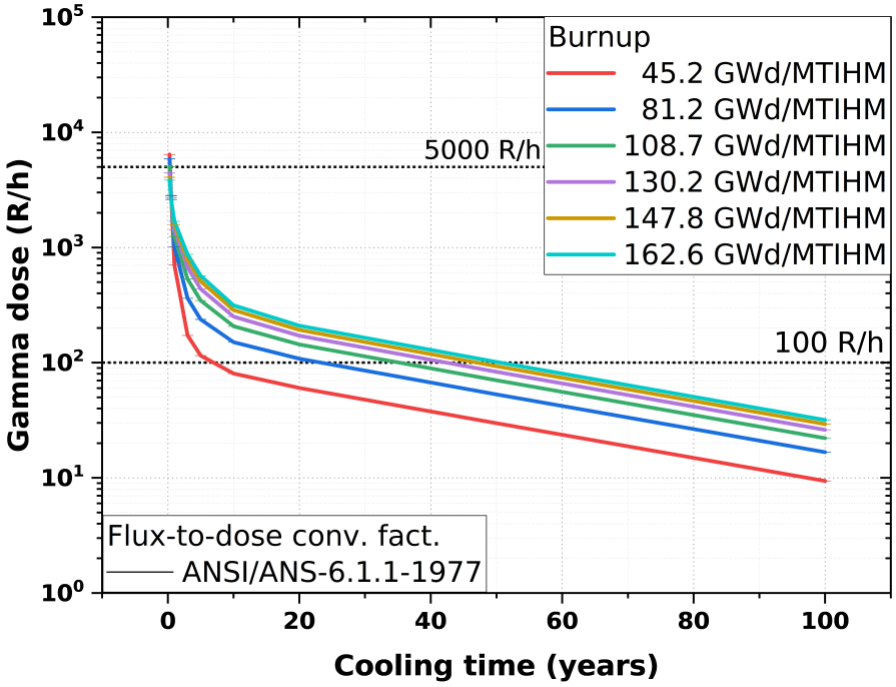

Figure A-4. Gamma dose from Type 2 pebbles in canister as a function of cooling time.

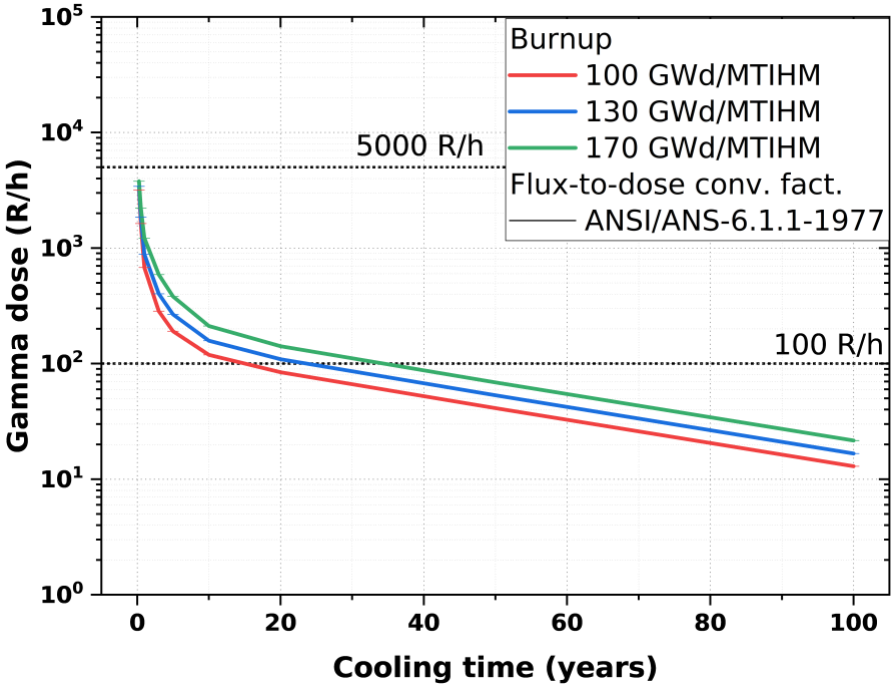

Figure A-5. Gamma dose from a Type 1 prismatic fuel block as a function of cooling time.

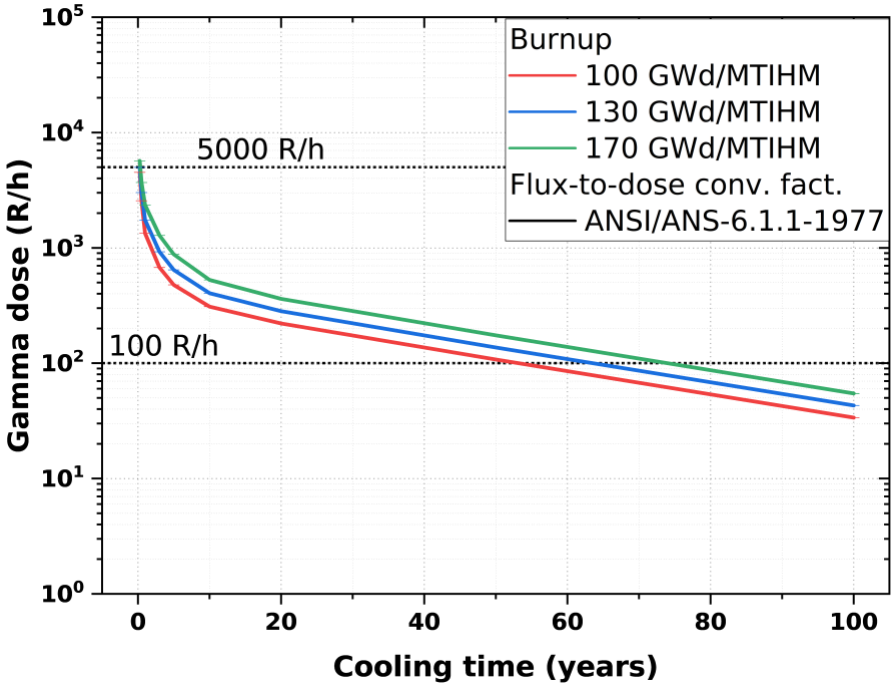

Figure A-6. Gamma dose from a Type 2 prismatic fuel block as a function of cooling time.

APPENDIX B. ADDITIONAL NEUTRON AND GAMMA EMISSION SPECTRA

APPENDIX B. ADDITIONAL NEUTRON AND GAMMA EMISSION SPECTRA

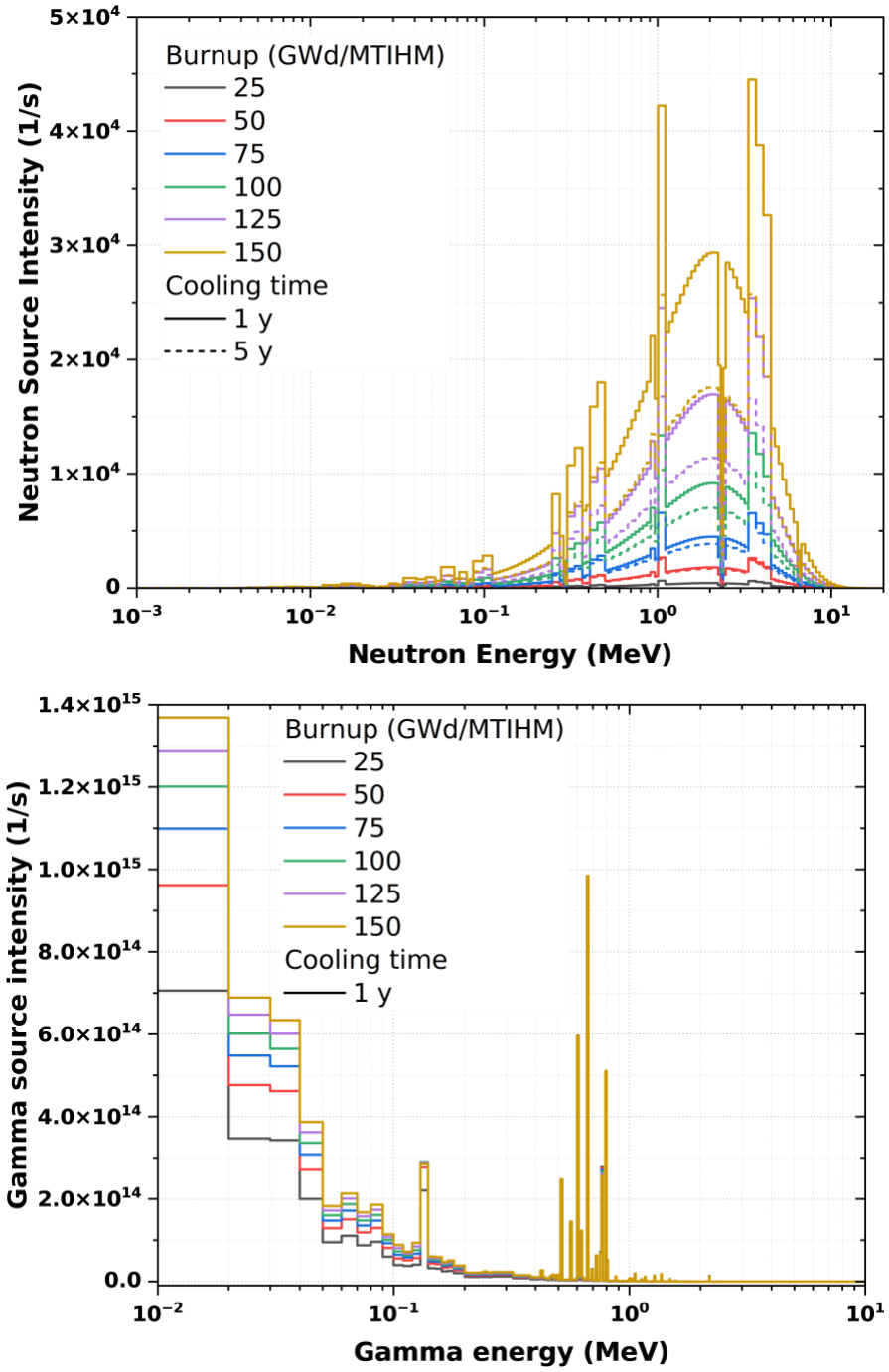

Figure B-1. Neutron and gamma sources of spent metallic fuel bundle.

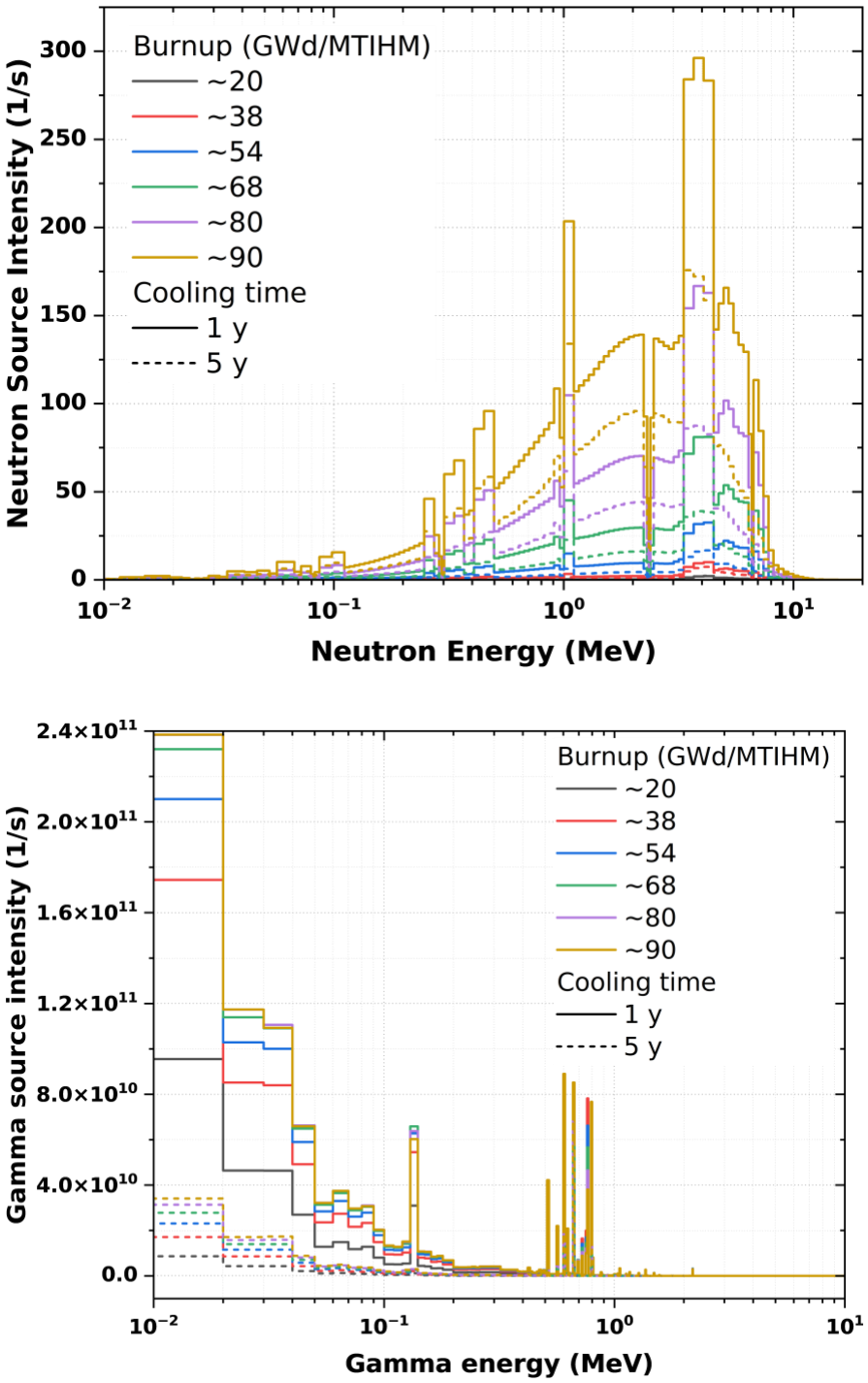

Figure B-2. Neutron and gamma sources of Type 1 pebbles in canister.

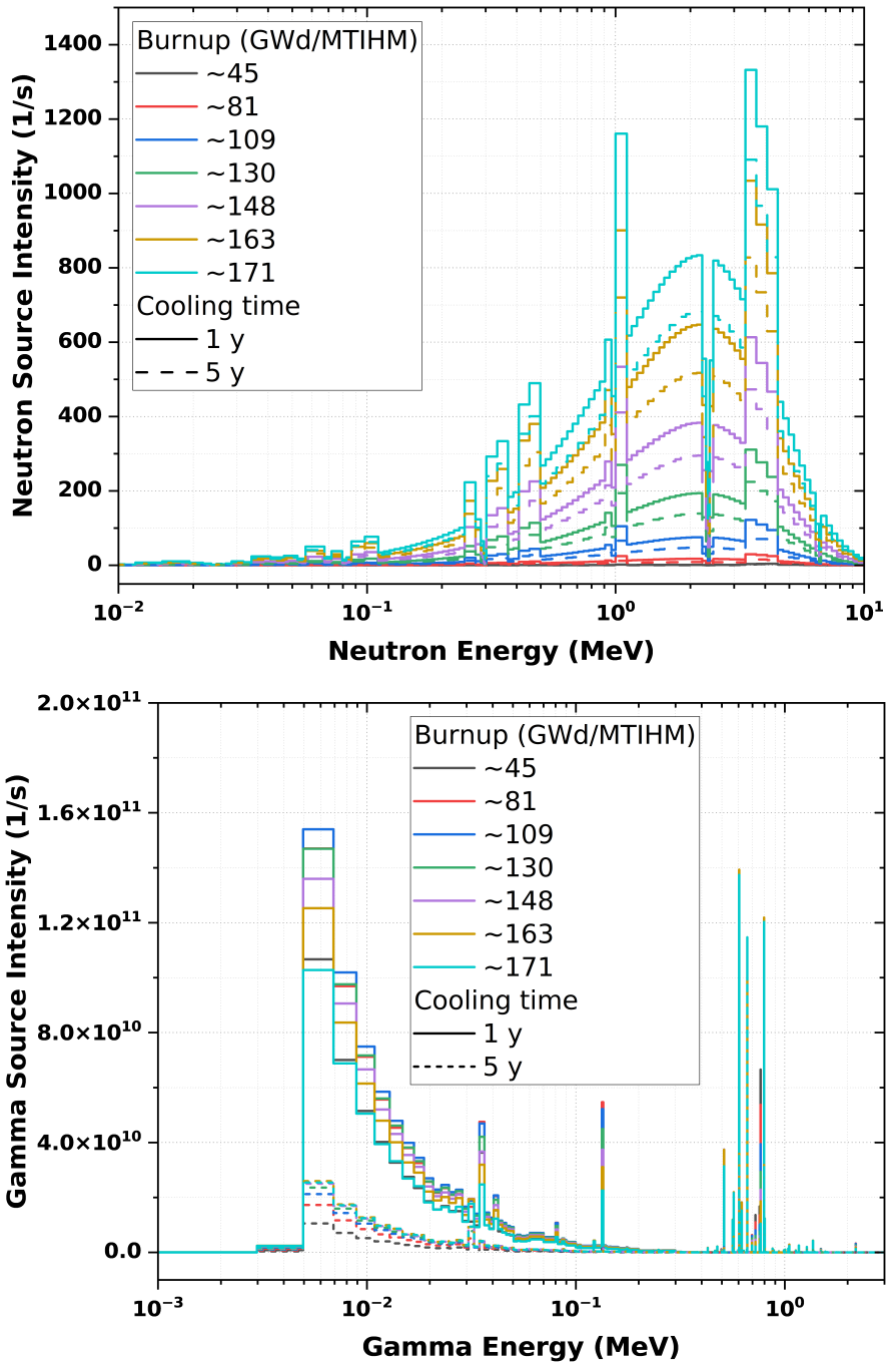

Figure B-3. Neutron and gamma sources of Type 2 pebbles in canister.

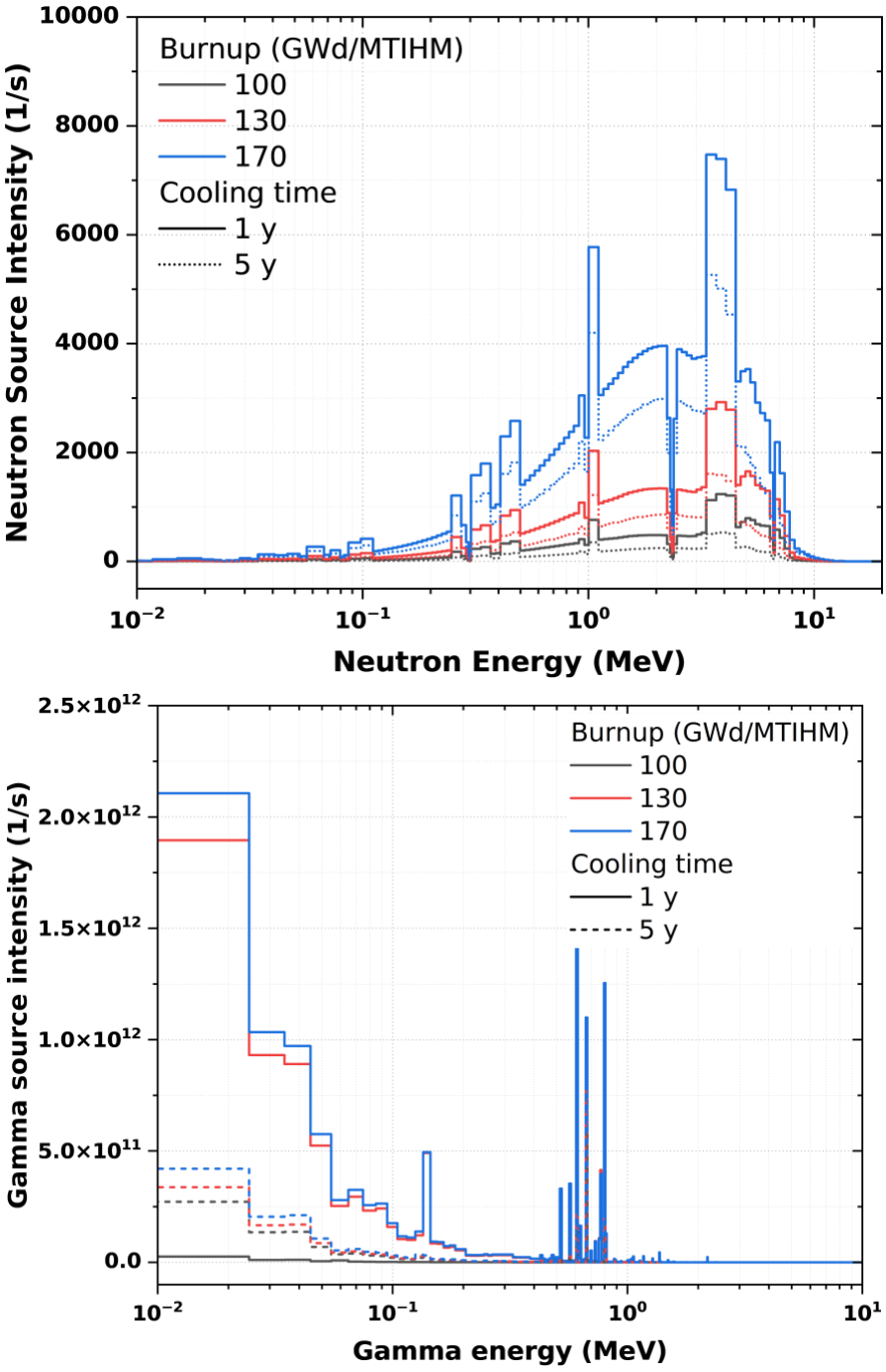

Figure B-4. Neutron and gamma sources of Type 1 prismatic fuel block.

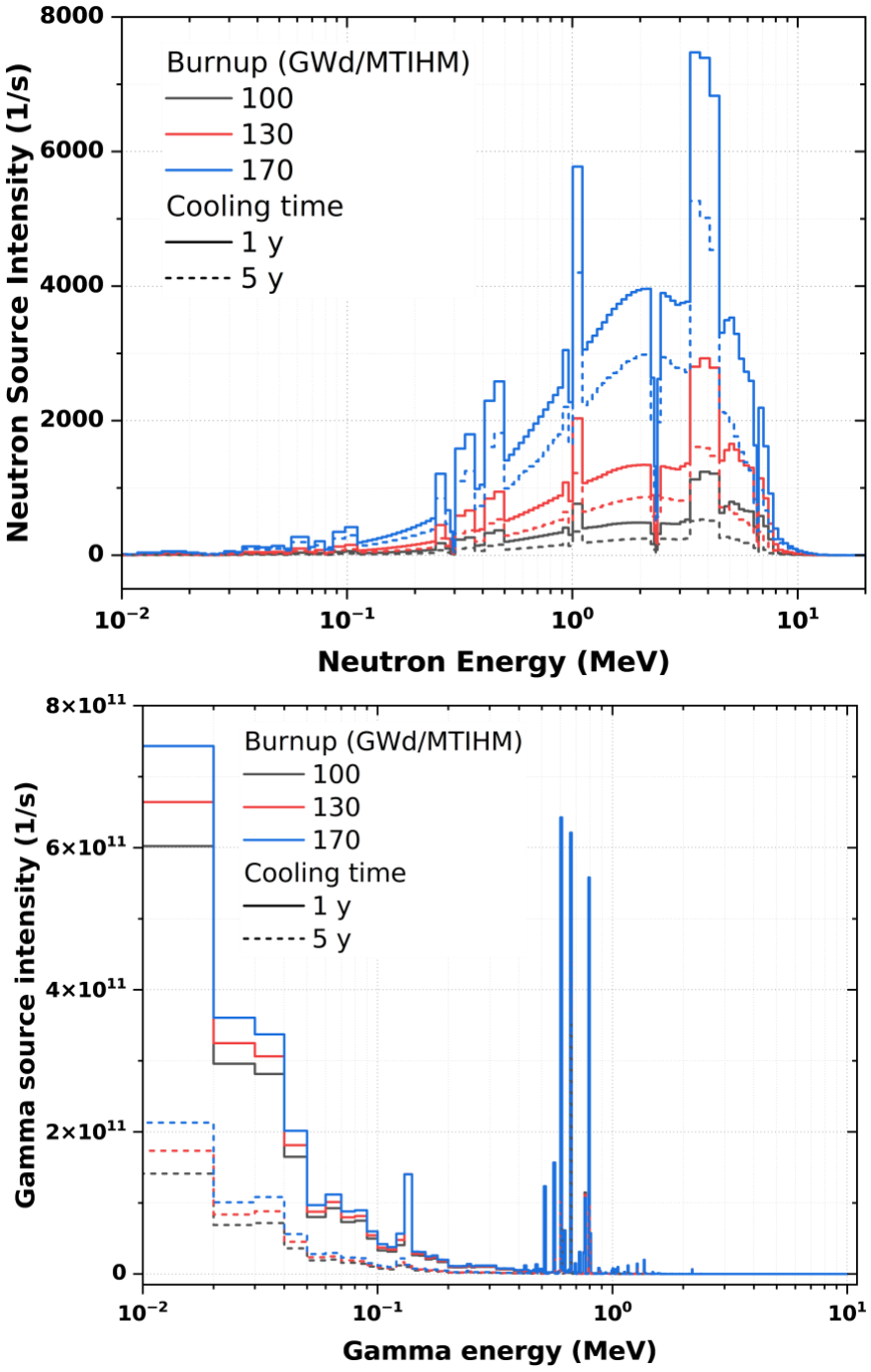

Figure B-5. Neutron and gamma sources of Type 2 prismatic fuel block.

APPENDIX C. ADDITIONAL GAMMA SPECTROMETRY RESULT

APPENDIX C. ADDITIONAL GAMMA SPECTROMETRY RESULT

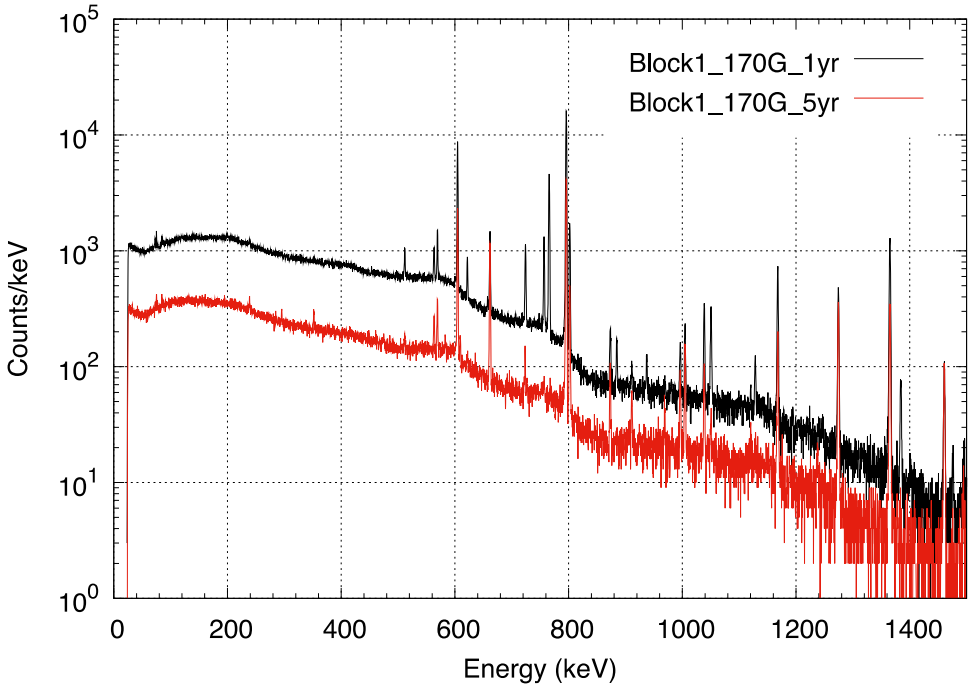

Figure C-1. Simulated HPGe gamma spectra from an irradiated Type 1 prismatic block with two different cooling times.

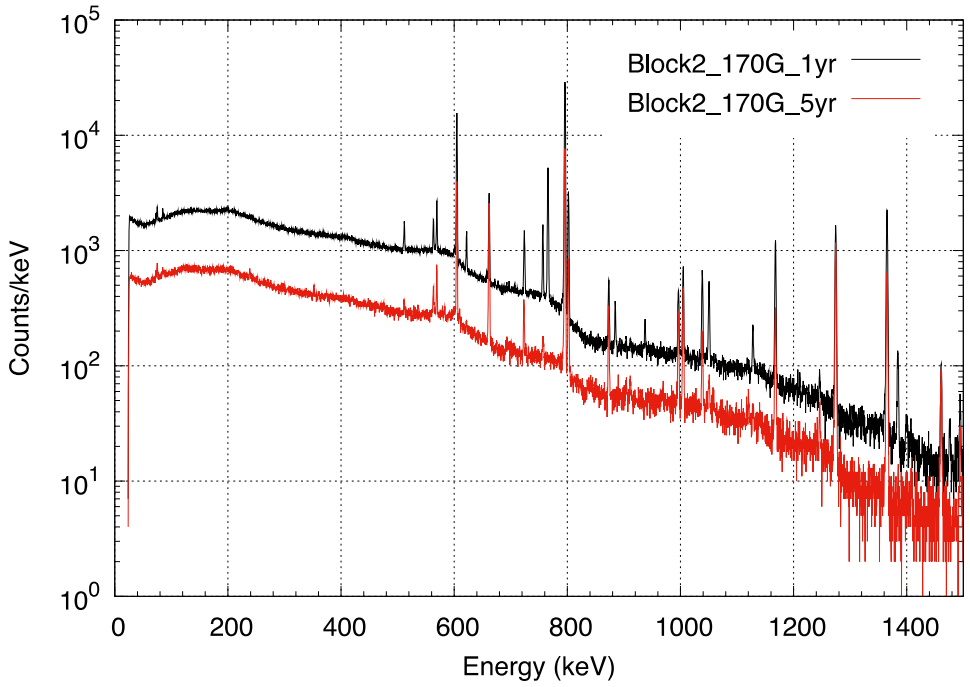

Figure C-2. Simulated HPGe gamma spectra from an irradiated Type 2 prismatic block with two different cooling times.

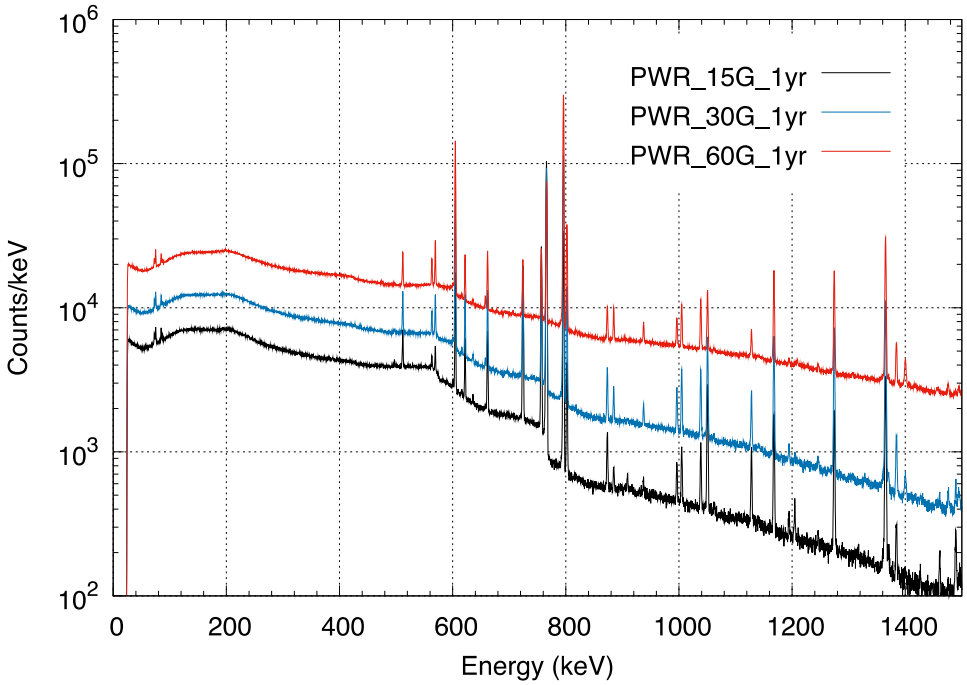

Figure C-3. Simulated HPGe gamma spectra from an irradiated PWR assembly with three different burnups and a cooling time of one year.

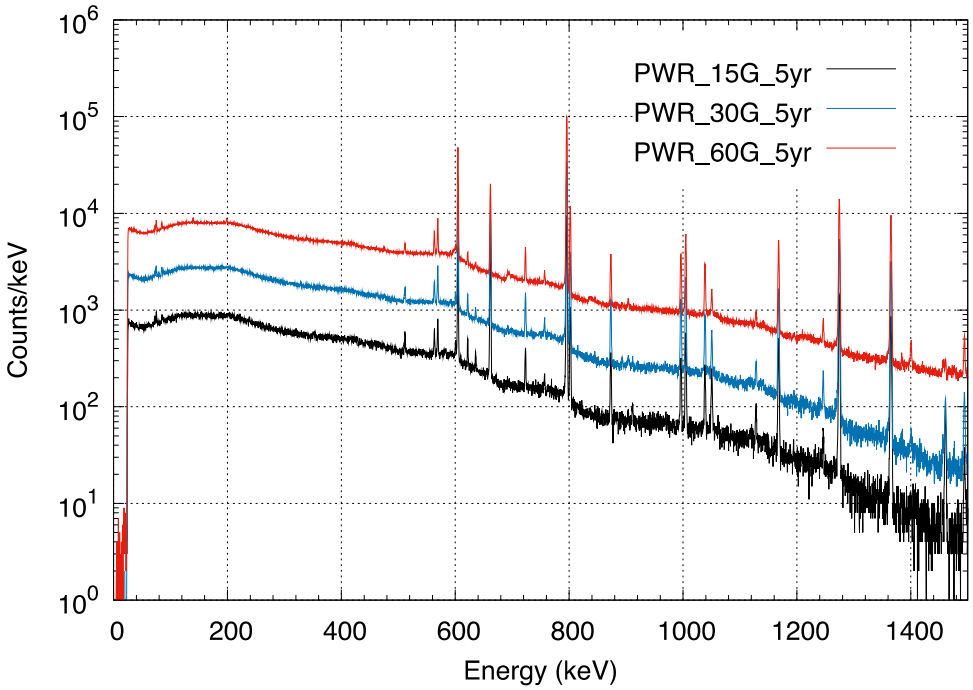

Figure C-4. Simulated HPGe gamma spectra from an irradiated PWR assembly with three different burnups and a cooling time of five years.

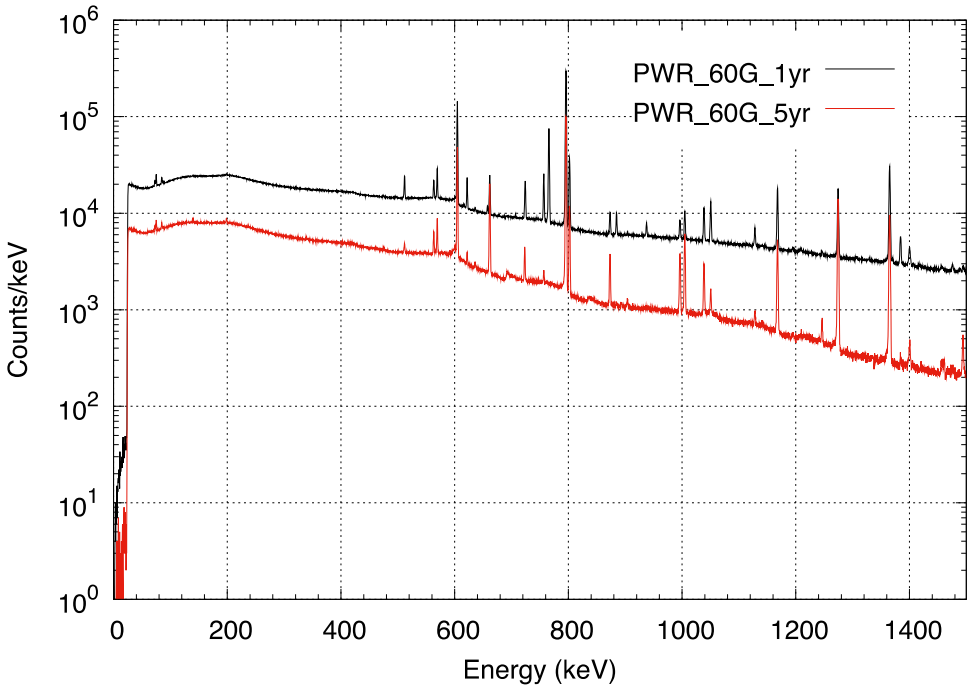

Figure C-5. Simulated HPGe gamma spectra from an irradiated PWR assembly with with two different cooling times.